Carboxydotrophic microorganisms

Natural and anthropogenic processes generate carbon monoxide (CO). They are responsible for a CO emission of 2500–2600 teragram (Tg) per year.

Most CO is emitted by natural processes including **atmospheric CH_4 oxidation**, **natural hydrocarbon oxidation**, **volcanic activity**, **production by plants** and **photochemical degradation of organic matter** in water, soil, and marine sediments or from the **enzymatic degradation of heme**.

Anthropogenic processes such as **incomplete combustion** of fossil fuels and various **industrial processes** are responsible for an annual release of 1200 Tg of CO to the atmosphere.

Kroneck et al. , 2014

Carboxydotrophic microorganisms

Chemical and biological processes are responsible for CO removal. The major part of **CO in the atmosphere becomes oxidized to CO_2 by rapid reaction with hydroxyl radicals in the troposphere** (2000–2800 Tg/yr), reducing the half-life of CO in the troposphere to a few months.

Biological processes are relevant to remove CO and keep it at low trace gas concentrations. **Microbes consume CO by using it as a source of carbon and energy**.
Soil and marine microbes reduce the global budget of CO by 20% per year, to which soil microbes contribute with 200–600 Tg of CO removal per year.

CO-oxidizing bacteria have a natural enrichment in the top layer of burning charcoal piles from where several of these soil microbes have been isolated. CO is also consumed by pathogenic Mycobacteria, like the tubercle bacillus *Mycobacterium tuberculosis*, which can grow on CO as sole source of carbon and energy.

Kroneck et al. , 2014

Carboxydotrophic microorganisms

Reaction equations and their standard Gibbs free energy (G0) for several modes of carboxydotrophic growth

Metabolism		Reaction	ΔG^0 (kJ)
Fermentative			
	Hydrogenogenic	$CO + H_2O \longrightarrow CO_2 + H_2$	–20
	Methanogenic	$4\ CO + 2\ H_2O \longrightarrow CH_4 + 3\ CO_2$	–210
	Acetogenic	$4\ CO + 2\ H_2O \longrightarrow CH_3COO^- + H^+ + 2\ CO_2$	–174
	Solventogenic (ethanol)	$6\ CO + 3\ H_2O \longrightarrow C_2H_5OH + 4\ CO_2$	–224
Respiratory			
	Oxygen	$2\ CO + O_2 \longrightarrow 2\ CO_2$	–514
	Sulfate	$4\ CO + SO_4^{2-} + H^+ \longrightarrow 4\ CO_2 + HS^-$	–231

Isolated microorganisms capable of conserving energy from the water–gas shift reaction

Species	Origin	Temperature optimum (°C)	Carboxydotrophic generation time (h)	Reference
Mesophilic bacteria				
Rhodospirillum rubrum	Various environments	30	5 (dark, acetate)	Kerby et al., 1995
Rubrivivax gelatinosa	Lake sediment	34	6.7 (dark, trypticase) 10 (light, autotrophically) 1.5 (light, malate)	Uffen, 1976; Maness et al., 2005
Rhodopseudomonas palustris	Anaerobic wastewater sludge digester	30	2 (light, autotrophically)	Jung et al., 1999

Diender et al. , 2015

Carboxydotrophic microorganisms

Isolated microorganisms capable of conserving energy from the water–gas shift reaction

Species	Origin	Temperature optimum (°C)	Carboxydotrophic generation time (h)	Reference
Thermophilic bacteria				
Caldanaerobacter subterraneus ssp. *pacificus*	Submarine hot vent, Okinawa Trough	70	7.1	Sokolova et al., 2001; Fardeau et al., 2004
Carboxydocella sporoproducens	Hot spring, Karymskoe Lake	60	1	Slepova et al., 2006
Carboxydocella thermoautotrophica	Terrestrial hot vent, Kamchatka Peninsula	58	1.1	Sokolova et al., 2002
Carboxydothermus hydrogenoformans	Freshwater hydrothermal spring, Kunashir Island	70	2	Svetlichny et al., 1991
Carboxydothermus islandicus	Hot spring, Hveragerdi	65	2	Novikov et al., 2011
Carboxydothermus pertinax	Volcanic acidic hot spring, Kyushu Island	65	1.5	Yoneda et al., 2012
Carboxydothermus siderophilus	Hot spring, Kamchatka Peninsula	65	9.3	Slepova et al., 2009
Dictyoglomus carboxydivorans	Hot spring, Kamchatka Peninsula	75	60	Kochetkova et al., 2011
Moorella stamsii	Digester sludge	65	N.D.	Alves et al., 2013
Thermincola carboxydiphila	Hot spring, Lake Baikal	55	1.3	Sokolova et al., 2005
Thermincola ferriacetica	Hydrothermal spring, Kunashir Island	60	N.D.	Zavarzina et al., 2007
Thermincola potens	Thermophilic microbial fuel cell	55	N.D.	Byrne-Bailey et al., 2010
Thermolithobacter carboxydivorans	Mud and water, Calcite Spring	73	1.3	Sokolova et al., 2007
Thermosinus carboxydivorans	Hot spring, Norris Basin	60	1.15	Sokolova et al., 2004a
Thermoanaerobacter thermohydrosulfuricus ssp. *carboxydovorans*	Geothermal spring, Turkey	70	N.D.	Balk et al., 2009
Desulfotomaculum carboxydivorans	Paper mill wastewater sludge	55	N.D.	Parshina et al., 2005b
Thermophilic archaea				
Thermococcus onnurineus	Deep-sea hydrothermal vent	80	5	Bae et al., 2006, 2012
Thermocuccus AM4	Hydrothermal vent	82	5	Sokolova et al., 2004b
Thermofilum carboxyditrophus	Kamchatka hot springs	90	N.D.	Kochetkova et al., 2011

Diender et al. , 2015

Carboxydotrophic microorganisms

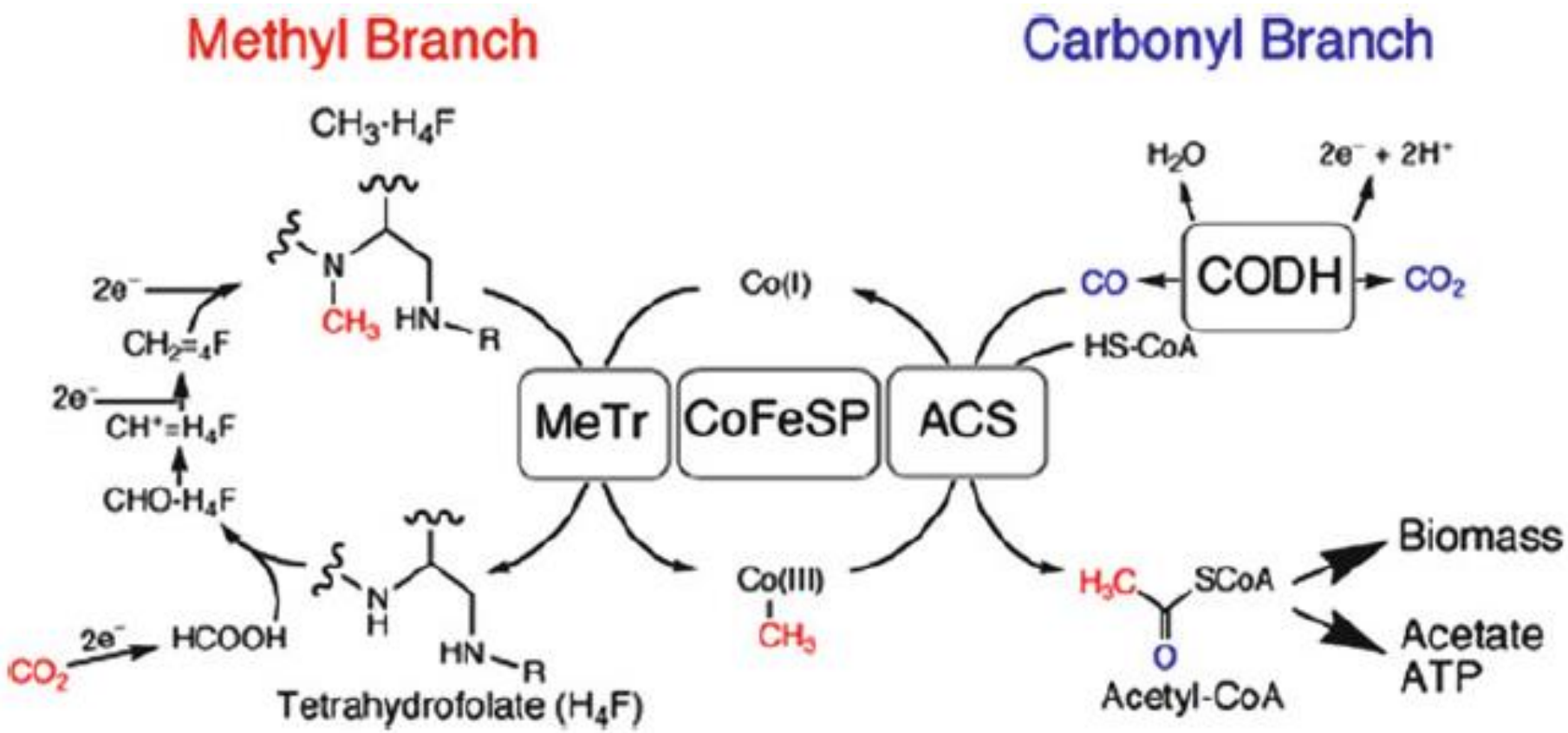

Figure 1 The Wood-Ljungdahl pathway. ACS, acetyl-CoA synthase; CODH, Ni,Fe-containing carbon monoxide dehydrogenase; CoFeSP, corrinoid iron-sulfur protein; MeTr, methyl-tetrahydrofolate:corrinoid iron-sulfur protein methyltransferase. The figure is modified from Ragsdale and Pierce [26].

Kroneck et al. , 2014

Carboxydotrophic microorganisms

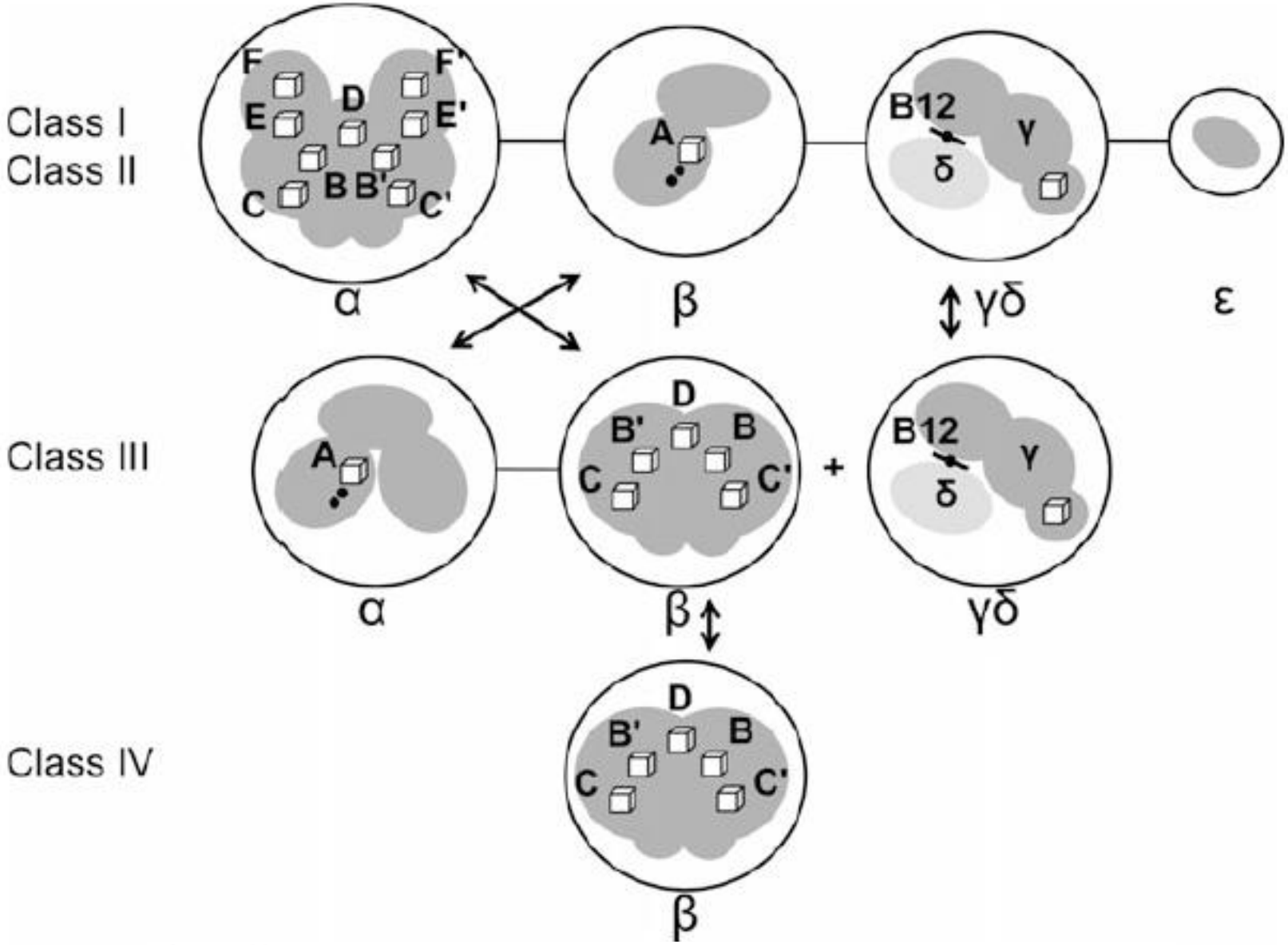

Figure 11 Subunit composition of Ni,Fe-containing CODHs. Connected circles indicate multiprotein complexes consisting of the corresponding subunits. Homology is indicated by arrows. The figure was adapted from Lindahl [74]. Details are given in the text.

Kroneck et al. , 2014

Cu,Mo-containing CO dehydrogenases

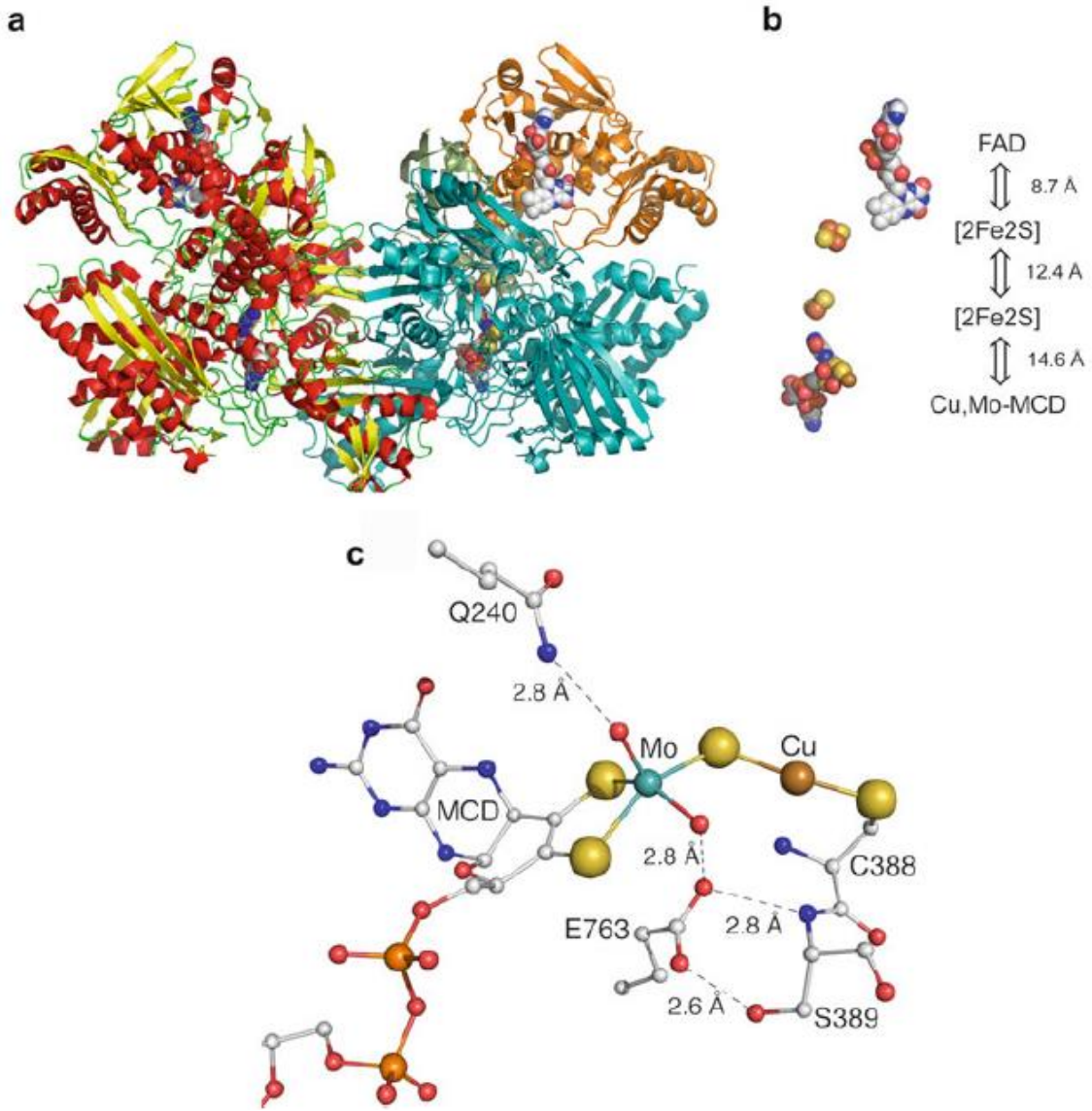

Figure 3 The structure of Cu,Mo-CODHs. (**a**) Overall structure of the dimer of trimers, $(LMS)_2$. The L subunit of the right monomer is colored in cyan, the M subunit in orange, and the S subunit in green. (**b**) Cofactors of one LMS monomer with shortest distance between the redox active sites of the cofactors. (**c**) Active site architecture including residues in the second coordination sphere of the metals.

Kroneck et al. , 2014

Monofunctional Ni,Fe-containing CO dehydrogenases

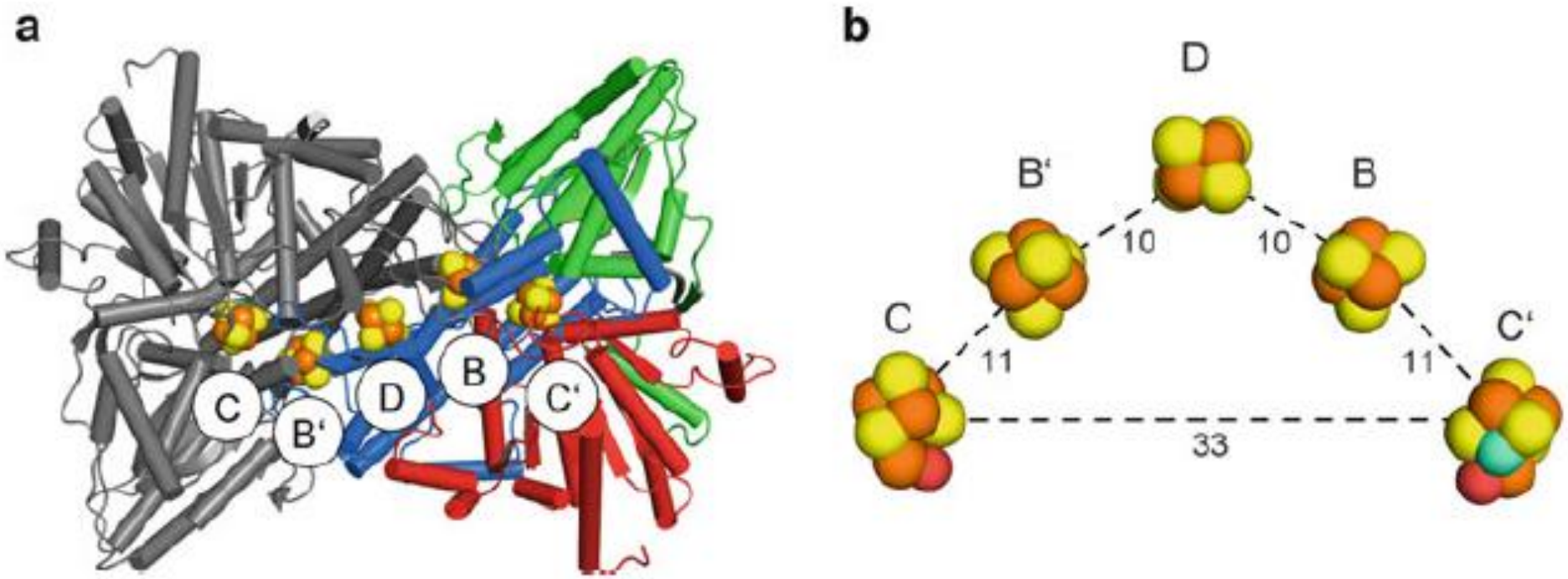

Figure 5 Homodimeric structure of monofunctional CODH II_{Ch}. (a) Cartoon-representation of dimeric Ni,Fe-CODH. The two subunits of CODH are shown with different colors, where one subunit is highlighted in blue, green, and red for the N-terminal, middle and C-terminal domain, respectively, and the other in grey. The metal clusters encountered are depicted as spheres (Fe is colored in orange, S in yellow, Ni in cyan, and O in red). (b) Cluster arrangement in CODH. Cluster D is connecting the two subunits covalently and is in electron transfer distance to clusters B and B'. Cluster C/C' is situated on the end of the electron transfer chain, in close distance to cluster B of the opposing subunit. The distances between Fe atoms of individual clusters are given in Ångstrom.

Kroneck et al. , 2014

Monofunctional Ni,Fe-containing CO dehydrogenases

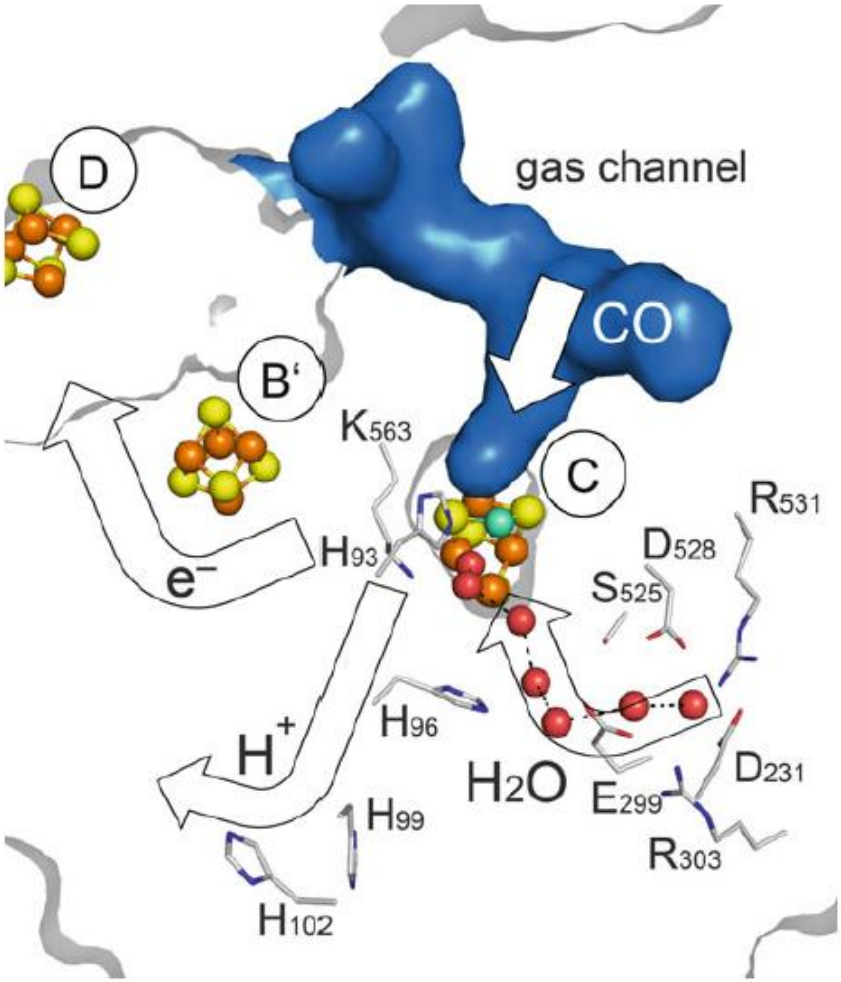

Figure 8 Channels involved in substrate/product transfer in monofunctional CODH II_{Ch}. Hydrophobic channels around cluster C have been calculated with the program Hollow [159] and are shown as blue surface. Metal clusters are depicted as spheres and colored in cyan for Ni, orange for Fe, and yellow for S. Water molecules are represented by red spheres. Charged and hydrophilic residues form a water channel network. The electron transfer network from clusters C↔B'↔D is indicated by an arrow. The proton relay shuttle is compromised of histidine residues H_{96}, H_{99}, and H_{102}, where the last residue has direct contact to the protein surface. The surface is contoured in grey.

Kroneck et al. , 2014

Bifunctional Ni,Fe-containing CO dehydrogenases

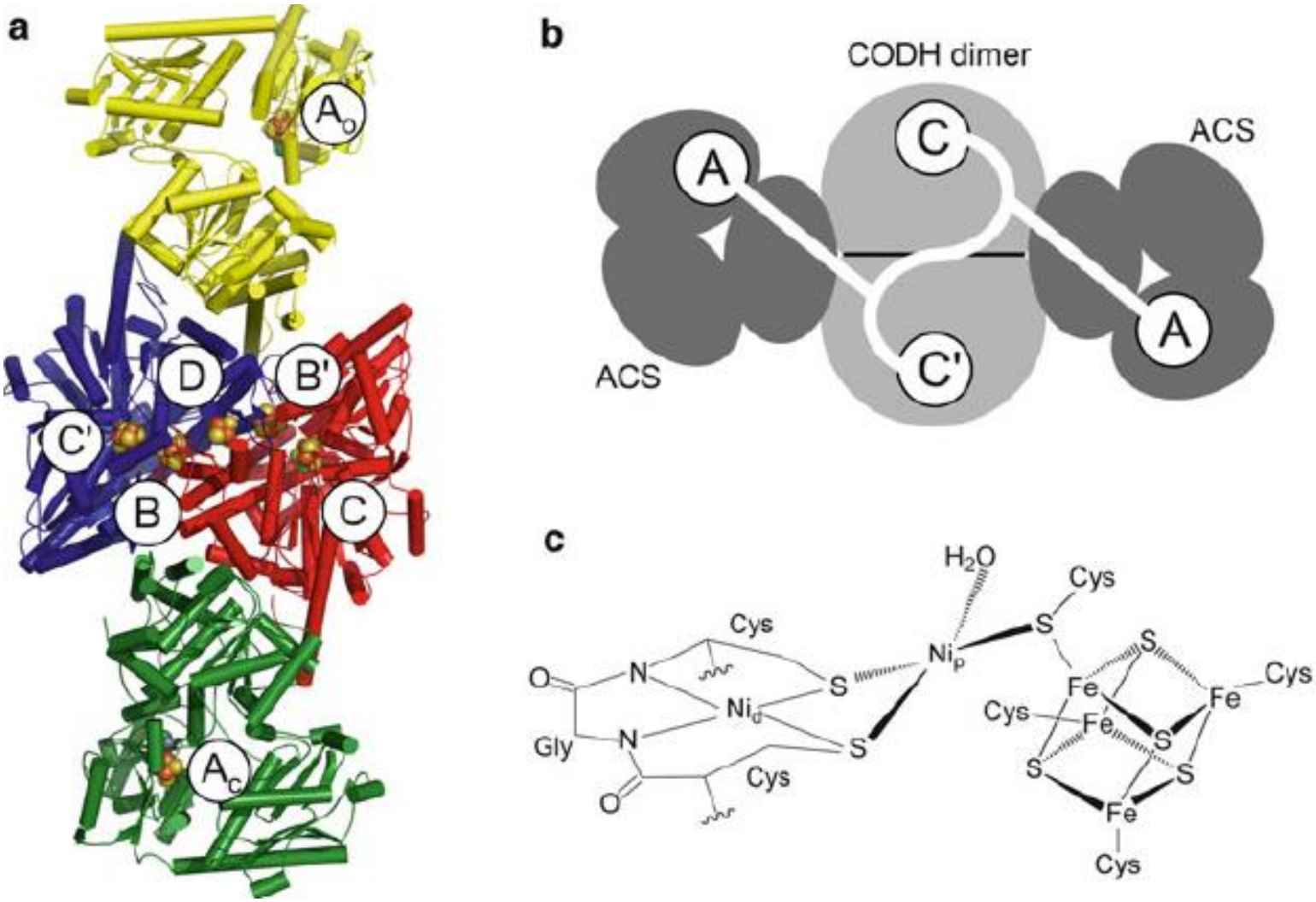

Figure 12 The structure of bacterial CODH/ACS. (a) Cartoon representation of the overall structure of the $\alpha_2\beta_2$ CODH/ACS complex from *Moorella thermoacetica* (PDB 1OAO) [111]. Metal clusters are presented as balls and sticks and are labeled with A to D. CODH subunits are colored in blue and red and ACS subunits are colored in yellow for the Ni-Ni-containing cluster A (A_o) and green for the Zn,Ni-containing cluster A (A_c). (b) Schematic representation of the gas channel connecting the CODH/ACS active sites. (c) Schematic representation of the Ni-Ni containing cluster A, based on PDB 1RU3 [81]. Details are given in the text.

Kroneck et al. , 2014

Carboxydotrophic microorganisms

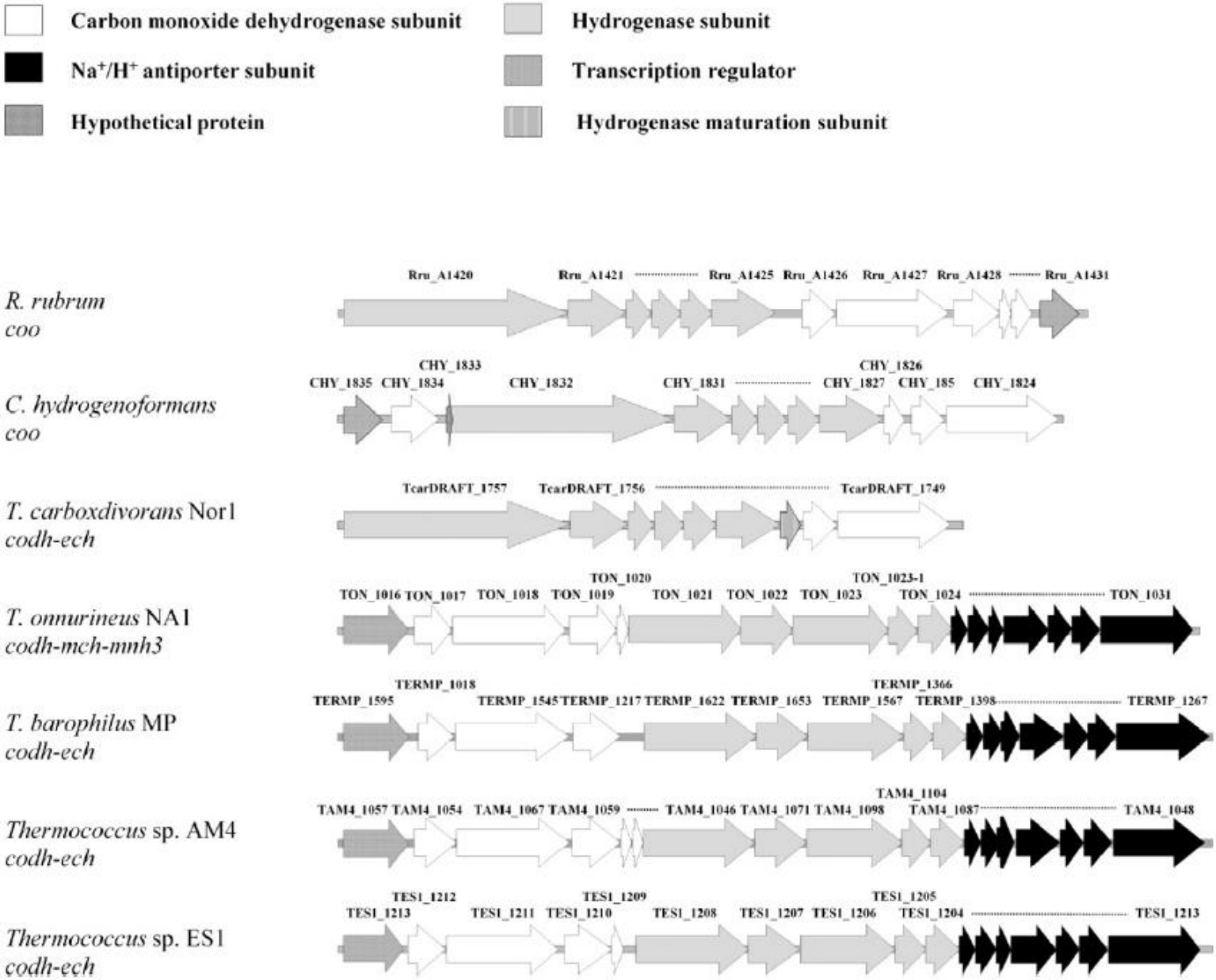

Rittmann et al. , 2015

Carboxydotrophic microorganisms

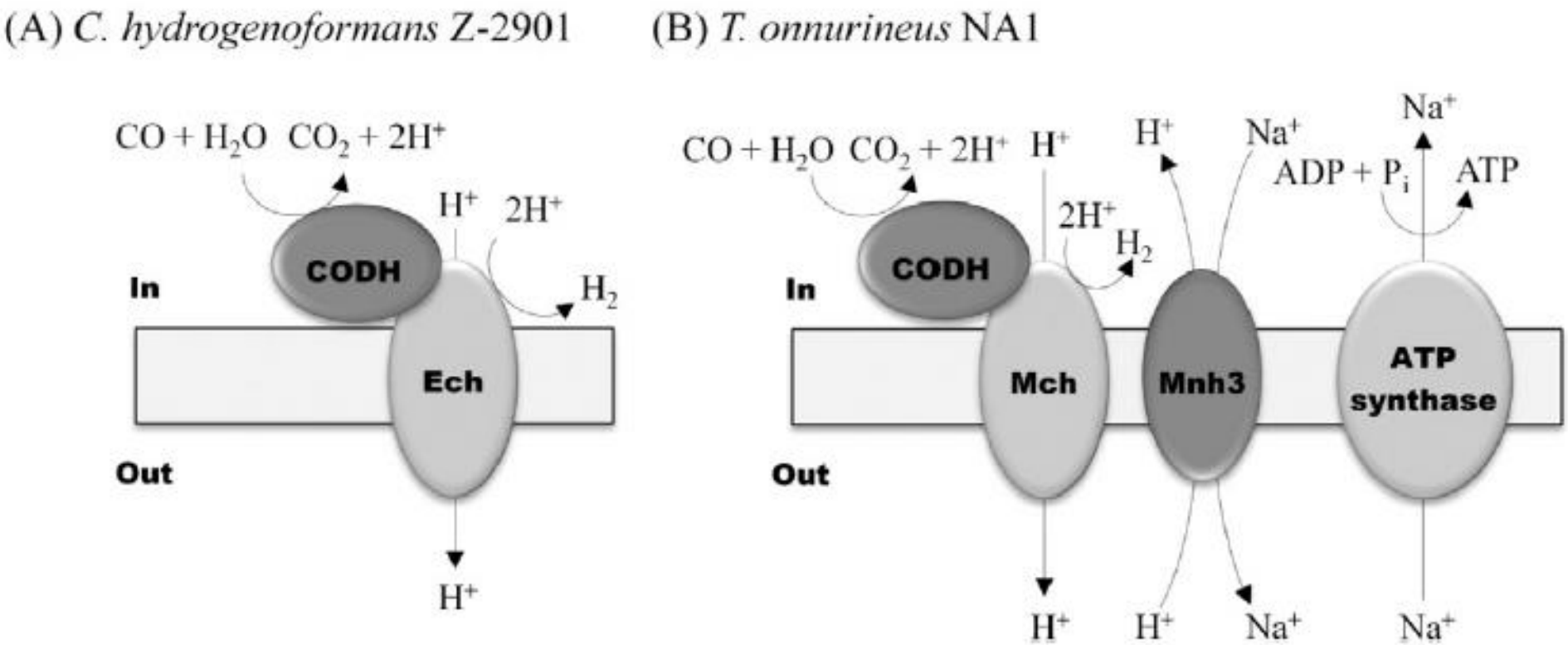

Fig. 4. Structural model of the CO-oxidizing, H2-forming enzyme complex in *Carboxydothermus hydrogenoformans* (Hedderich, 2004) (A) and *Thermococcus onnurineus* NA1 (B) and the proposed mechanism of coupling of CO oxidation with ATP synthesis.

Rittmann et al. , 2015

Carboxydotrophic microorganisms

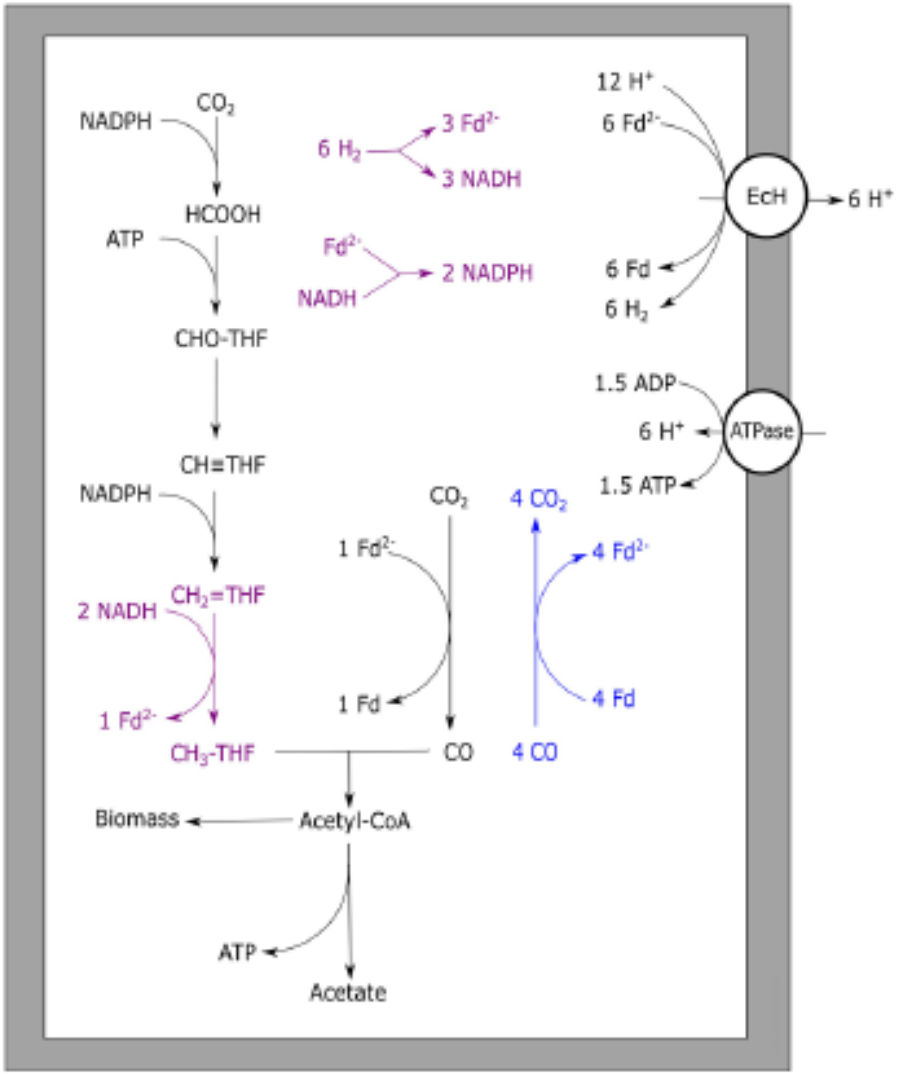

FIGURE 2 | Carbon monoxide metabolism of *Moorella thermoacetica*. Stoichiometric conversion of CO to acetate by *M. thermoacetica* is disaplayed. Reactions marked blue indicate CO oxidizing activity by CODH, bifurcating reactions are marked purple. The EcH is assumed to transport one proton per hydrogen formed whereas the ATPase is assumed to generate one ATP per four protons translocated. EcH, energy converting hydrogenase; ATPase, ATP synthase; Fd, ferredoxin; THF, tetrahydrofolate.

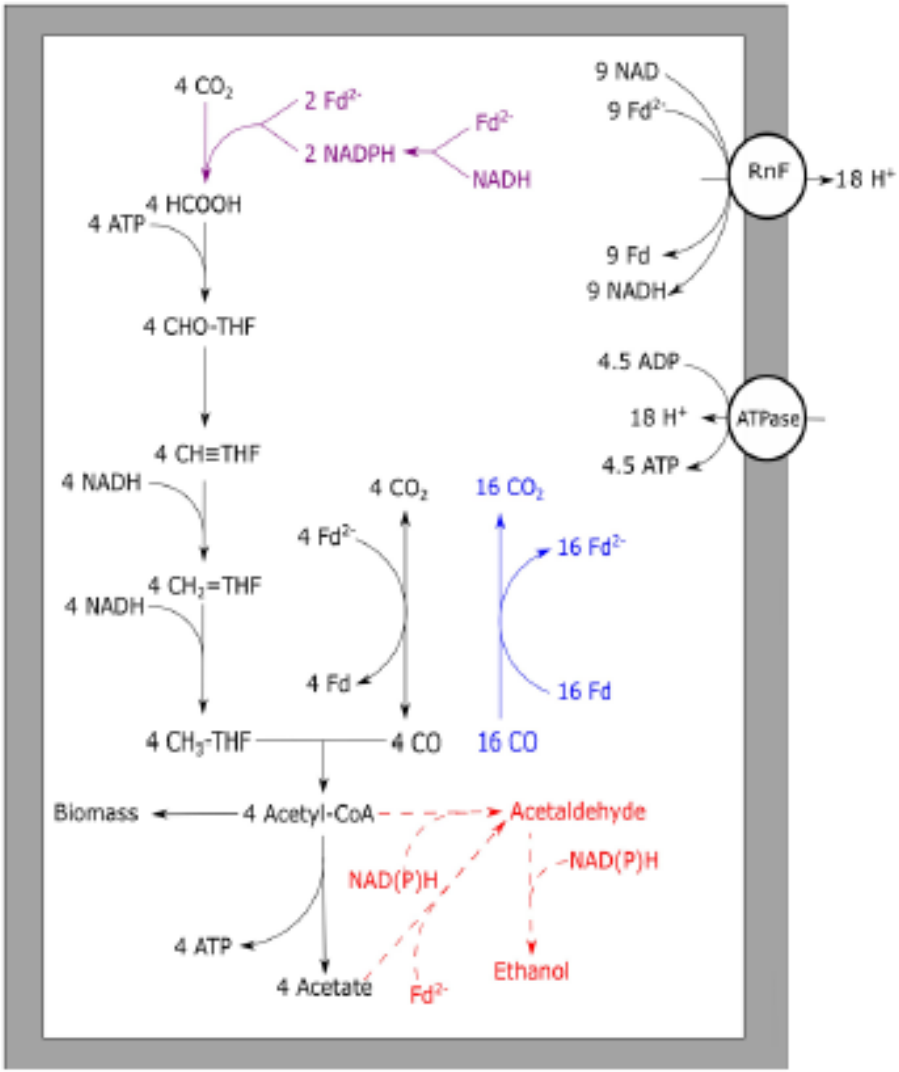

FIGURE 4 | Carbon monoxide metabolism of *Clostridium ljungdahlii*. Stoichiometric conversion of CO to acetate for *C. ljungdahlii* is displayed. The pathways of ethanol formation are indicated by the dotted line in red, and are not taken into account for the energy yield displayed. Reactions marked blue indicate CO oxidizing activity by CODH, bifurcating reactions are marked purple. The RnF complex is assumed to transport two protons per Fd oxidized whereas the ATPase is assumed to generate one ATP per four protons translocated. Rnf, RnF complex; ATPase, ATP synthase; Fd, ferredoxin; THF, tetrahydrofolate.

Diender et al. , 2015

Carboxydotrophic microorganisms

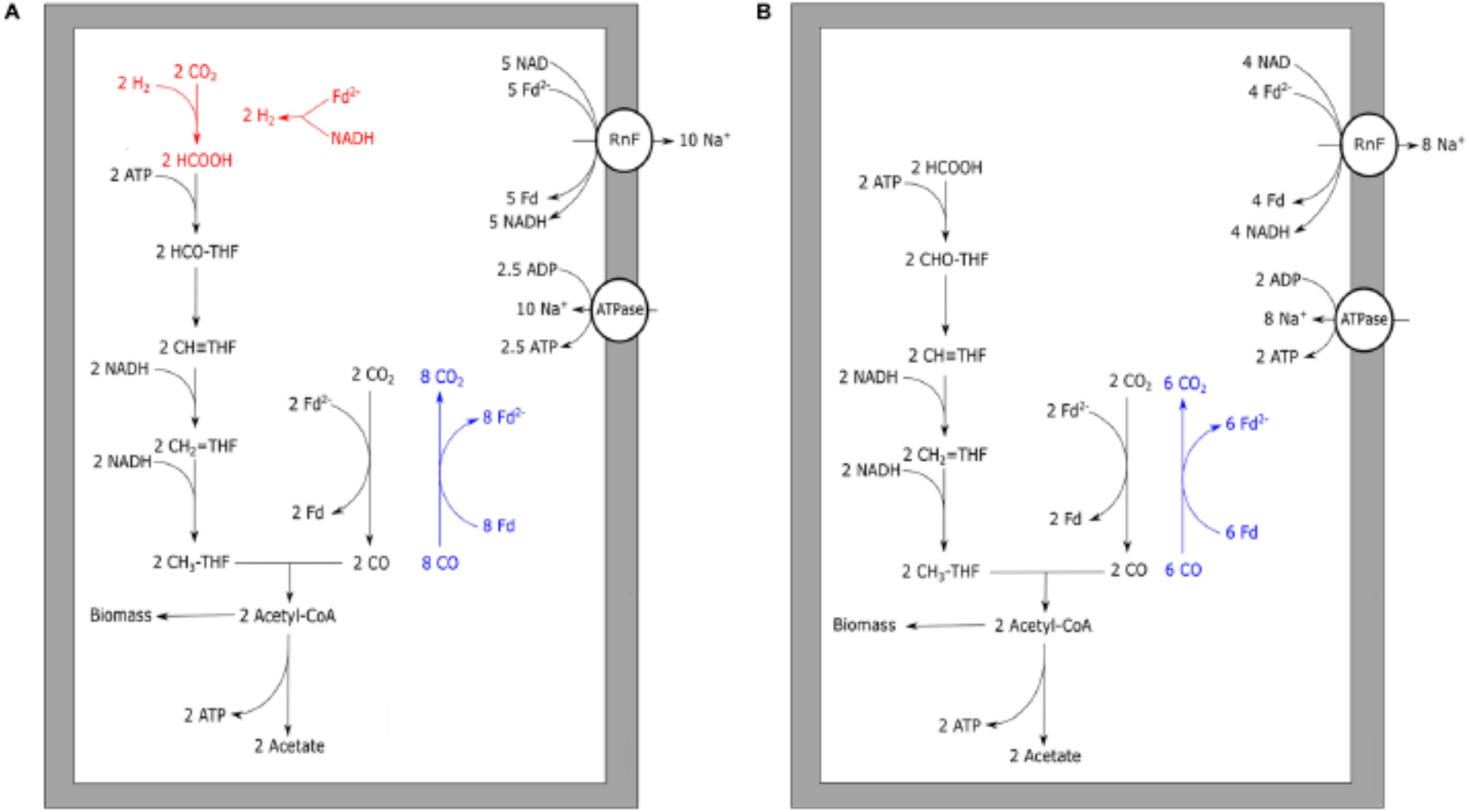

FIGURE 3 | Carbon monoxide metabolism of *Acetobacterium woodii*. Acetogenic CO metabolism of *A. woodii* is displayed. **(A)** The proposed theoretical pathway and energetic yield of CO conversion to acetate. Pathways prone to CO inhibition are shown in red. **(B)** Proposed metabolism and energetic yield of acetogenic metabolism driven by CO co-fermented with formate. Reactions marked blue indicate CO oxidizing activity by CODH. The RnF complex is assumed to transport two sodium ions per Fd oxidized whereas the ATPase is assumed to generate one ATP per four sodium ion translocated. Rnf, RnF complex; ATPase, ATP synthase; Fd, ferredoxin; THF, tetrahydrofolate.

Diender et al. , 2015

universität wien

Methanogenesis

Dr. Simon K.-M. R. Rittmann

Methanogens

➢are obligate anaerobic prokaryotes from the domain Archaea, exclusively belong to the phylum Euryarchaeota (and possibly Bathyarchaeota, Lokiarchaeota); produce methane as end product of their energy metabolism; use carbon substrates such as C_1-, C_2- and methylated compounds

M. marburgensis

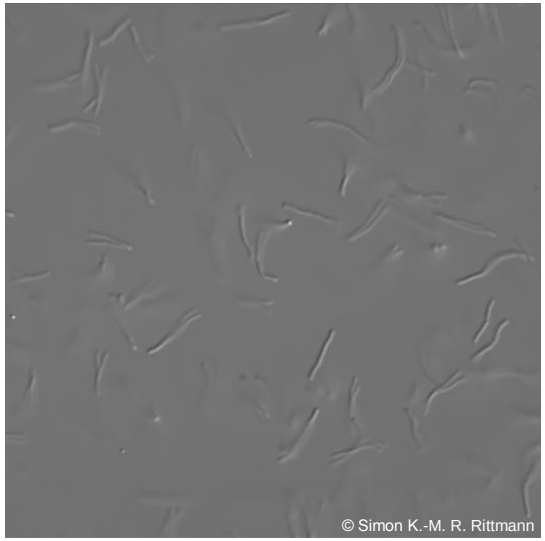

Methanothermobacter marburgensis DSM 2133, phase contrast micrograph (magnification x 1000)

M. barkeri

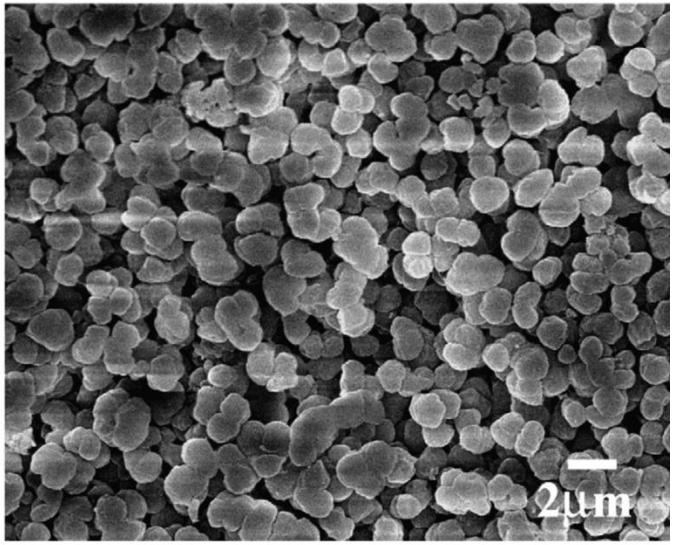

Nomura *et al*., 2007, Advanced Powder Technology

M. solegelidi

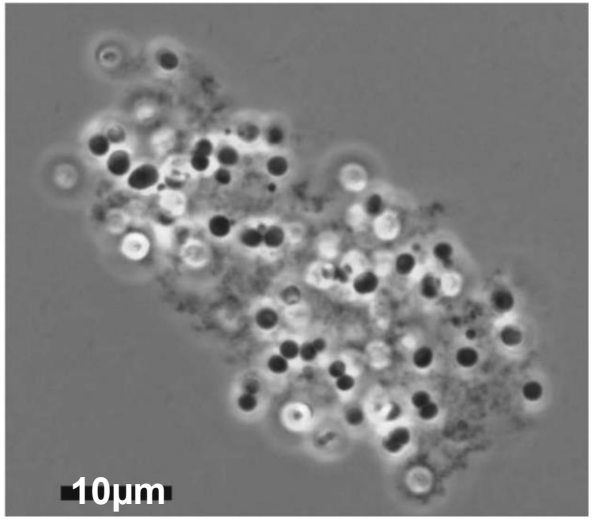

Wagner *et al*., 2007, IJSEM

The cell wall is composed of pseudomurein.

Cell wall of Sarcina is composed of a S-layer lattice, but under special environmental conditions Sarcina also form a methanochondoitin layer encapsulating an association of cells enabling intercellular e^- transfer.

Six classes of methanogens

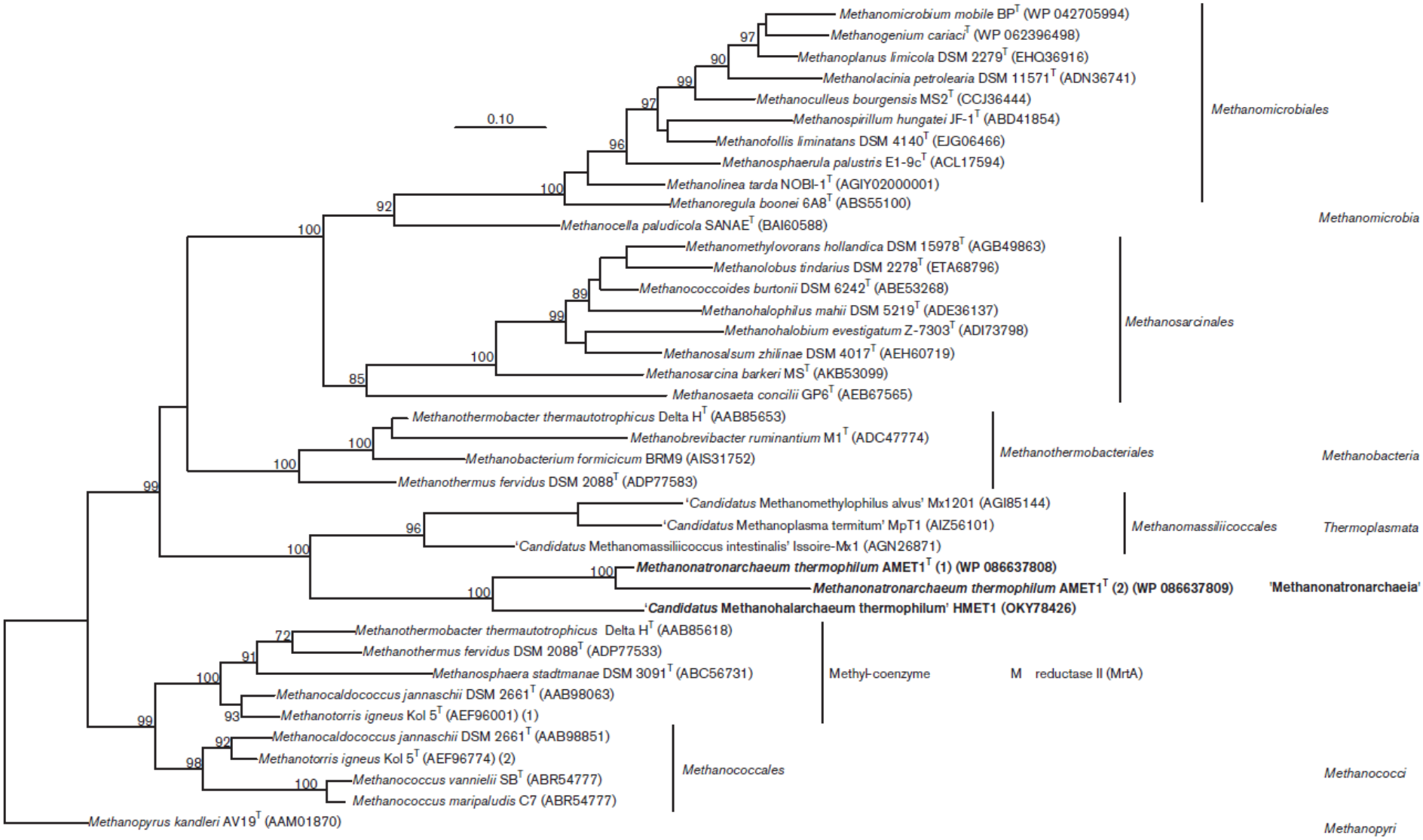

Fig. 3. Phylogeny of novel halo(alkali)philic methanogens from hypersaline lakes based on the 16S rRNA gene (a) and full amino acid sequences of the α-subunit of methyl coenzyme M reductase (McrA or MrtA) (b). The trees were built with the PhyML program and the approximate likelihood-ratio test for branches [33]. Bootstrap values above 70 % are shown at the nodes. Bar, 0.10 changes per position.

Sorokin *et al.*, 2018

Eight orders of methanogens

1. Methanobacterales
2. Methanocellales
3. Methanococcales
4. Methanomassiliicoccales
5. Methanomicrobiales
6. Methanonatronarchaeles
7. Methanopyrales
8. Methanosarcinales

Borrel *et al*.,2013, Iino *et al*., 2013, Sorokin *et al*., 2018

Methanogenesis – Global carbon cycle

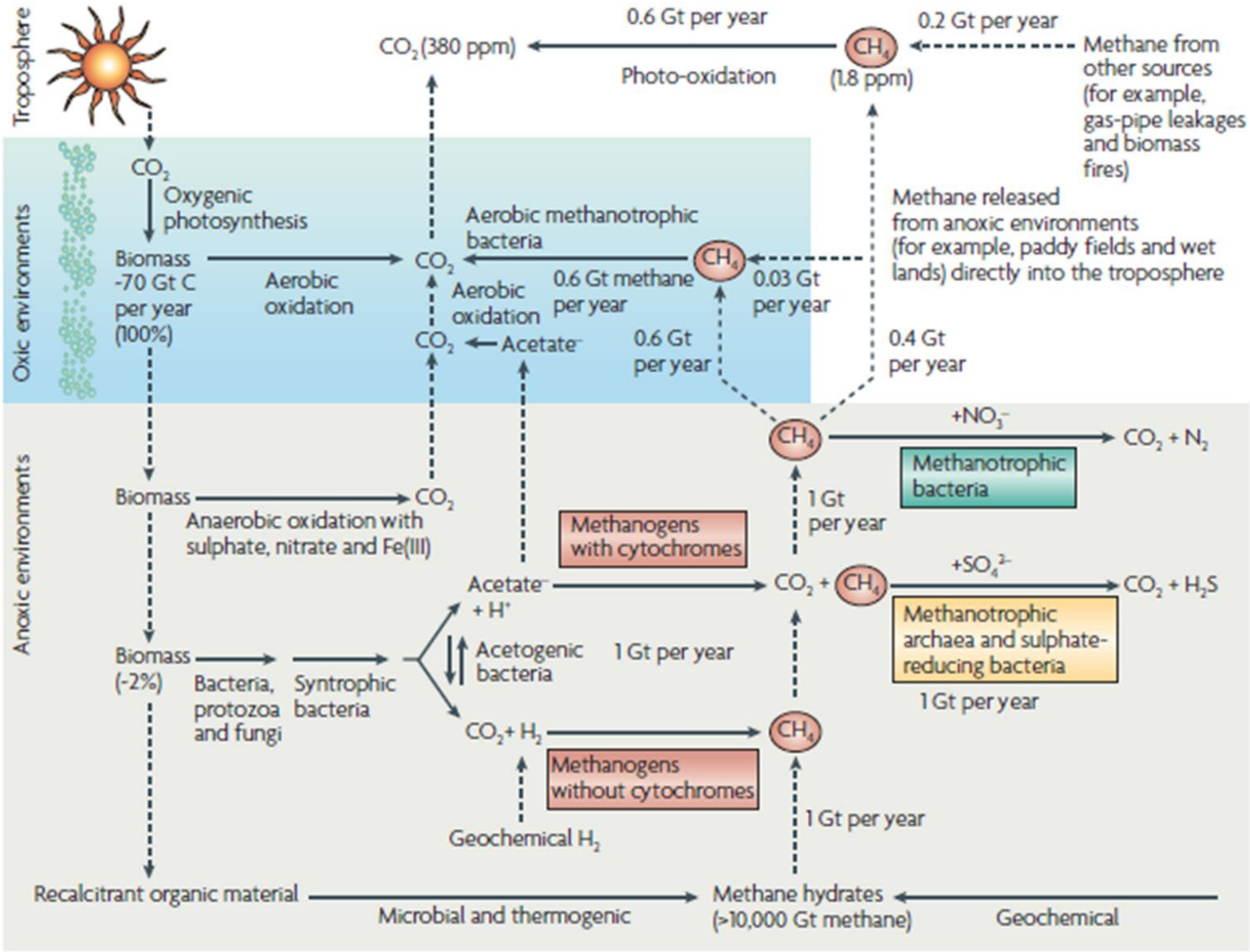

Thauer *et al*. 2008

Methanogenesis – Global carbon cycle

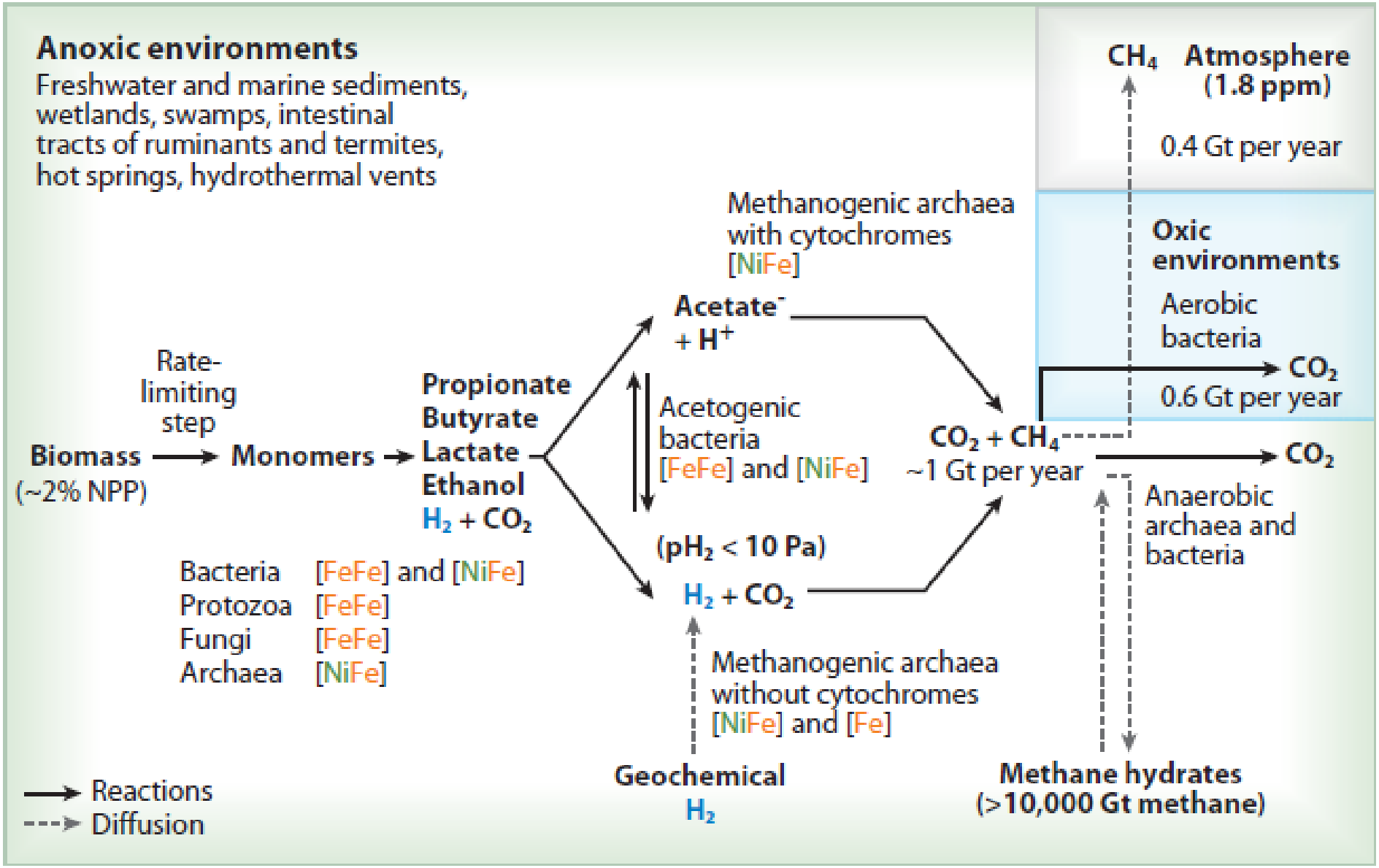

Thauer *et al.* (2010) Ann. Rev. Biochem.

Sources of GHG emissions

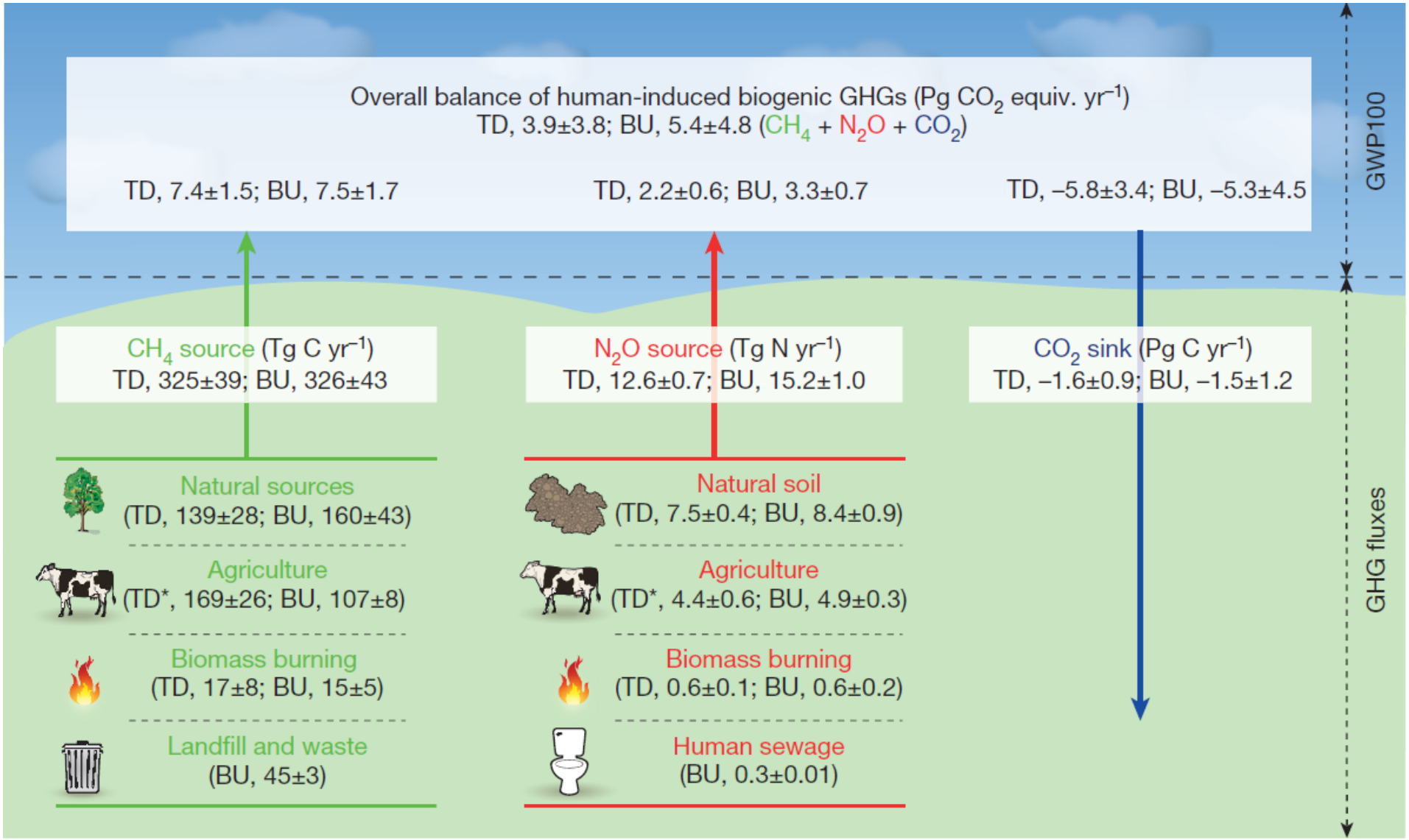

TD… top down, BU… bottom up

Tian *et al.*, 2016

Sources of CH_4 emissions

Sources	Methane emission (Tg of CH_4 per year)	Percentage (%)[a]
Natural sources		
Wetlands	92–237	15–40
Termites	20	3
Ocean	10–15	2–3
Methane hydrates	5–10	1–2
Subtotal	127–282	21–47
Anthropogenic sources		
Ruminants	80–115	13–19
Energy generation[b]	75–110	13–18
Rice agriculture	25–100	7–17
Landfills	35–73	6–12
Biomass burning	23–55	4–9
Waste treatment	14–25	2–4
Subtotal	267–478	45–80
Total sources	500–600	

Source: Modified from Lowe[2] and Prather and Ehhalt.[140]

[a]Estimates of the relative contribution of methane emission from a source to the total global emissions of 600 Tg of CH_4 per year.

[b]Methane deposits released by coal mining, petroleum drilling, and petrochemical production.

Liu and Whitman, 2008

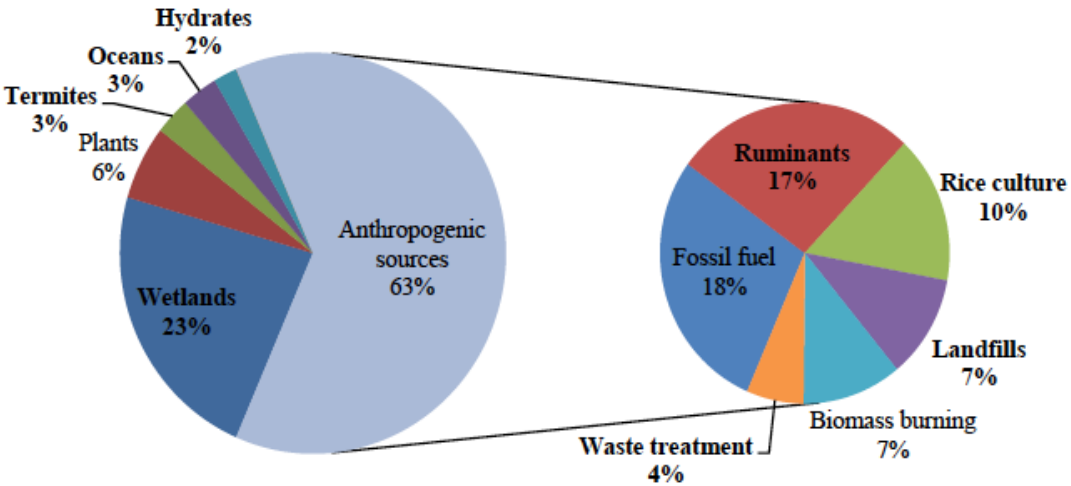

Nazaries *et al.*, 2013

Ruminants, agriculture and fossil fuel exploitation are large anthropogenic sources of methane emissions

Ruminants and methane

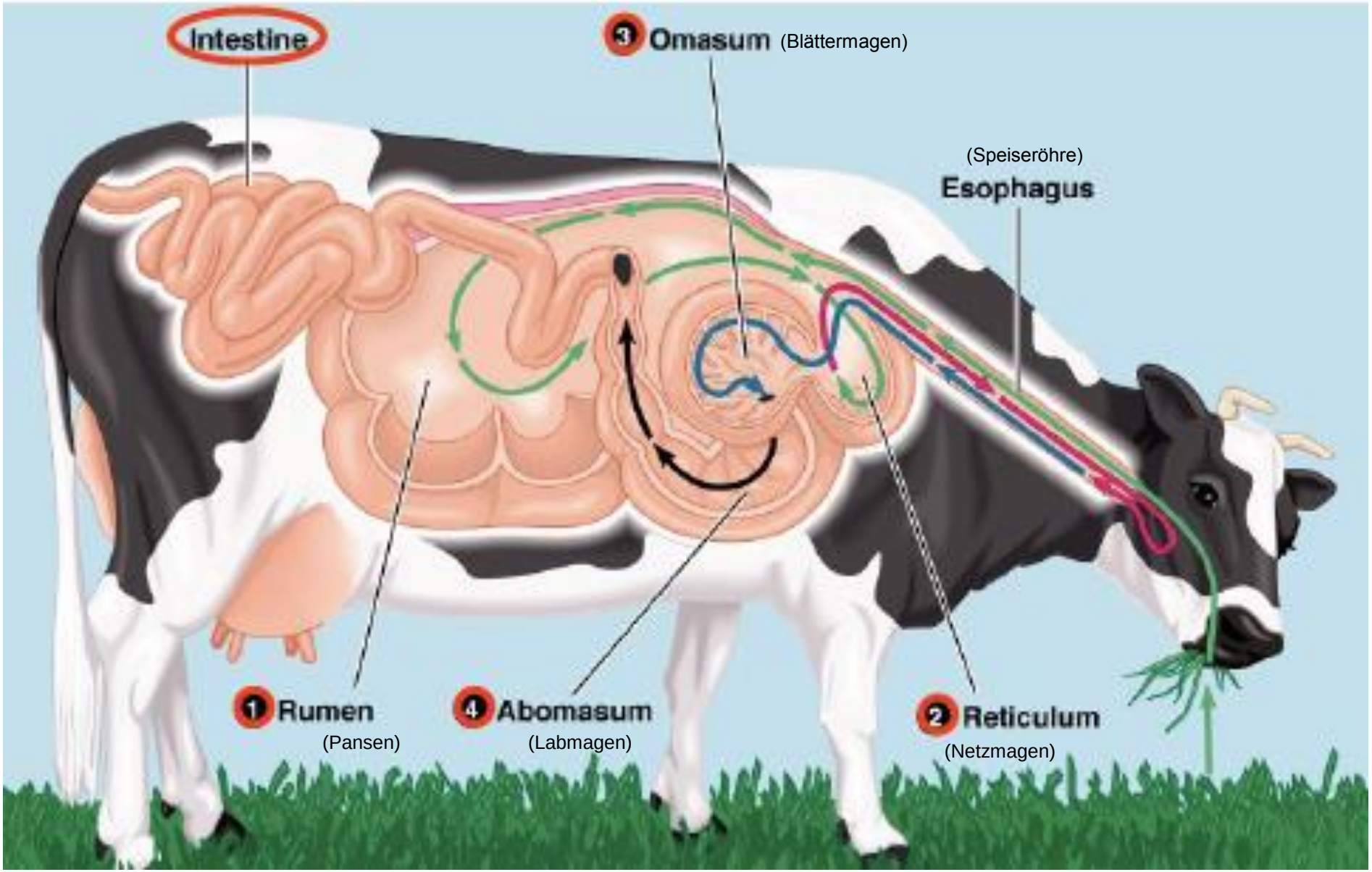

Rumen and reticulum are hydrolysis and fermentation chambers, anaerobic, 100-150 L, 200-250 liters CH_4 d^{-1} (~ 3.4 mmol L^{-1} h^{-1}).

Ruminants and methane

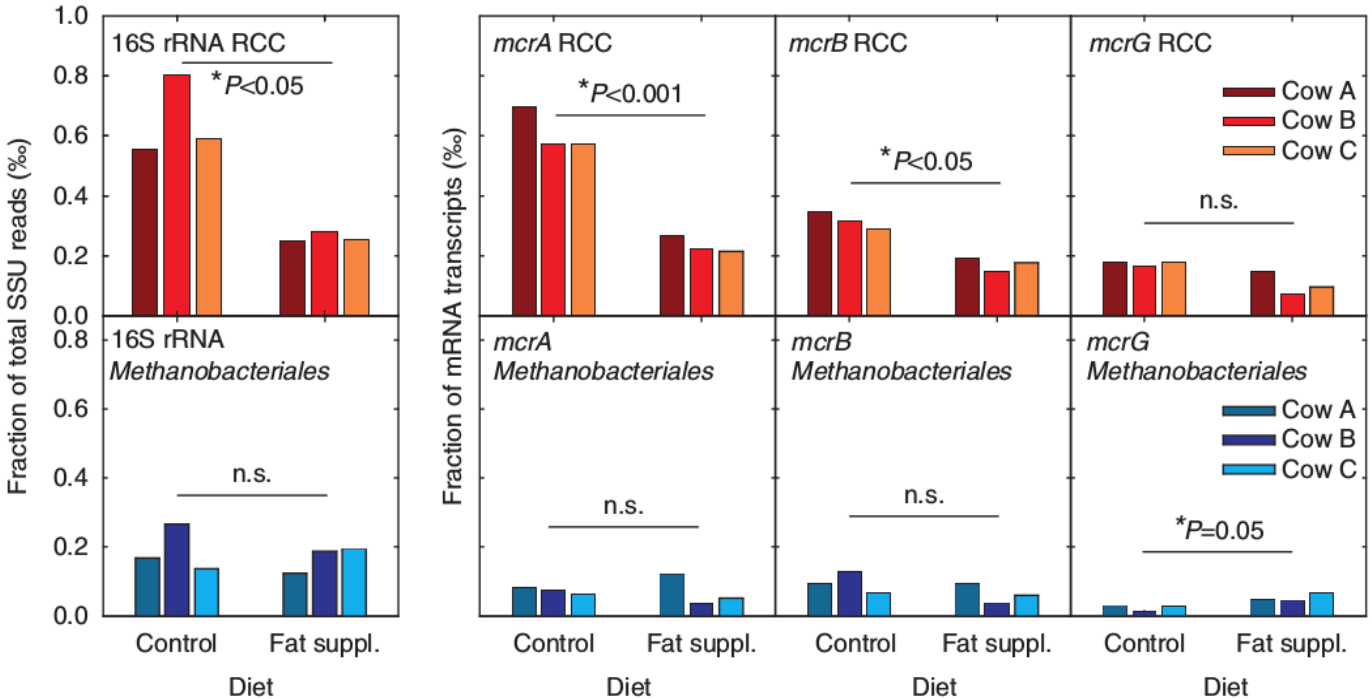

Figure 1 | Effect of RSO on methanogens *in vivo*. Relative abundances of transcripts from RCC (upper row) and from *Methanobacteriales* (bottom row) from individual cows on control and rapeseed oil (RSO)-supplemented diets, respectively. Relative fraction of archaeal SSU ribo-tags affiliated to RCC and *Methanobacteriales* is shown as % of total SSU reads, and fraction of *mcrA*, *mcrB* and *mcrG* transcripts detected for RCC and other methanogens (that is, *Methanobrevibacter ruminantium* and *Methanosphaera stadtmanae*), shown as ‰ of all mRNA transcripts with a significant homologue in Genbank nr (e-value < 1e-5) for each sample. *P*-values ≤ 0.05 are considered representing significant effects of fat supplementation (*marked) using paired *t*-test. The *mcrG* of RCC was trend-wise affected by fat supplementation ($P < 0.10$). n.s., not significant; suppl, supplement.

Poulsen *et al*., 2012

TMA, *Methanomassiliicoccales* and health

Origin and fate of TMA in the human gut, and the Archaebiotics concept. Gut microbiota synthesis of TMA is realized from TMAO , choline, PC and L-carnitine. The TMA is then absorbed and goes to the liver, routes (A) or (B). In the case of route (A), a partial or total defect in a flavin-containing monooxygenase 3 (FMO 3)-oxidation into TMAO leads to increased level and diffusion of TMA in breath, urine and sweat. When FMO 3 (liver oxidation) is functional (B), the increase of TMAO in blood is associated with atherosclerosis.2,7,11 Therefore, converting TMA directly in the gut using Archaebiotics belonging to the seventh methanogenic order, naturally-occurring in the gut, route (C) should be envisaged. Interestingly, these archaea are only able to perform methanogenesis using methyl compounds (see Fig. 2), because the two other pathways are absent (CO2 reduction with H2 and aceticlastic pathway): this would increase the efficiency of TMA conversion.

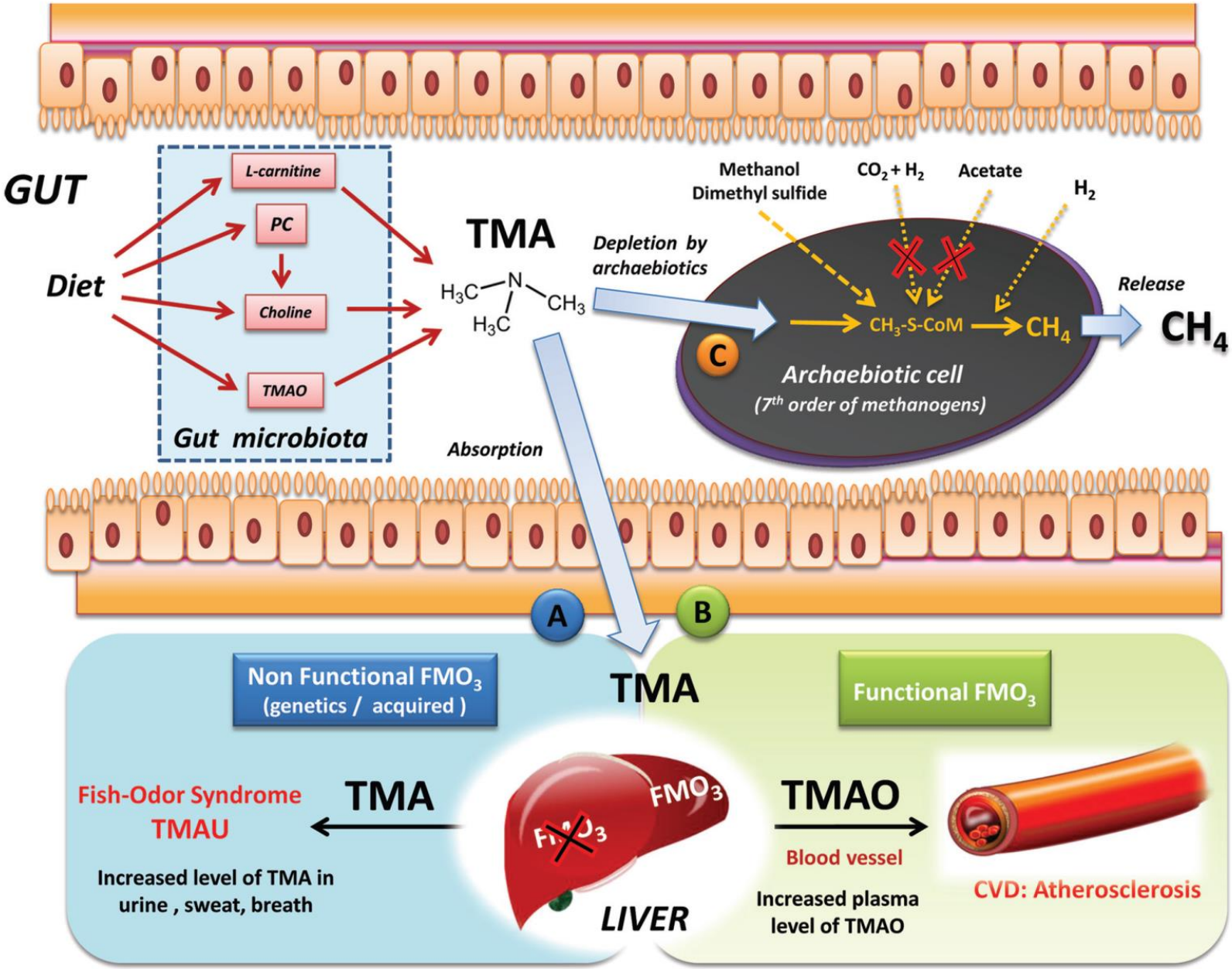

Brugère *et al.*, 2014

Methane from coal

Methane from coal

Coal seams produce natural gas (methane) through the activity of microbial food chains or the methanogen *Methermicoccus* discovered by Mayumi *et al.*

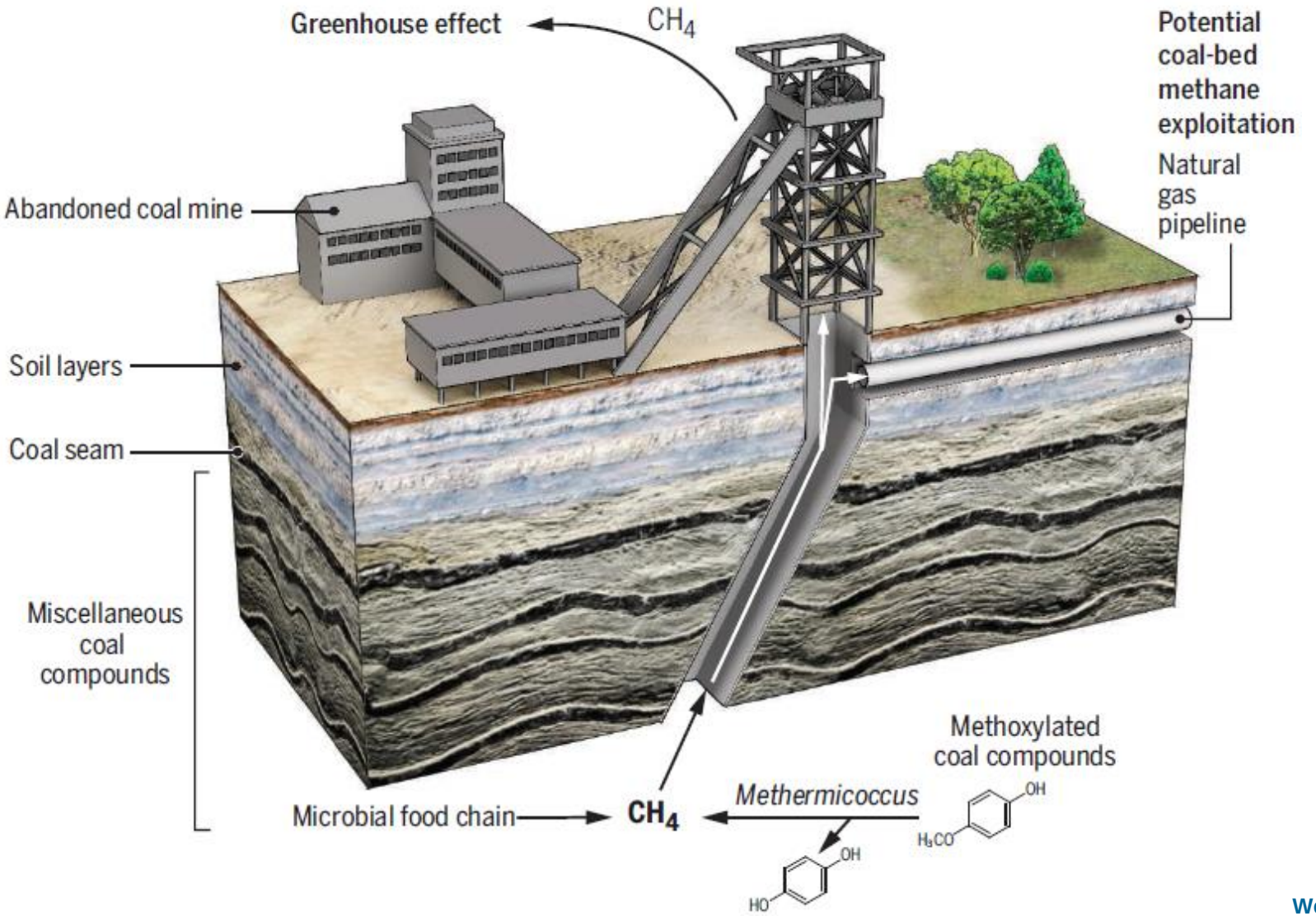

Methane from coal

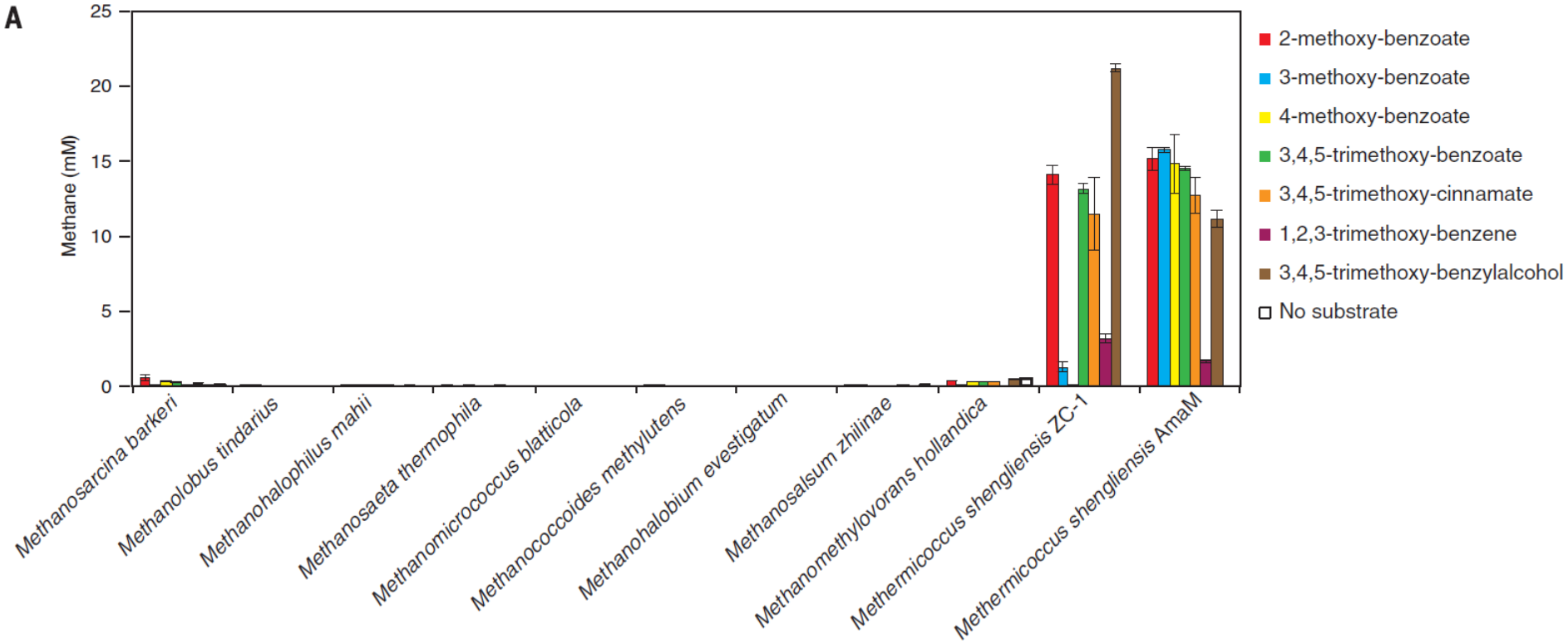

Mayumi *et al.*, 2016

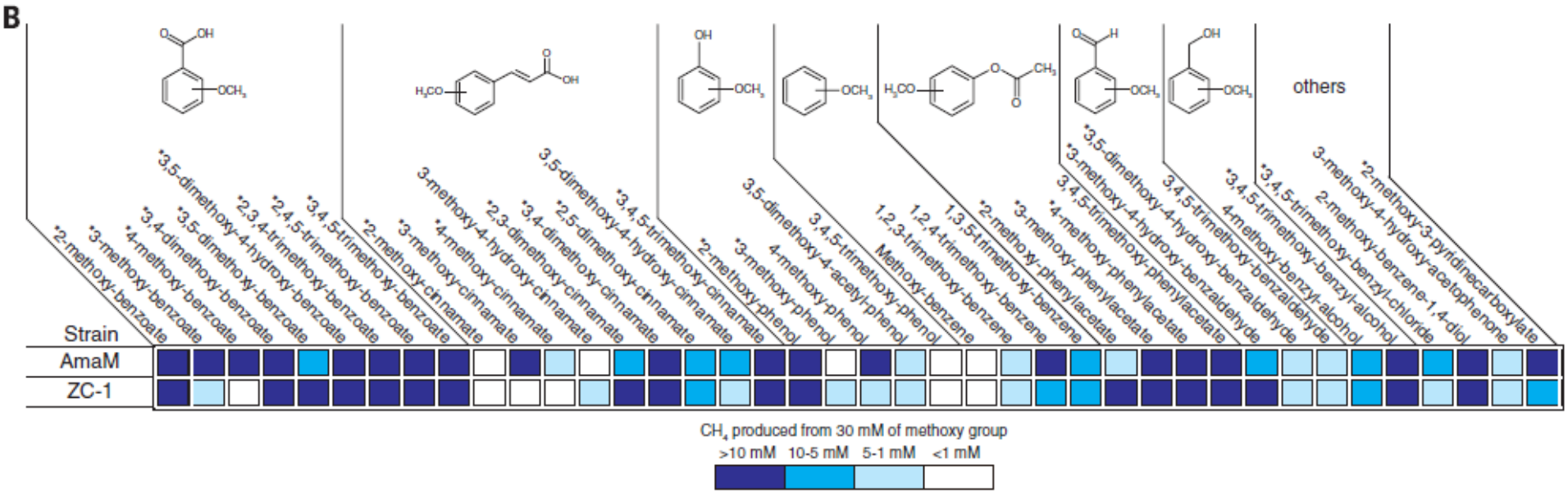

Methoxydotrophic methanogenesis from various MACs. (A) Methanogenesis from seven types of MACs by 10 type strains and one isolate belonging to the order Methanosarcinales. Each MAC was supplied with methoxy groups to a final concentration of 30 mM. Methane produced was measured after incubation for 9 months. Data are means of three individual incubations; error bars represent SD of these triplicates. (B) Substrate ranges of Methermicoccus shengliensis strains AmaM and ZC-1 for 40 types of MACs; an asterisk designates MACs analyzed for the media with coal samples. For each substrate, the average amount of methane produced (n = 3) is expressed by one of four ranges. Detailed methane production data are shown in table S1.

Mayumi *et al.*, 2016

Methane from coal

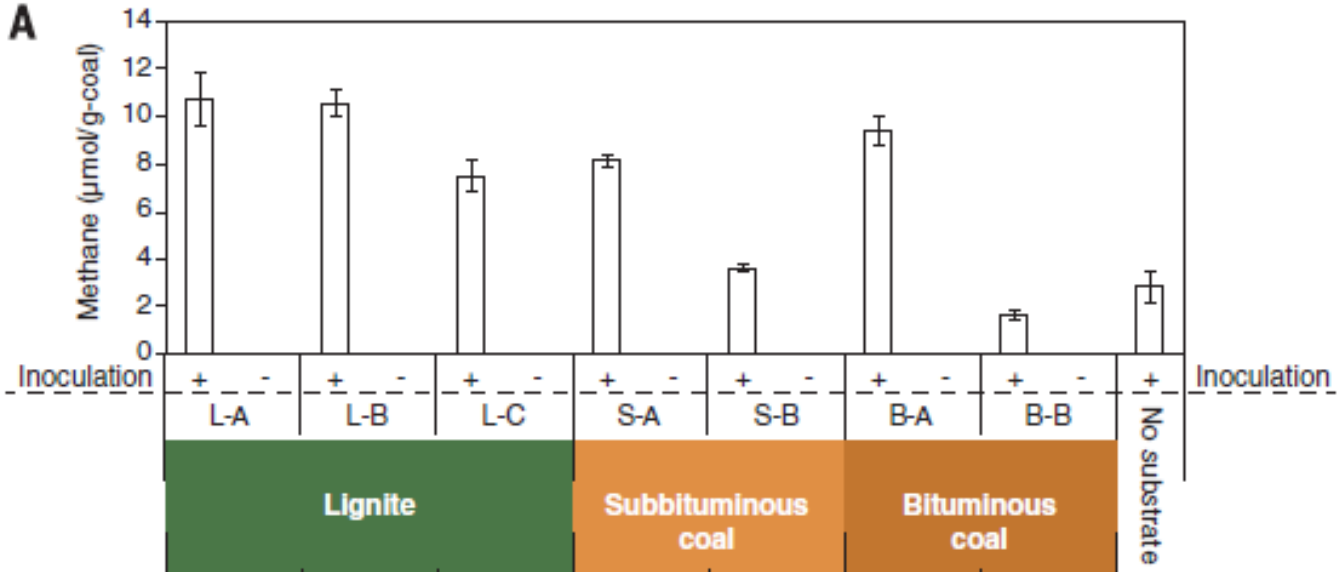

B

Substrates (µmol/g-coal)	L-A	L-B	L-C	S-A	S-B	B-A	B-B
3-methoxy-benzoate	0.02	0.08	0.12	0.14	0.09	0.07	ND
4-methoxy-benzoate	0.02	0.16	0.22	0.29	0.07	0.02	ND
3,4-dimethoxy-benzoate	ND	0.01	0.03	TR	ND	ND	ND
3,5-dimethoxy-benzoate	ND	TR	ND	TR	ND	ND	ND
Methanol	0.40	2.01	1.60	ND	ND	ND	ND
Methylamine	0.14	0.13	0.09	0.12	ND	ND	ND
Dimethylamine	ND	0.12	0.10	ND	ND	ND	ND
Trimethylamine	ND	ND	ND	ND	ND	ND	ND
Total	0.58	2.51	2.16	0.55	0.16	0.09	ND

Fig. 2. Methanogenesis from coal samples by *Methermicoccus shengliensis* AmaM. (**A**) Methane production in a medium with lignite, subbituminous coal, or bituminous coal. Information for each coal sample is shown in fig. S2. A small amount of methane in the media without substrate was detected as a result of carryover from methanol-grown preculture. Data are means of three individual incubations; error bars represent SD of these triplicates. +, inoculated; –, not inoculated. (**B**) MACs, methanol, and methylamines detected in the media with coal samples before inoculation of *M. shengliensis* AmaM. The GC-MS analyses were performed in duplicate; average concentrations are shown. ND, not detected; TR, detected but below the range of concentration for which the calibration curve could be applied.

Mayumi *et al.*, 2016

Methane from coal

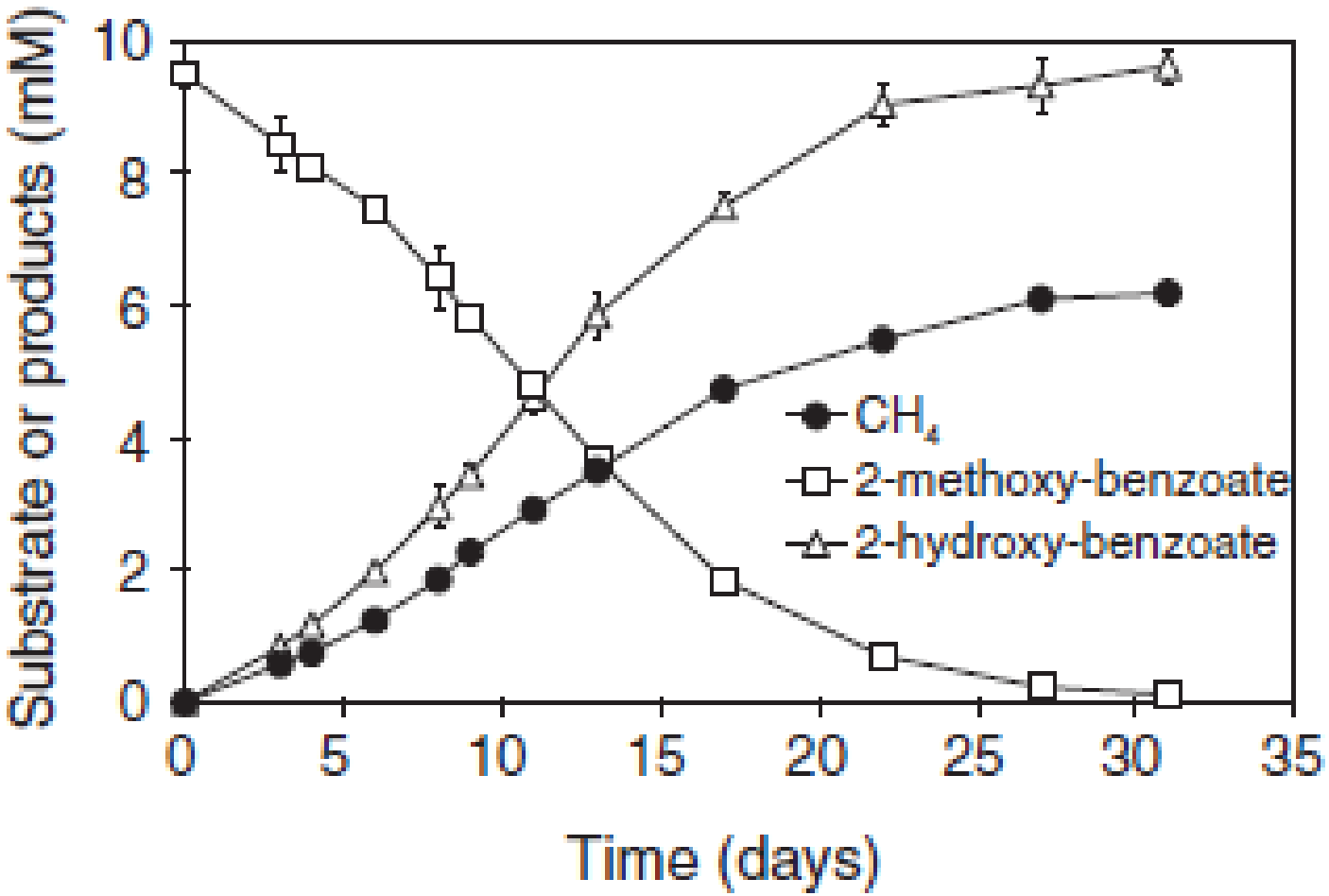

Fig. 3. Methanogenesis from 2-methoxy-benzoate by *Methermicoccus shengliensis* AmaM. All symbols represent means of three individual incubations; error bars represent SD of these triplicates.

Mayumi *et al.*, 2016

Methane from coal

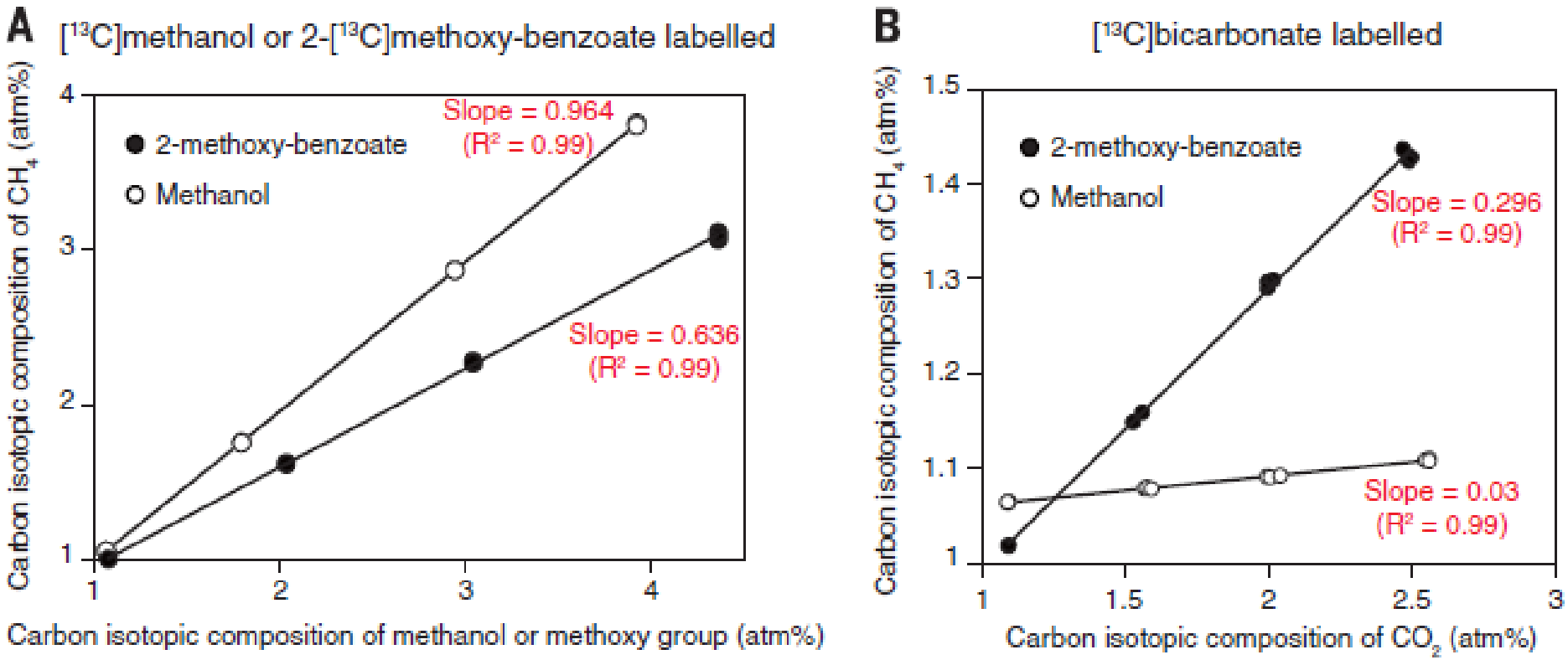

Fig. 4. Stable isotope tracer experiments to elucidate the mode of metabolism in methoxydotrophic methanogenesis. (**A**) Carbon isotopic relationship between methane produced by *M. shengliensis* AmaM and either methanol or the methoxy group of 2-methoxy-benzoate added to the media. The slopes of the regression lines show the efficiency of carbon incorporation from each substrate into methane. (**B**) Carbon isotopic relationship between methane produced from either methanol or 2-methoxy-benzoate and carbon dioxide. The slopes of the regression lines show the efficiency of carbon incorporation from carbon dioxide into methane. Each symbol represents one of three individual incubations.

Mayumi *et al.*, 2016

Methanogenesis – Thawing permafrost

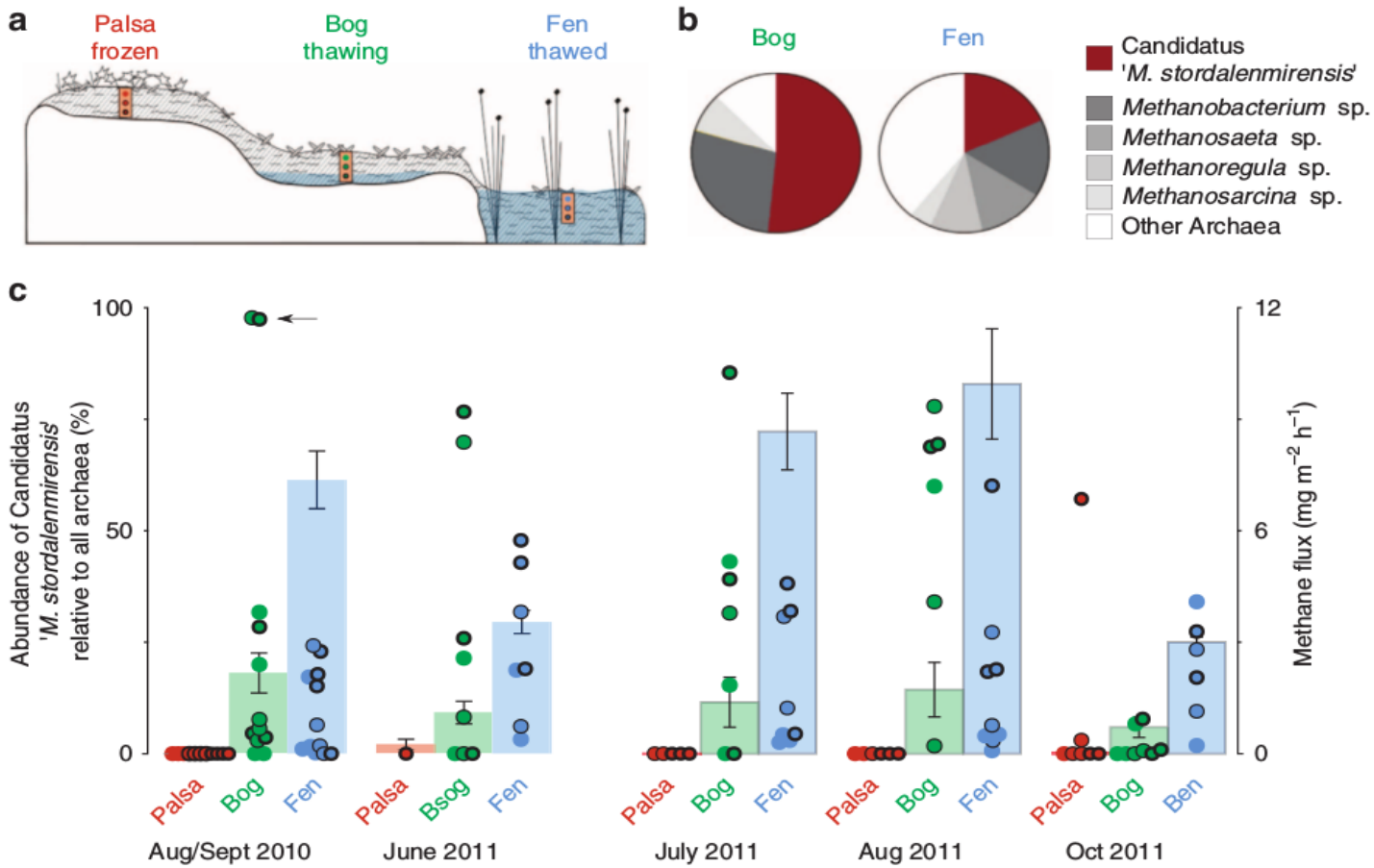

Figure 1 | Seasonal abundance of *Candidatus 'M. stordalenmirensis'* along a thaw gradient. (**a**) Schematic of the sampling sites at Stordalen Mire, Sweden; the white area indicates permafrost, hashed area indicates the active layer and blue area indicates water. Boxes denote coring sites and coloured dots represent the sampling site and depth: intact (brown), thawing (green) and thawed (blue), and thick, thin and no borders representing deep, middle and surface, respectively. (**b**) Relative abundance of dominant methanogens in the bog and fen sites, compared with the total number of archaeal sequences. (**c**) Relative abundance of '*M. stordalenmirensis*' in microbial communities between 2010 and 2011. Coloured dots represent sampling site and depth: intact (brown), thawing (green) and thawed (blue), and thick, thin and no borders representing deep, middle and surface, respectively. Arrow indicates the two samples used for metagenomic sequencing. Histograms indicate associated methane flux for each site averaged across the week before cores were taken (2010 and June 2011 represent a 10 year flux average[7], July–October 2011 measured *in situ*). All error bars represent s.e.

Mondav *et al.* (2014) Nature Communications

Methanogenesis – Thawing permafrost

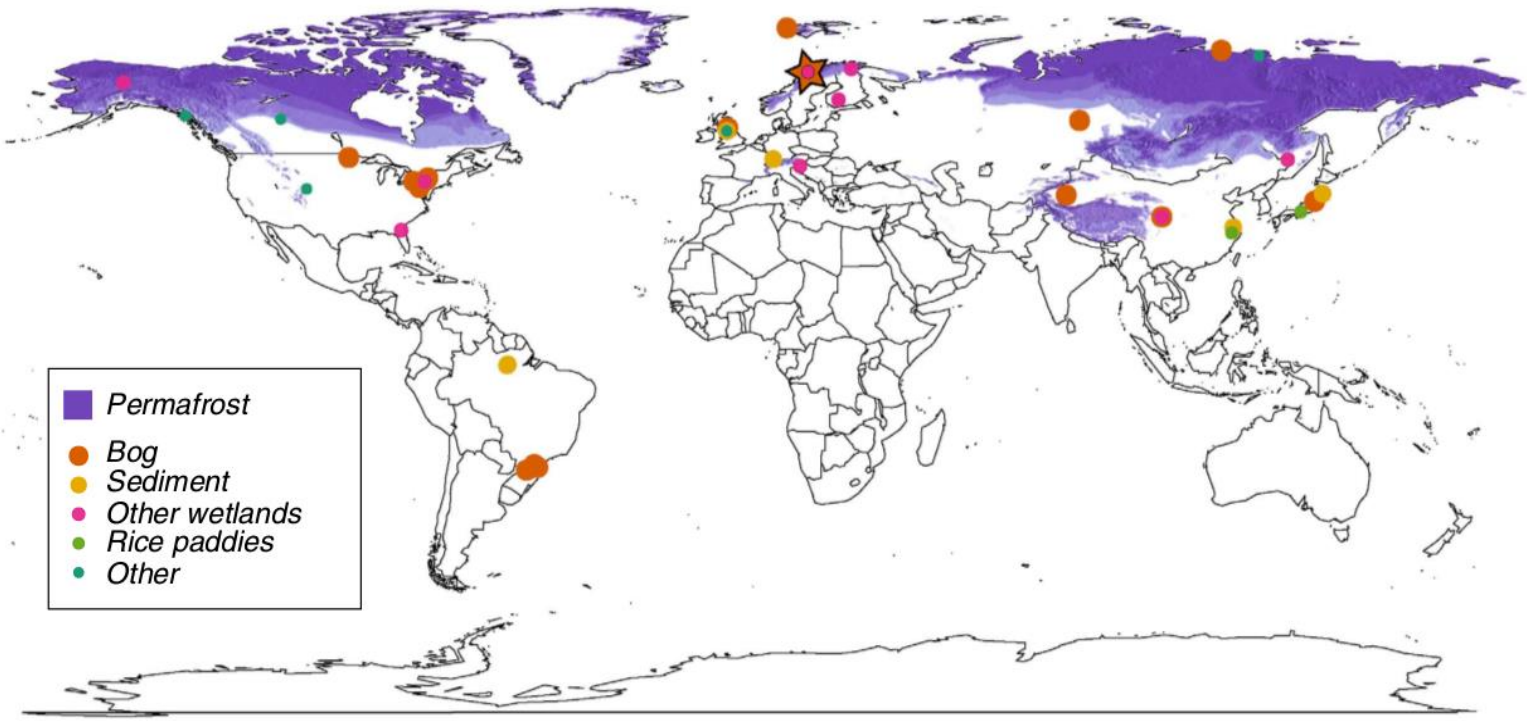

Figure 3 | Global distribution of *Candidatus* '*M. stordalenmirensis*'-like sequences. Each dot represents an instance where one or more published *SSU rRNA* gene sequences with >97% identity to '*M. stordalenmirensis*' was observed. Dots are colour coded according to ecosystem type, and the star indicates Stordalen Mire. Purple shading indicates permafrost distribution and classification. This figure was drawn using the R[58] package 'maps' version 2.2-6 (http://cran.r-project.org/web/packages/maps/) then modified with Gimp (gimp.org) and Inkscape (inkscape.org). Overlayed permafrost distribution was derived from http://svs.gsfc.nasa.gov/goto?3511 (NASA/Goddard Space Flight Center Scientific Visualization Studio, National Snow and Ice Data Center, World Data Center for Glaciology).

Mondav *et al.*, 2014

Methanogenesis – psychrophilic strains

Table 1. Summary of currently known psychrophilic strains and their main temperature and pH features.

Strain	Temp. [°C]			pH			Ref.
	min.	opt	max	min.	opt.	max.	
Methanospirillum psychrodurum	4	25	32	6.5	7	8	[92]
Methanosarcina baltica	3	21	28	6.3	7.2	7.5	[32]
Methanosarcina lacustris	1	25	35	4.5	7	8.5	[93]
Methanolobus psychrophilus	0	18	25	6	7–7.2	8	[94]
Methanogenium marinum	5	25	25	5.5	6–6.6	7.7	[95]
Methanogenium frigidum	0	15	17	6.3	7.5–7.9	8	[33]
Methanohalobium evestigatum	50	n.a. [1]	n.a.	n.a.	7.4	n.a.	[96]
Methanogenium cariaci	15	20–25	35	6	6.8–7.2	7.5	[97]
Methanogenium boonei	5	19.4	25.6	6.4	n.a.	7.8	[98]
Methanoculleus marisnigri	15	20–25	48	6	6.2–6.6	7.6	[99]
Methanoculleus chikugoensis	15	25	40	6.7	6.7–7.2	8	[100]
Methanococcoides alaskense	2.3	23.6	28.4	6.3	n.a.	7.5	[101]
Methanococcoides burtonii	1.7	23.4	29.5	6.8	n.a.	8.2	[102]
Methanospirillum stamsii	5	20–30	37	6.0	7.0–7.5	10	[31]
Methanosarcina soligelidi	0	28	54	4.8	7.8	9.9	[34]
Candidatus "Methanoflorens stordalenmirensis"	n.a.	n.a.	n.a.	n.a.	n.a.	n.a.	[36]

[1] not available.

Taubner et al., 2015

Methanogenesis – growth rate

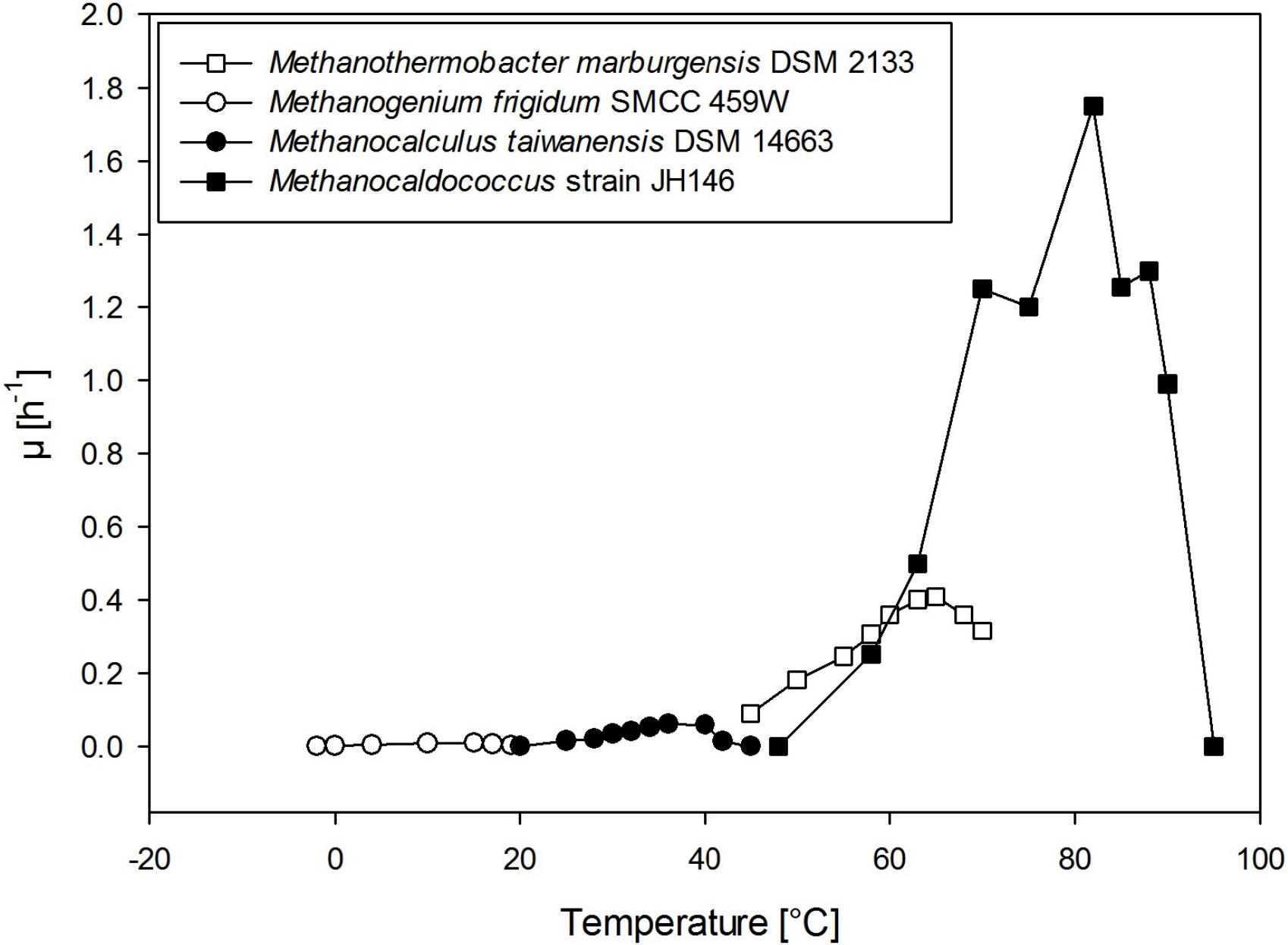

A plot of specific growth rates (μ) of four methanogenic strains

Taubner et al., 2015

Methanogenesis – 4 pathways

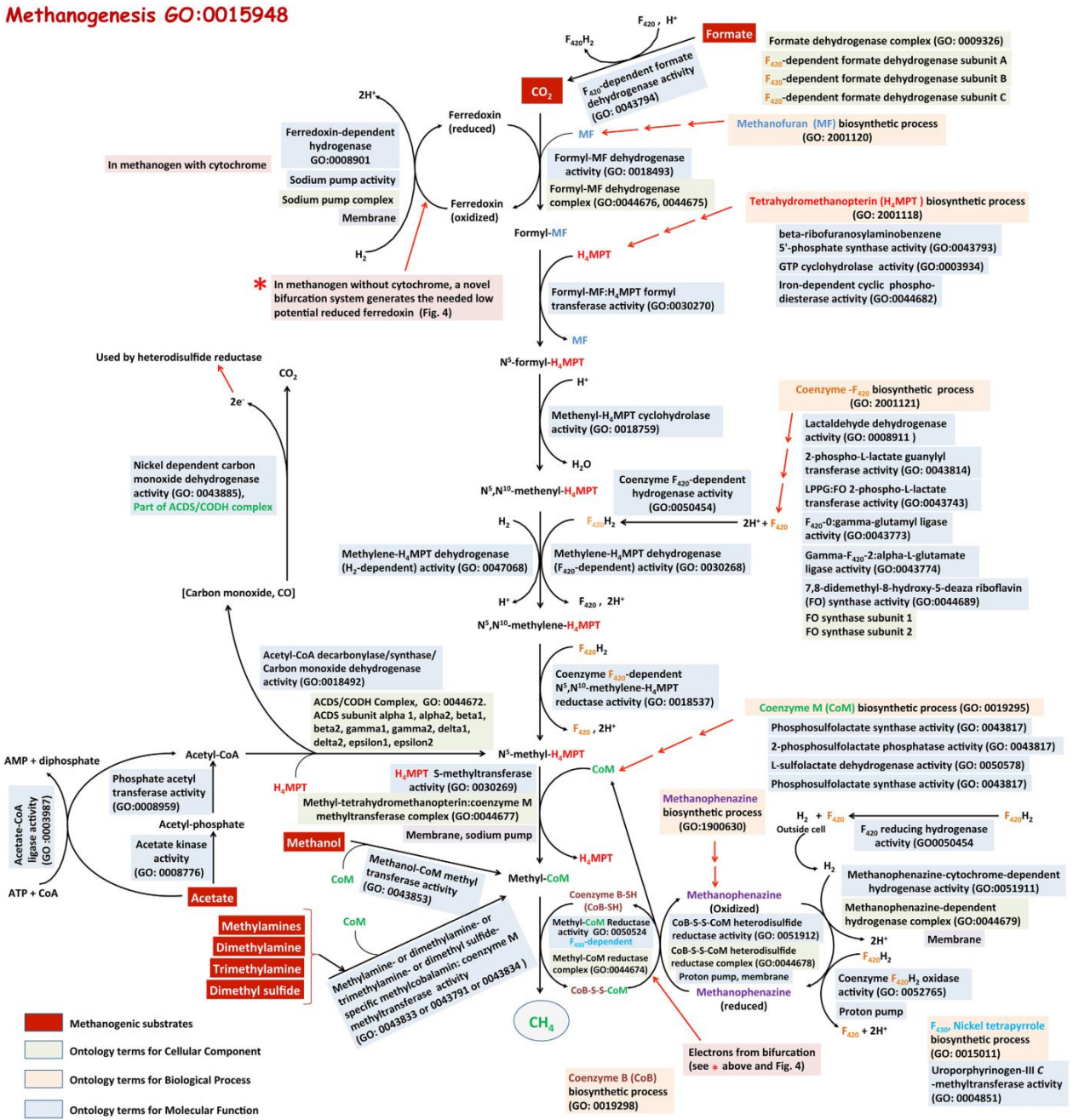

Purwatini et al., 2014

Methanogenesis – 4 pathways

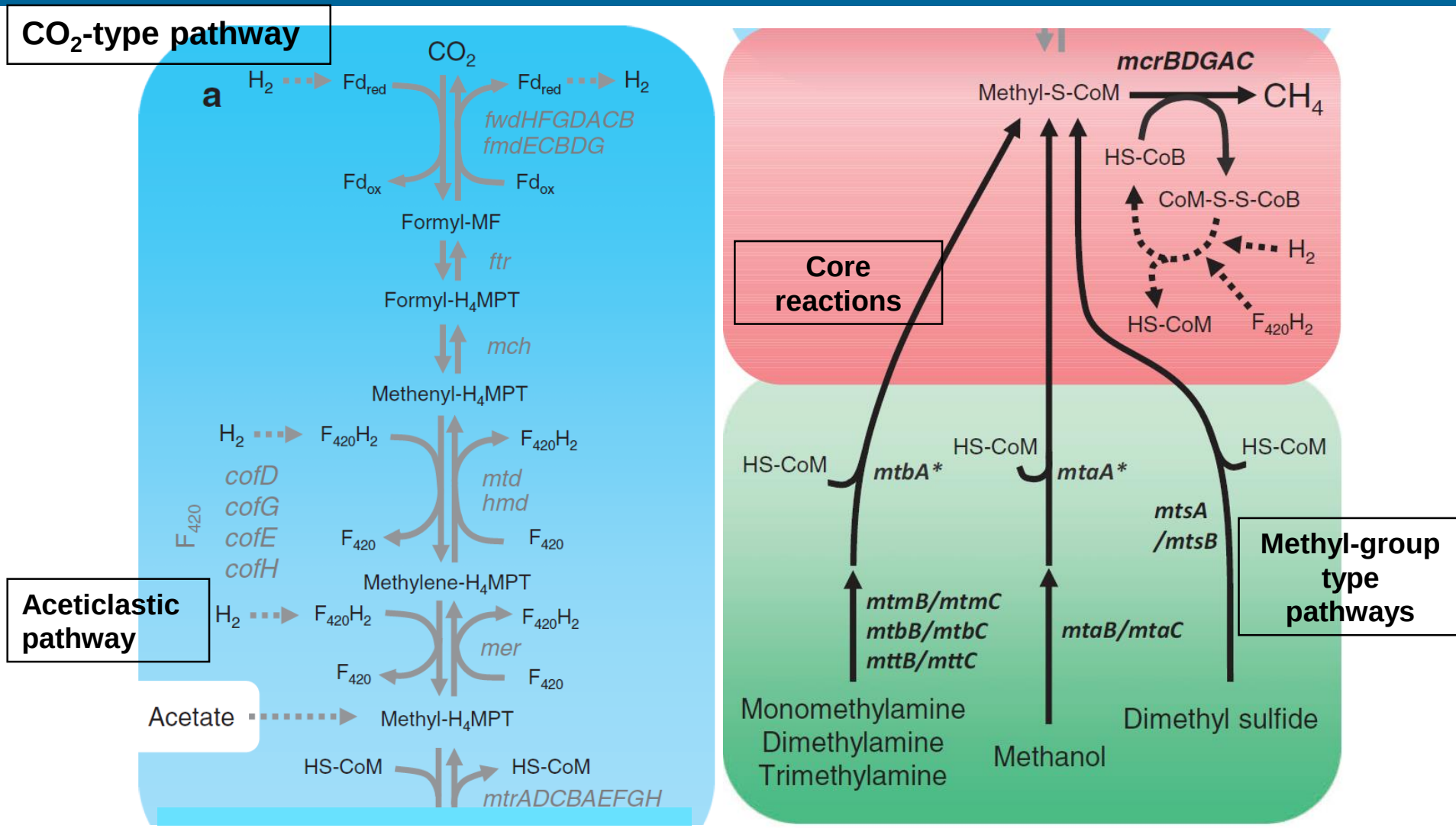

Thermodynamically, two reactions are exergonic and, hence, involved in energy conservation:

1)The methyl transfer from H_4MPT to CoM by methyl-tetrahydromethanopterin:CoM methyltransferase (Mtr)

2)The reduction of the CoM-S-S-CoB heterodisulfide by heterodisulfide reductase (Hdr)

Thauer et al., 2008; Borrel et al., 2013

Methanogenesis – Gibbs free energy

Reaction	$\Delta G^{o\prime}$ [a] (kJ/mol CH_4)	Organisms
I. CO_2-type		
$4\ H_2 + CO_2 \rightarrow CH_4 + 2\ H_2O$	−135	Most methanogens
$4\ HCOOH \rightarrow CH_4 + 3\ CO_2 + 2\ H_2O$	−130	Many hydrogenotrophic methanogens
$CO_2 + 4$ isopropanol $\rightarrow CH_4 + 4$ acetone $+ 2\ H_2O$	−37	Some hydrogenotrophic methanogens
$4\ CO + 2H_2O \rightarrow CH_4 + 3\ CO_2$	−196	*Methanothermobacter* and *Methanosarcina*
II. Methylated C1 compounds		
$4\ CH_3OH \rightarrow 3\ CH_4 + CO_2 + 2\ H_2O$	−105	*Methanosarcina* and other methylotrophic methanogens
$CH_3OH + H_2 \rightarrow CH_4 + H_2O$	−113	*Methanomicrococcus blatticola* and *Methanosphaera*
$2\ (CH_3)_2\text{-}S + 2\ H_2O \rightarrow 3\ CH_4 + CO_2 + 2\ H_2S$	−49	Some methylotrophic methanogens
$4\ CH_3\text{-}NH_2 + 2\ H_2O \rightarrow 3\ CH_4 + CO_2 + 4\ NH_3$	−75	Some methylotrophic methanogens
$2\ (CH_3)_2\text{-}NH + 2\ H_2O \rightarrow 3\ CH_4 + CO_2 + 2\ NH_3$	−73	Some methylotrophic methanogens
$4\ (CH_3)_3\text{-}N + 6\ H_2O \rightarrow 9\ CH_4 + 3\ CO_2 + 4\ NH_3$	−74	Some methylotrophic methanogens
$4\ CH_3NH_3Cl + 2\ H_2O \rightarrow 3\ CH_4 + CO_2 + 4\ NH_4Cl$	−74	Some methylotrophic methanogens
III. Acetate		
$CH_3COOH \rightarrow CH_4 + CO_2$	−33	*Methanosarcina* and *Methanosaeta*

SOURCE: Modified from Hedderich and Whitman[1] and Zinder.[43]

[a]The standard changes in free energies were calculated from the free energy of formation of the most abundant ionic species at pH 7. For instance, CO_2 is $HCO_3^- + H^+$ and HCOOH is $HCOO^- + H^+$.

Liu &Whitman 2008

Carboxydotrophic methanogens

Methanogenic archaea capable of metabolizing CO

Species	Native physiology	Experimental procedure used	Inhibitory levels[A]	Products from CO	Generation time on CO (h)	Reference
Mesophilic						
Methanobrevibacter arboriphilicus	Hydrogenotrophic	Enzyme assay	N.D.	N.D.	N.D.	Hammel et al., 1984
Methanosarcina acetivorans C2A	Aceticlastic	Cultivation/enzyme assay	>150 kPa	Methane, acetate, formate	~20	Rother and Metcalf, 2004; Oelgeschläger and Rother, 2009
Methanosarcina barkeri	Aceticlastic	Cultivation/enzyme assay	>100 kPa	Hydrogen, Methane	~65	O'Brien et al., 1984; Bott et al., 1986
Methanobacterium formicicum	Hydrogenotrophic	Cultivation	N.D.	N.D.	No growth	Kluyver and Schnellen, 1947
Methanosaeta concilii	Aceticlastic	Enzyme assay	N.D.	N.D.	No growth	Jetten et al., 1989
Thermophilic						
Methanothermobacter thermoautotrophicus	Hydrogenotrophic	Cultivation/enzyme assay	50 kPa	Methane, hydrogen	~200	Daniels et al., 1977; Wasserfallen et al., 2000
Methanosarcina thermophila	Aceticlastic	Cultivation	>2 kPa	Hydrogen, Methane	N.D.	Zinder and Anguish, 1992
Methanothrix sp. *Strain CALS-1*	Aceticlastic	Cultivation	<2 kPa	Methane	No growth	Zinder and Anguish, 1992
Archaeoglobus fulgidus[B]	Sulfate reducer	Cultivation	>136 kPa	Acetate, formate	~10	Henstra et al., 2007a

Not determined parameters are marked N.D.

[A]*Forward arrows (>) indicate inhibitory levels have not been reached; numbers displayed are the maximal level tested. Reverse arrows (<) indicate the tested level was the highest tested and the inhibitory concentration lies below this level.*

[B]*Archaeoglobus fulgidus is not capable of generating methane, but is displayed here due to its capacity to generate acetate and formate from CO, like M. acetivorans.*

Diender et al. , 2015

Carboxydotrophic methanogens

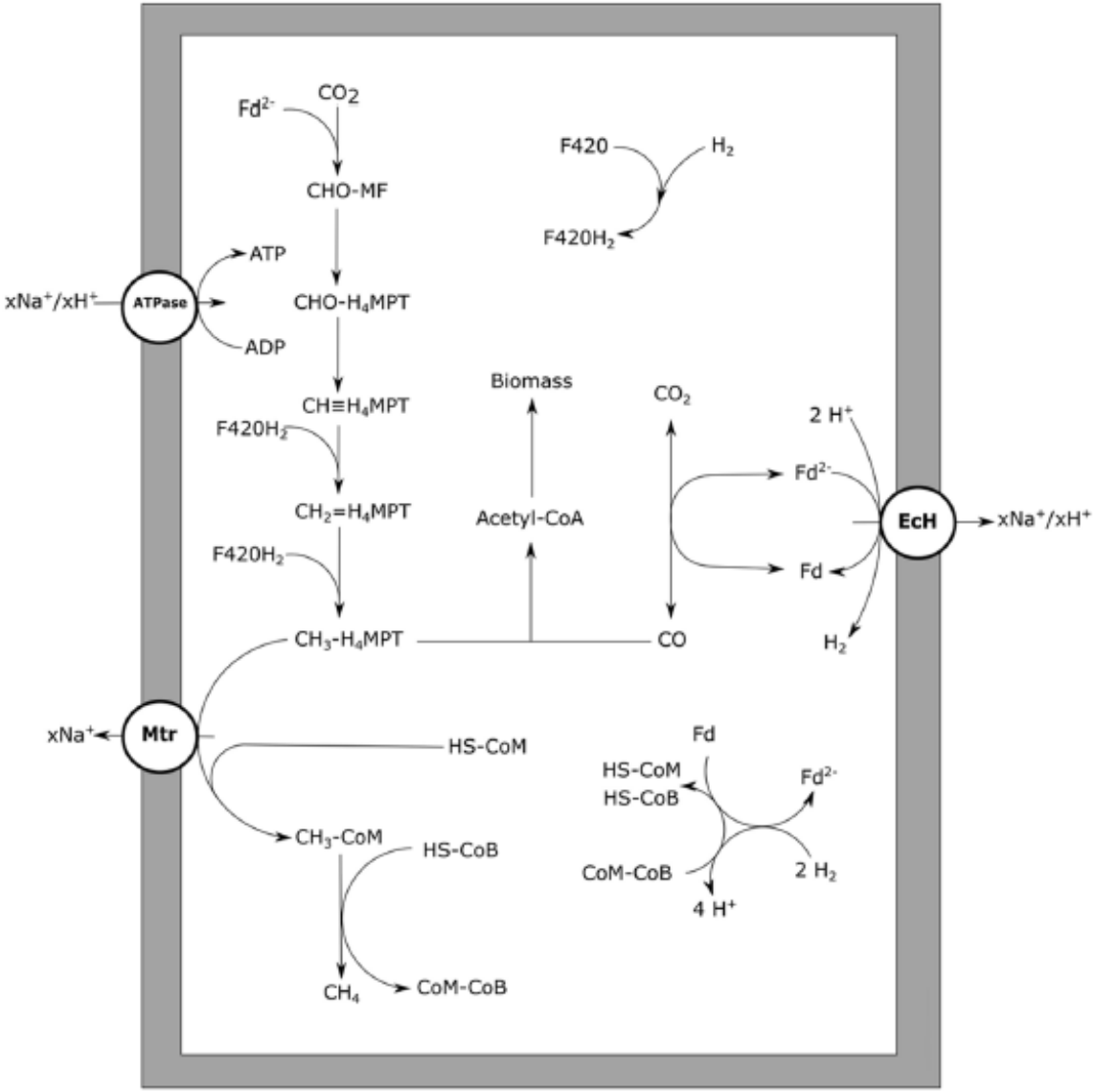

FIGURE 5 | Carbon monoxide metabolism of hydrogenotrophic methanogens. CO driven methanogenesis with hydrogen as an intermediate is displayed. xH^+ or xNa^+ indicate translocation of an undefined number of protons or sodium ions, respectively. Reactions are not displayed stoichiometrically. EcH, energy converting hydrogenase; Mtr, methyl-H_4MPT:HS-CoM methyltransferase; ATPase, ATP synthase; Fd, ferredoxin; MF, methanofuran; H_4MPT, tetrahydromethanopterin; HS-CoM, coenzyme M; HS-CoB, coenzyme B.

Diender et al. , 2015

Carboxydotrophic methanogens

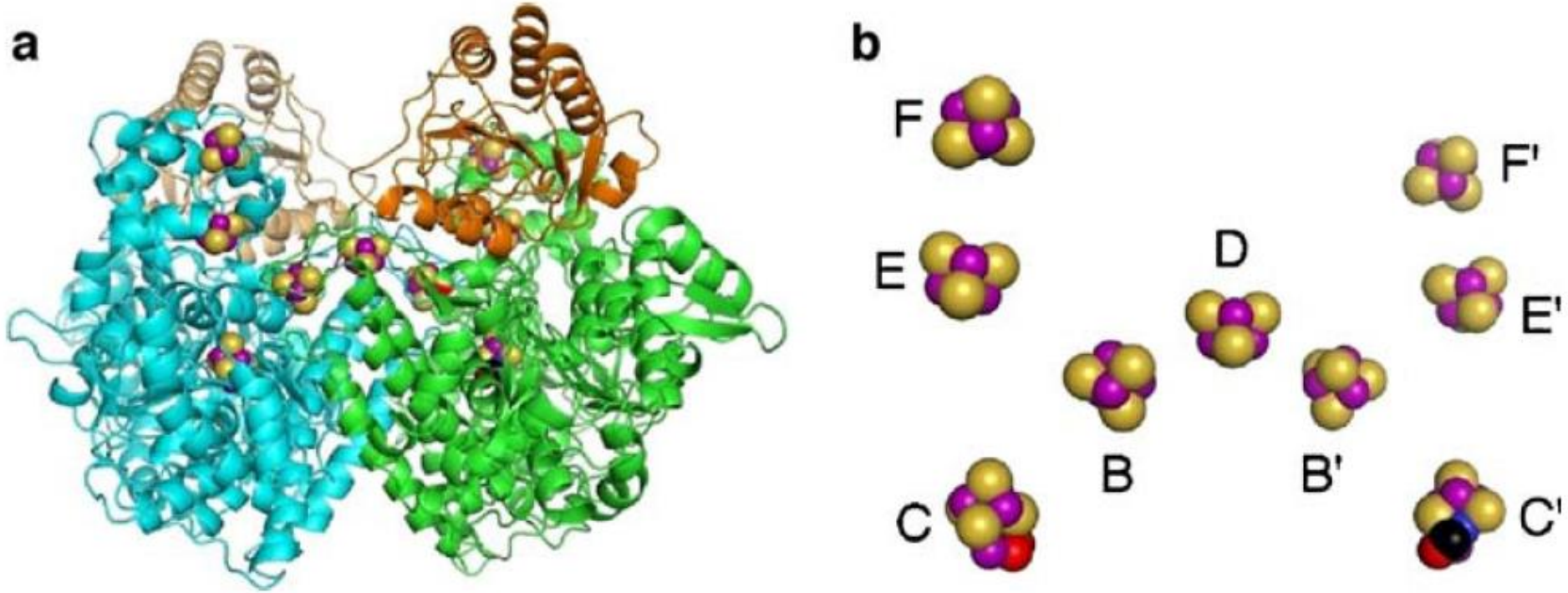

Fig. 6 The *Methanosarcina barkeri* $\alpha_2\varepsilon_2$ CdhAE component.**a** Side view shown as *ribbons* with the α-subunits colored in *cyan* and *green* and the ε-subunits in *tan* and *orange*. Metal cluster atoms are shown as *spheres*, with iron atoms in *purple*, nickel atoms in *blue*, and the remaining atoms in *CPK*. **b** Side view of the metal clusters. By permission (Gong et al. 2008)

Ferry, 2010

Carboxydotrophic methanogens

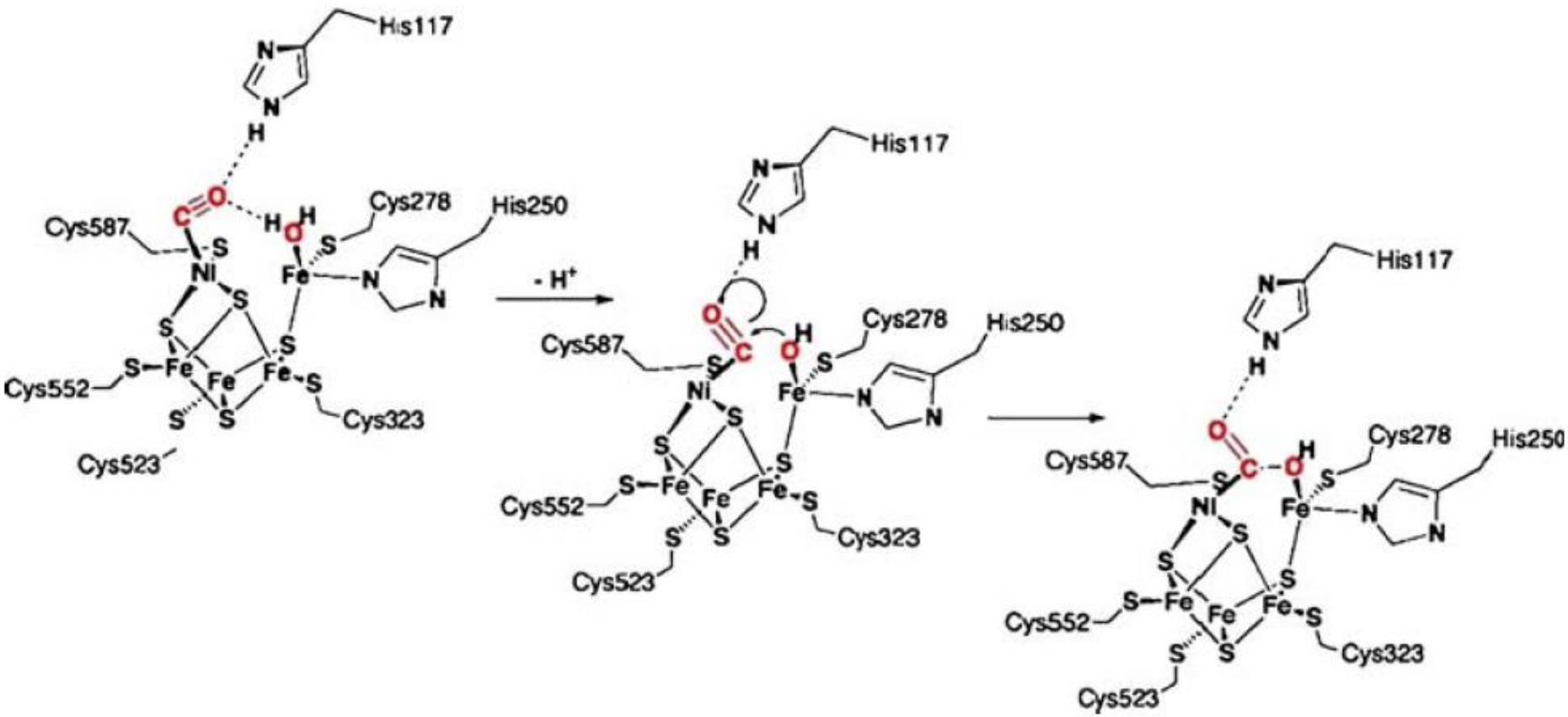

Fig. 7 Proposed coupling of the CO and H_2O species in the C cluster of the *Methanosarcina barkeri* CdhAE component

Ferry, 2010

Carboxydotrophic methanogens

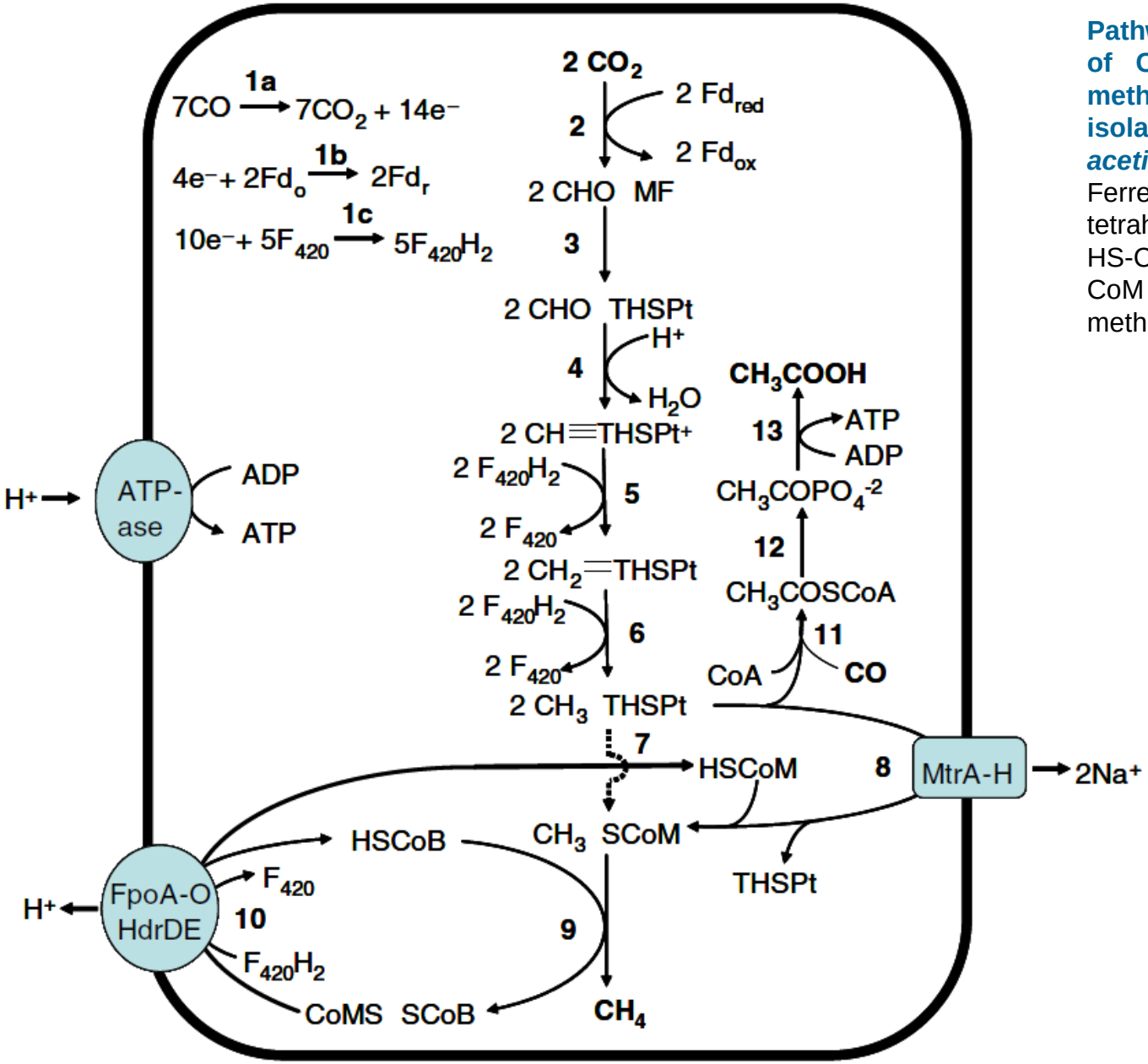

Pathway for conversion of CO to acetate and methane by the marine isolate *Methanosarcina acetivorans*. Fd Ferredoxin, THSPt tetrahydrosarcinapterin, HS-CoB coenzyme B, HS CoM coenzyme M, MF methanofuran

Ferry, 2010

Methanogens with & without cytochromes

Reaction number	Equation	$\Delta G^{o\prime}$ (kJ per mole)
1	$4\,H_2 + CO_2 \rightarrow CH_4 + 2\,H_2O$	−131
2	$CO_2 + MFR + Fd_{red}^{2-} + 2\,H^+ \rightleftharpoons CHO\text{-}MFR + Fd_{ox} + H_2O$	0
3	$CHO\text{-}MFR + H_4MPT \rightleftharpoons CHO\text{-}H_4MPT + MFR$	−5
4	$CHO\text{-}H_4MPT + H^+ \rightleftharpoons CH{\equiv}H_4MPT^+ + H_2O$	−5
5	$CH{\equiv}H_4MPT^+ + F_{420}H_2 \rightleftharpoons CH_2{=}H_4MPT + F_{420} + H^+$	+6
6	$CH_2{=}H_4MPT + F_{420}H_2 \rightleftharpoons CH_3\text{-}H_4MPT + F_{420}$	−6
7	$CH_3\text{-}H_4MPT + HS\text{-}CoM \rightleftharpoons CH_3\text{-}S\text{-}CoM + H_4MPT$	−30 (coupled with 2 Na^+ translocations)
8	$CH_3\text{-}S\text{-}CoM + HS\text{-}CoB \rightleftharpoons CH_4 + CoM\text{-}S\text{-}S\text{-}CoB$	−30
9	$H_2 + Fd_{ox} \rightleftharpoons Fd_{red}^{2-} + 2\,H^+$	+16 (coupled to 2 H^+, or possibly 2 Na^+, translocations)
10	$H_2 + F_{420} \rightleftharpoons F_{420}H_2$ (x 2)	−11
11	$H_2 + MP \rightleftharpoons MPH_2$	−50 (coupled with 2 H^+ translocations)
12	$MPH_2 + CoM\text{-}S\text{-}S\text{-}CoB \rightleftharpoons MP + HS\text{-}CoM + HS\text{-}CoB$	−5 (coupled with 2 H^+ translocations)
13	$ADP + P_i \rightleftharpoons ATP + H_2O$	−32 (coupled to 4 H^+, or possibly 4 Na^+, translocations)
14	2 H^+ (outside) + 1 Na^+ (inside) $\rightleftharpoons$ 2 H^+ (inside) + 1 Na^+ (outside)	0
15	$2\,H_2 + CoM\text{-}S\text{-}S\text{-}CoB + Fd_{ox} \rightleftharpoons HS\text{-}CoM + HS\text{-}CoB + Fd_{red}^{2-} + 2\,H^+$	−39
16	$CH_3OH + HS\text{-}CoM \rightleftharpoons CH_3\text{-}S\text{-}CoM + H_2O$	−17.5

F_{420}, coenzyme F_{420}; Fd, ferredoxin; H_4MPT, tetrahydrosarcinapterin; HS-CoB, coenzyme B; HS-CoM, coenzyme M; MFR, methanofuran; MP, methanophenazine.

Thauer *et al.*, 2008

Methanogens with cytochromes

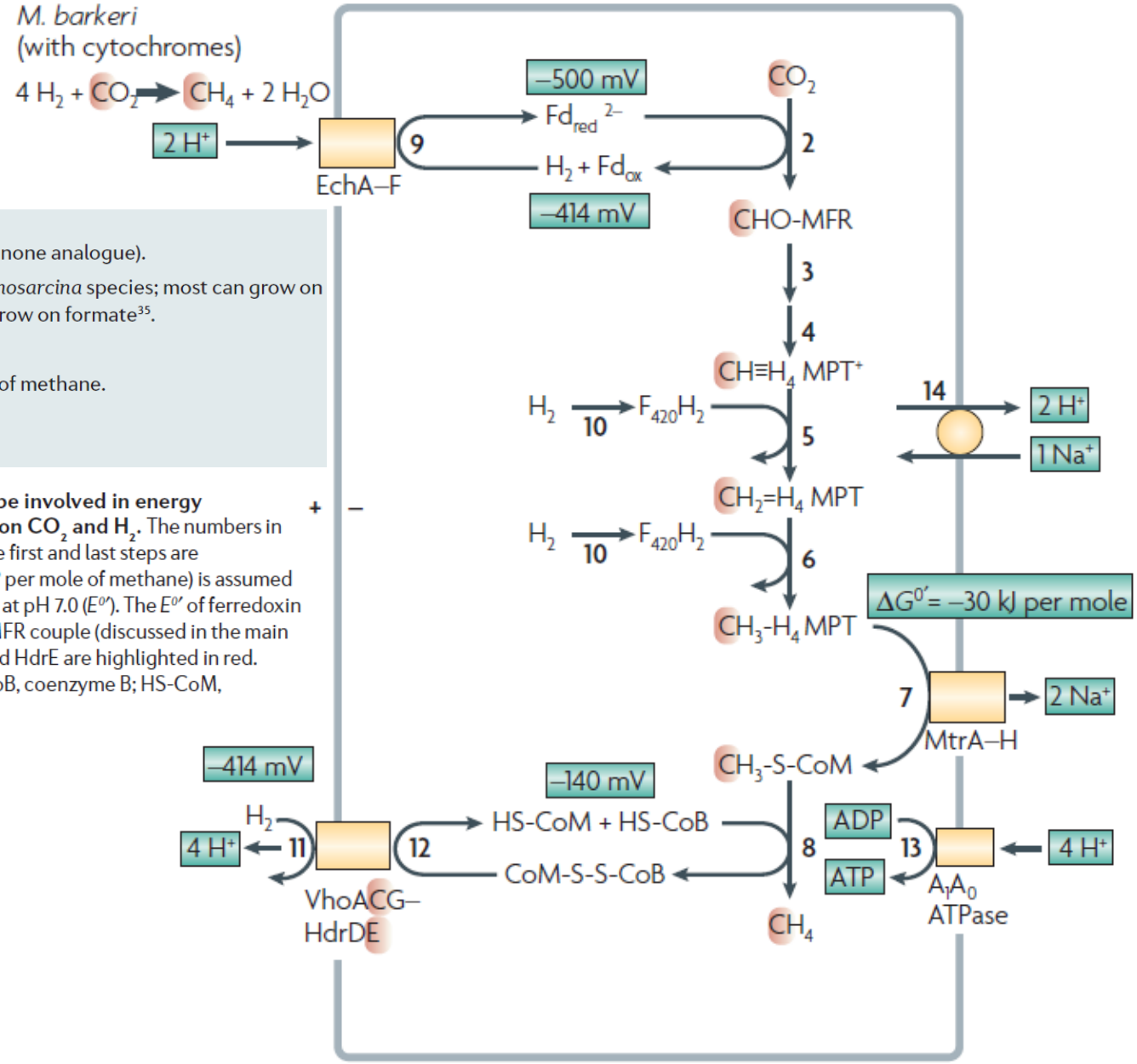

Methanogens with cytochromes

- Contain methanophenazine (a functional menaquinone analogue).
- Growth on H_2 and CO_2 is restricted to some *Methanosarcina* species; most can grow on acetate, methanol and methylamines and cannot grow on formate[35].
- Threshold H_2 partial pressure is generally >10 Pa.
- Growth yields on H_2 and CO_2 of up to 7 g per mole of methane.
- Doubling times are generally >10 hours.
- No hyperthermophilic species.

Figure 2 | **The coupling sites that are proposed to be involved in energy conservation in *Methanosarcina barkeri* growing on CO_2 and H_2.** The numbers in bold correspond to the reaction numbers in BOX 1. The first and last steps are chemiosmotically coupled. The ATP gain (moles of ATP per mole of methane) is assumed to be 1.5. The redox potentials are standard potentials at pH 7.0 ($E^{0\prime}$). The $E^{0\prime}$ of ferredoxin was set at –500 mV, which is the $E^{0\prime}$ of the CO_2/CHO-MFR couple (discussed in the main text). C_1 units and the cytochrome *b* subunits VhoC and HdrE are highlighted in red. Fd, ferredoxin; H_4MPT, tetrahydrosarcinapterin; HS-CoB, coenzyme B; HS-CoM, coenzyme M; MFR, methanofuran.

Thauer *et al.*, 2008

Acetoclastic methanogens

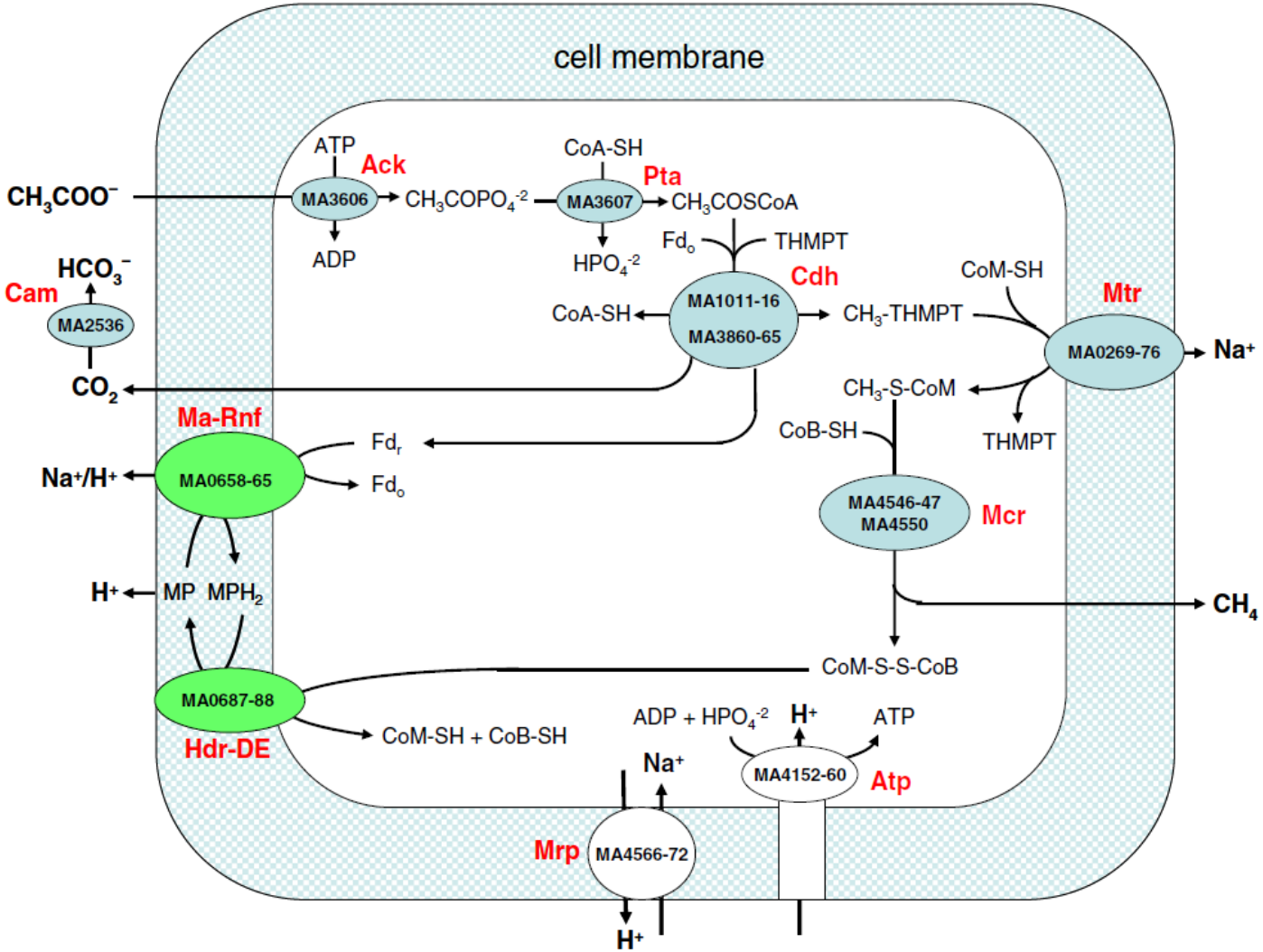

Fig. 5 Pathway for the conversion of acetate to methane by *Methanosarcina acetivorans*. *Ack* Acetate kinase, *Pta* phosphotransacetylase, *CoA-SH* coenzyme A, *THMPT* tetrahydromethanopterin, Fd_r reduced ferredoxin, Fd_o oxidized ferredoxin, *Cdh* CO dehydrogenase/acetyl-CoA synthase, *CoM-SH* coenzyme M, *Mtr* methyl-THMPT: CoM-SH methyltransferase, *CoB-SH* coenzyme B, *Cam* carbonic anhydrase, *Ma-Rnf M. acetivorans* Rnf, *MP* methanophenazine, *Hdr-DE* heterodisulfide reductase, *Mrp* multiple resistance/pH regulation Na^+/H^+ antiporter, *Atp* H^+-transporting ATP synthase. Carbon transfer reactions are catalyzed by the enzymes shown in *blue*. Electron transfer reactions are catalyzed by enzymes shown in *green*. By permission (Li et al. 2006)

Ferry, 2010

Methanogens with cytochromes

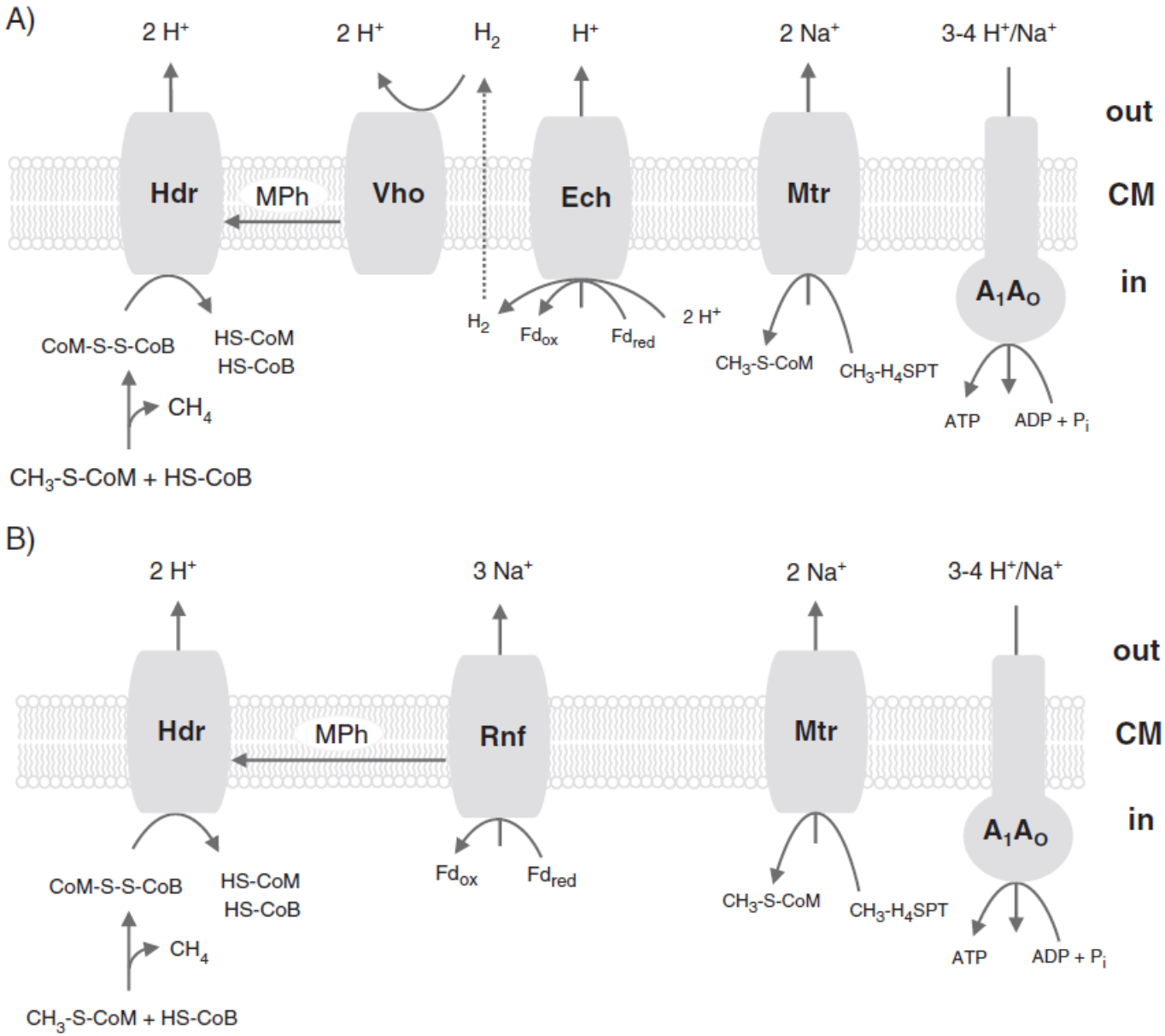

Fig. 4. Process of ion translocation during acetate utilization. (A) *Ms. mazei*, (B) *Ms. acetivorans*. The scheme gives an overview of ion translocation events and does not indicate the mechanism of ion translocation. Vho, Mph-reducing hydrogenase; Ech, Ech hydrogenase; Rnf, Rnf complex; Hdr, heterodisulfide reductase; Mtr, methyl-H_4SPT–coenzyme M methyltransferase; A_1A_O, ATP synthase; CM, cytoplasmic membrane.

Welte & Deppenmeier, 2014

Methanogens with cytochromes

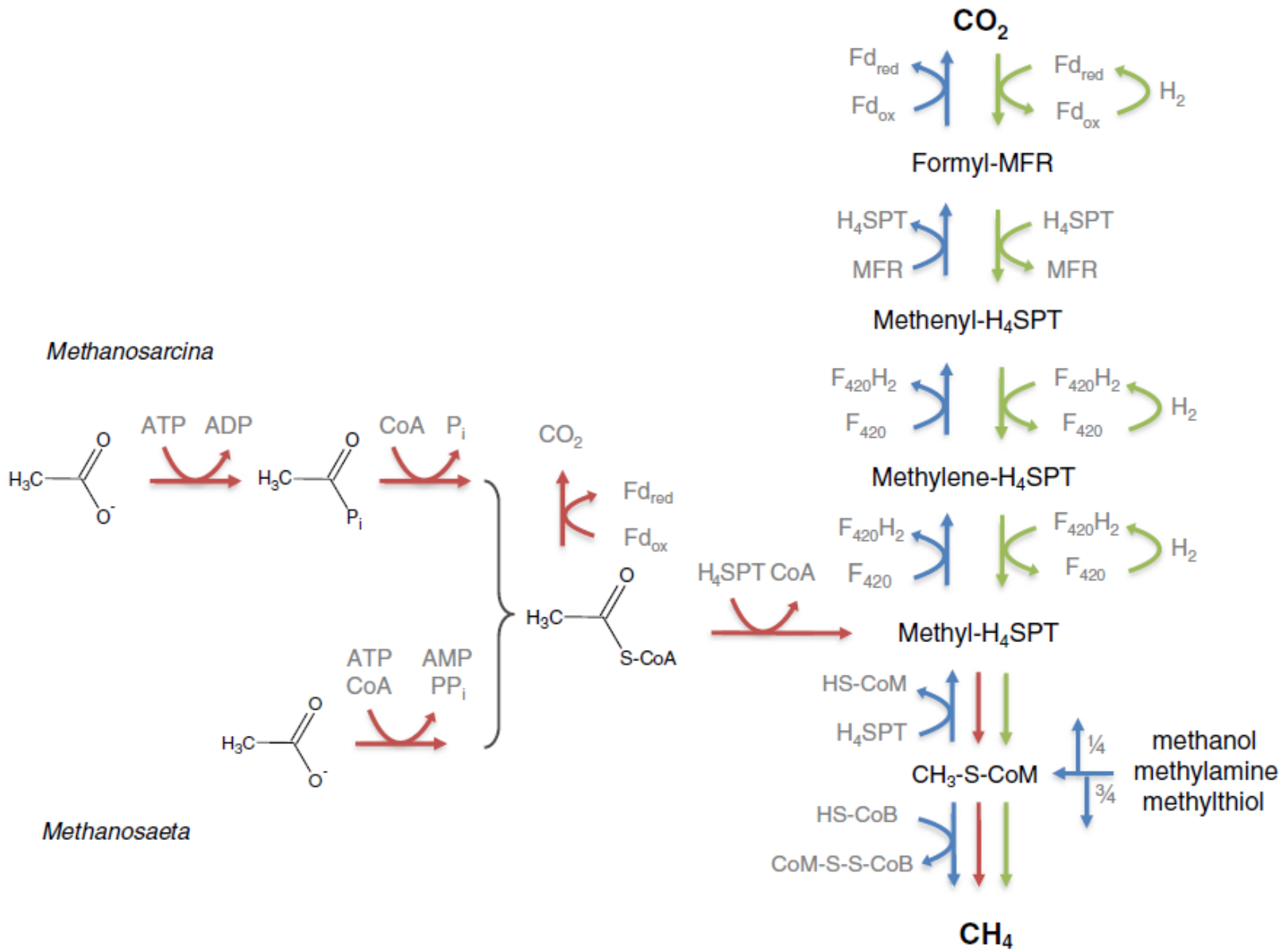

Fig. 2. Pathways of methanogenesis. Carbon fluxes through the three pathways of methanogenesis in *Methanosarcina* and *Methanosaeta* strains. Red arrows indicates aceticlastic methanogenesis with the different acetate activation mechanisms in *Methanosarcina* and *Methanosaeta*. Blue arrows indicate reactions of methylotrophic methanogens. Green arrows indicate the pathway of hydrogenotrophic methanogenesis by a subgroup of *Methanosarcina* strains, e.g. *Ms. mazei*.

Welte & Deppenmeier, 2014

Methanogens with cytochromes

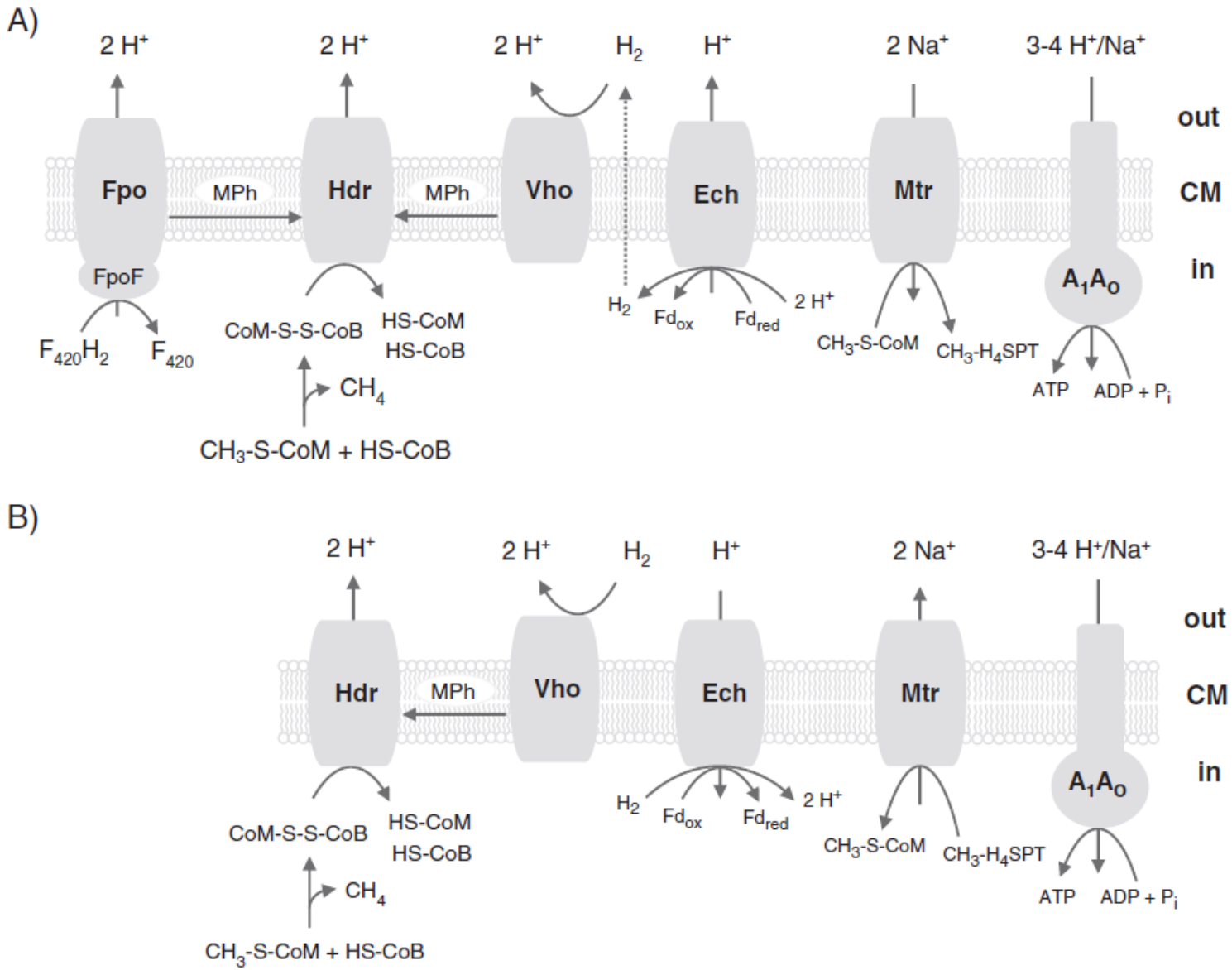

Fig. 3. All ion-translocating enzymes of *Ms. mazei* in action. (A) methylotrophic methanogenesis, (B) hydrogenotrophic methanogenesis. The scheme gives an overview of ion translocation events and does not indicate the mechanism of ion translocation. Vho, Mph-reducing hydrogenase; Ech, Ech hydrogenase; Hdr, heterodisulfide reductase. Fpo, $F_{420}H_2$ dehydrogenase; FpoF, input module of the Fpo complex; Mtr, methyl-H_4SPT–coenzyme M methyltransferase; A_1A_O, ATP synthase; CM, cytoplasmic membrane. Please note that in *Ms. acetivorans* Vho and Ech are replaced by the Na^+-translocating Rnf complex.

Welte & Deppenmeier, 2014

Methanogens with cytochromes

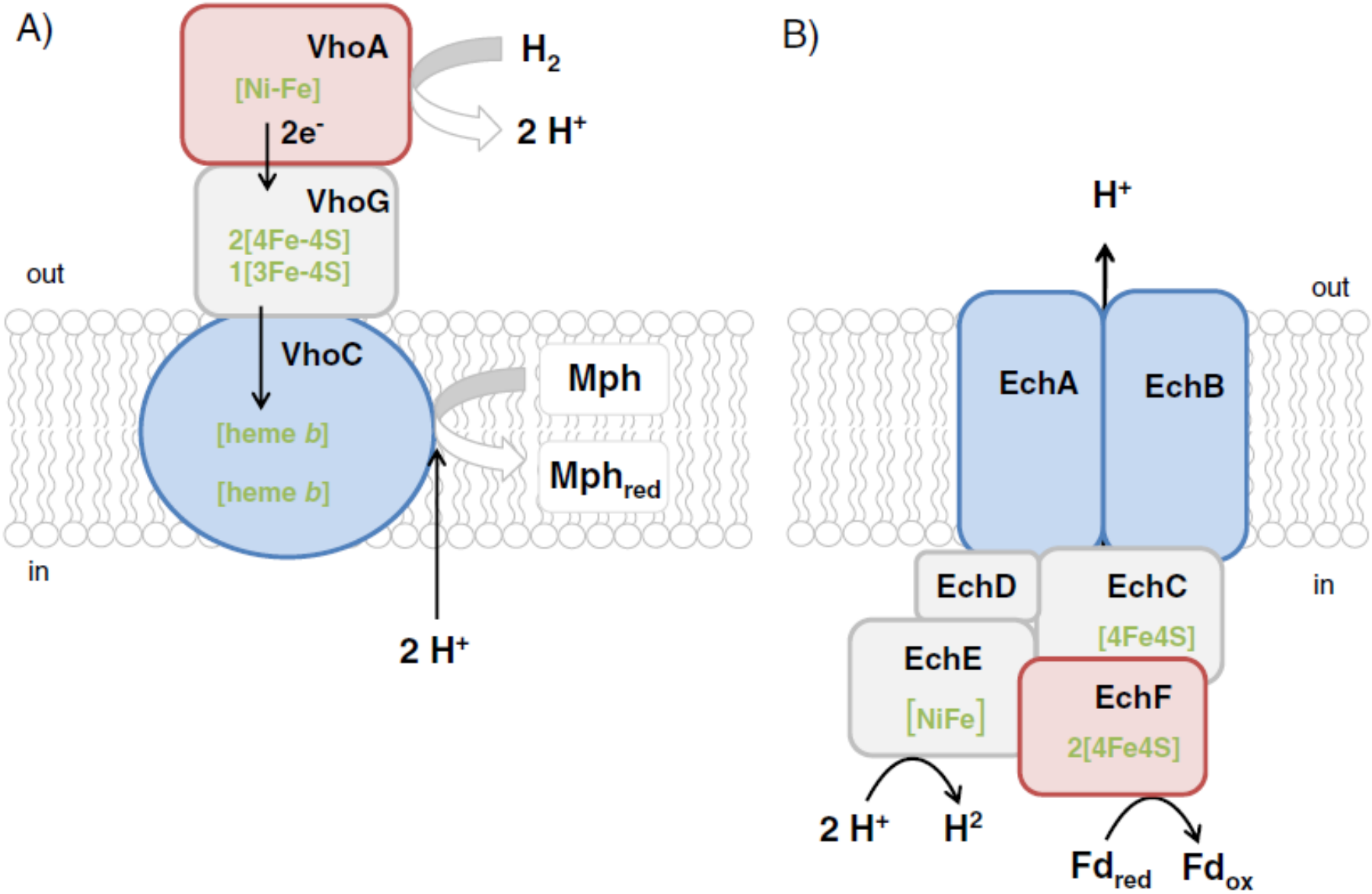

Fig. 5. Structure of hydrogenases. Schematic overview of subunits and prosthetic groups found in the Mph-reducing hydrogenase Vho (A) and Ech hydrogenase (B). Red colour indicates the initial oxidizing subunit, blue colour indicates membrane integral subunits.

Welte & Deppenmeier, 2014

Methanogens with cytochromes

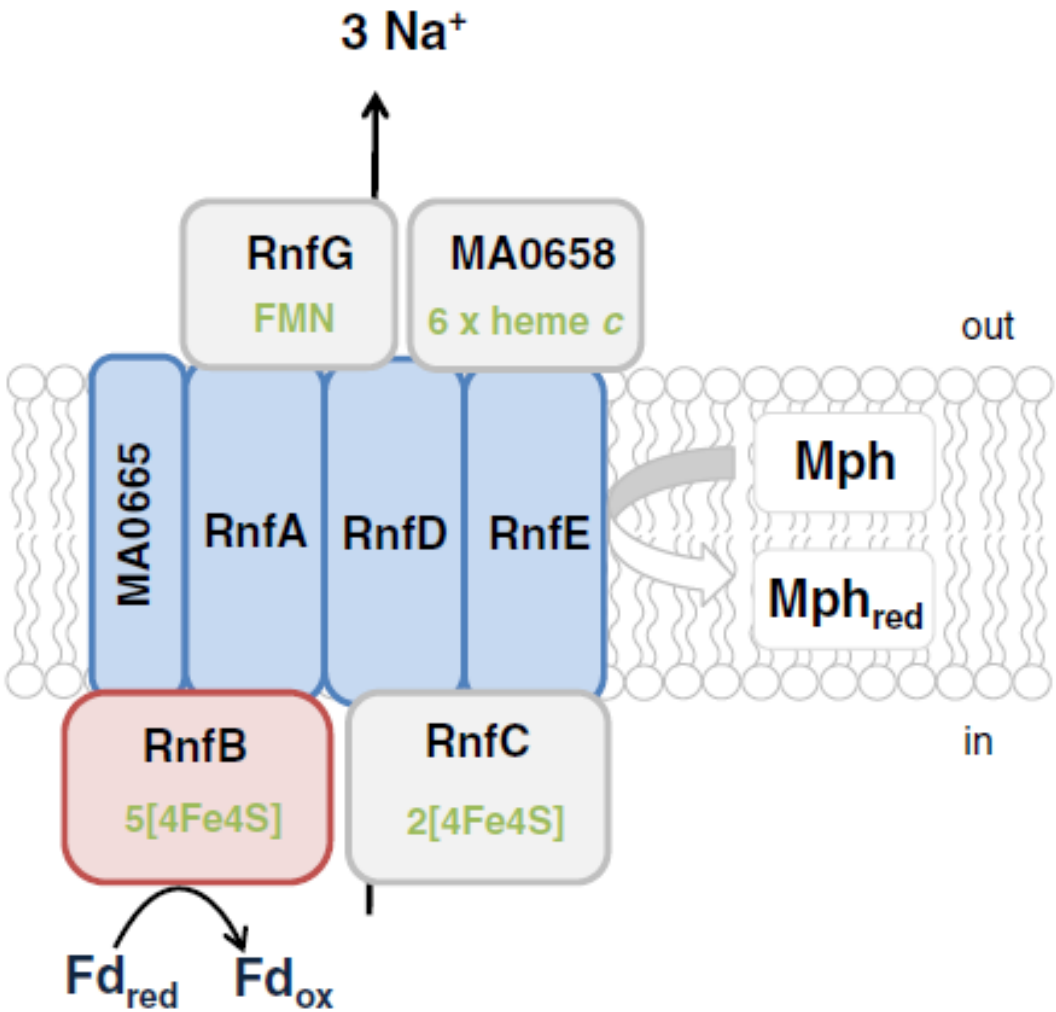

Fig. 6. Rnf complex. Tentative model of the Rnf complex of *Ms. acetivorans*. The additional small hydrophobic subunit (MA0665) is indicated as part of the membrane module. The multi-heme cytochrome *c* is termed MA0658. The exact topology of the subunits, the electron flow and the sodium ion translocation mechanism have not been determined in the methanogenic enzyme. Red colour indicates the initial oxidizing subunit, blue colour indicates membrane integral subunits.

Welte & Deppenmeier, 2014

Methanogens with cytochromes

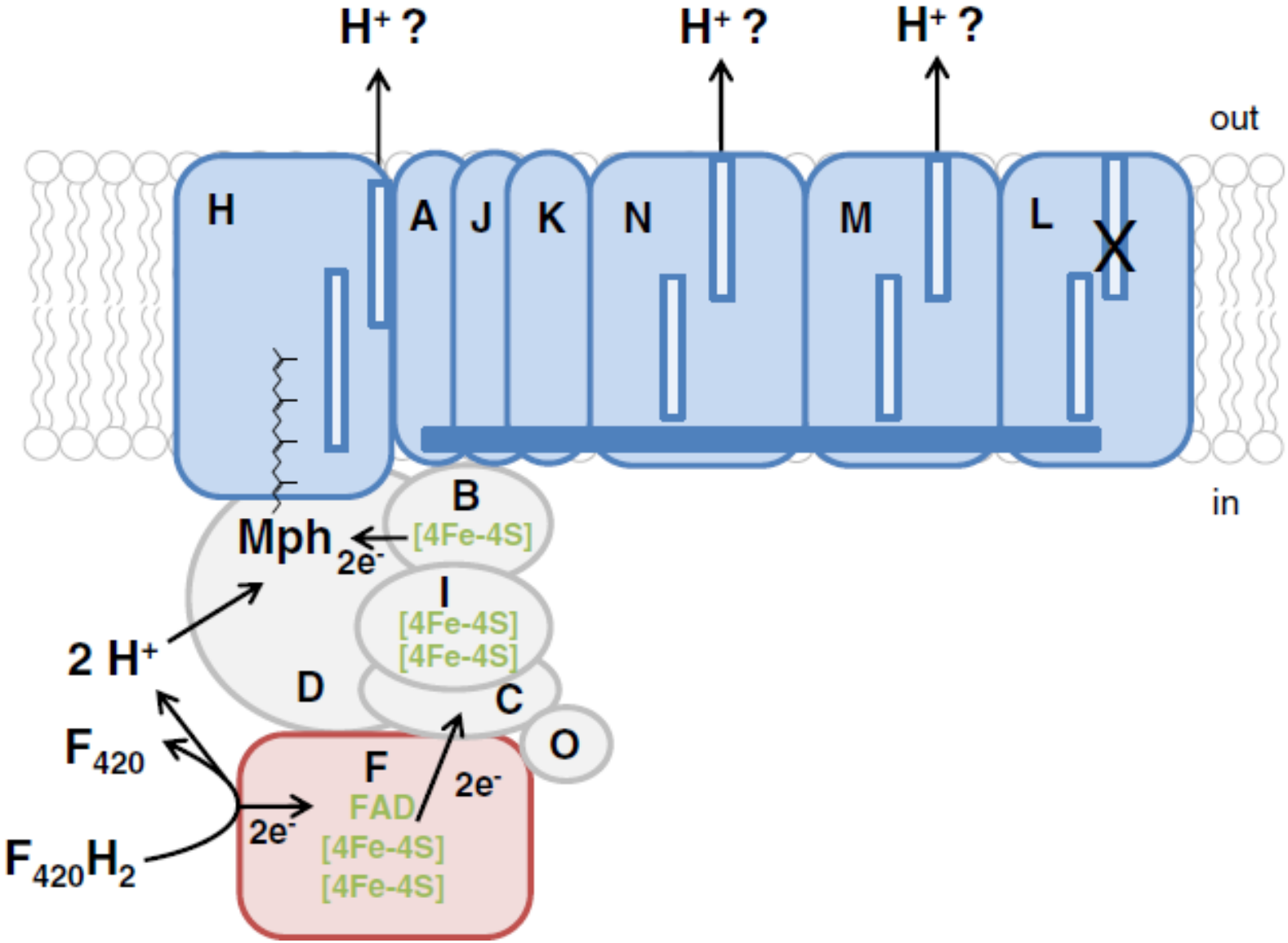

Fig. 7. Tentative model of the $F_{420}H_2$ dehydrogenase. The figure indicates the subunit arrangement, prosthetic groups and the electron flow. Predicted discontinuous TM helices in FpoHLMN are shown as light blue boxes. Putative helix HL is indicated by a dark blue box. Question marks indicate that the exact site of H^+ translocation is not known. The predicted discontinuous TM helix of FpoL is marked by X because it might be inactive. The function of the hydrophilic subunit FpoO is not known. Therefore, its properties are not discussed. Red colour indicates the initial oxidizing subunit, blue colour indicates membrane integral subunits.

Welte & Deppenmeier, 2014

Methanogens with cytochromes

A)

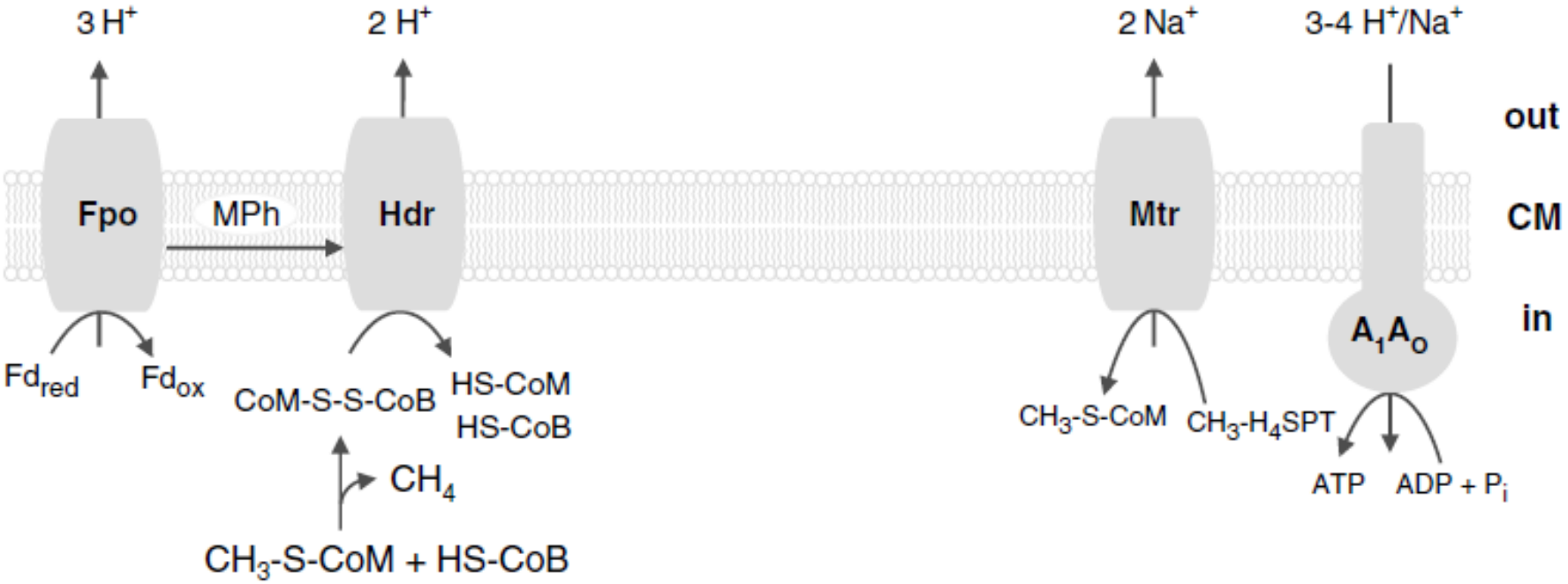

B)

```
MM_2486     122 KLAR......EVDIQEGDER.............................................. 136
MA1500      122 KLAR......EVDIKEGDEK............................................. 136
Mbar_A3407  122 KLAR......EVDLEEGDEK............................................. 136
Mthe_1054   122 RIAVKKFSDKEVAELEAEAKRQAEEKKKAAAAAAKEKAAK.........AKGKENKAKTKPSEGGEA 180
Mcon_3064   126 FLATKRFSAKEVADLEAEAKRIAAEKAAAKKAAAKDAAAAGDKKPAKEGANAEKKKAVAKPAEGGAS 193
Mhar_1414   122 DIAVGLYSDQELAELAEEARKAEEEKKRKAAEAAKAKKEKAAKAADEGDKGSGEKAAKKKKAE.... 185
```

Fig. 10. Process of energy conservation in *Methanosaeta* species. (A) Model of electron transport and ion translocation during aceticlastic growth of *Mt. thermophila*. Fpo, $F_{420}H_2$ dehydrogenase without input module FpoF; Hdr, heterodisulfide reductase; Mtr, methyl-H_4SPT–coenzyme M methyltransferase; A_1A_O, ATP synthase. (B) Alignment of FpoI homologues of different methanogenic archaea. FpoI of *Methanosaeta* sp. contain a C-terminal extension with an accumulation of basic lysine residues. MM_2486, *Ms. mazei* NP_634510.1 (the corresponding gene in the database contains a wrong start codon. In the alignment, the correct start amino acid further downstream was chosen); MA1500, *Ms. acetivorans* NP_616434.1; Mbar_A3407, *Ms. barkeri* YP_306860.1; Mthe_1054, *Mt. thermophila* YP_843478.1; Mcon_3064, *Mt. concilii* YP_004385202.1; Mhar_1414, *Mt. harundinacea* YP_005920401.1.

Welte & Deppenmeier, 2014

Methanogens with cytochromes

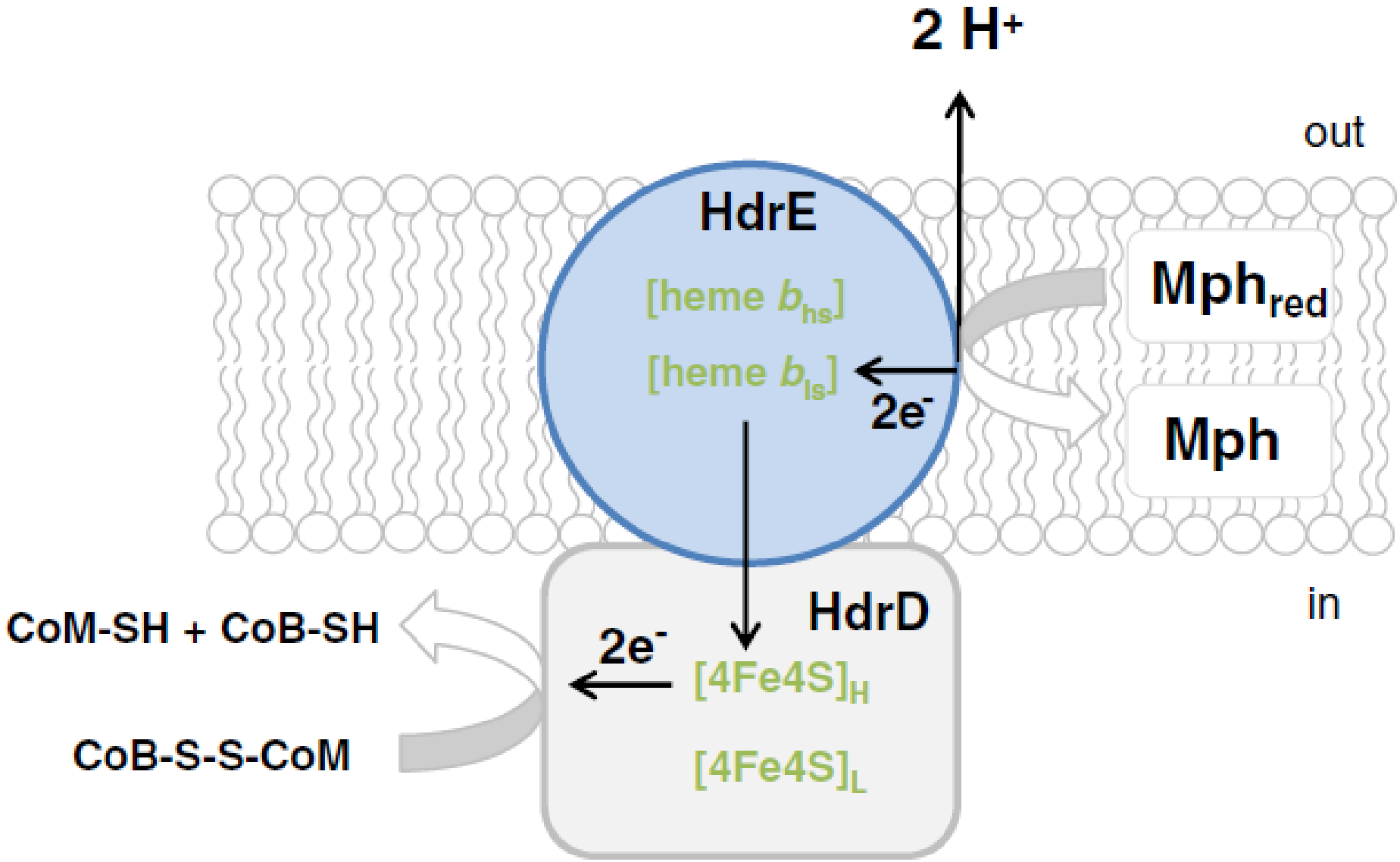

Fig. 9. Simplified scheme of the HdrDE-type heterodisulfide reductase. Direct involvement of electron transport was demonstrated for the low-spin heme (heme b_{ls}) but not for the high-spin heme (heme b_{hs}). The high potential FeS cluster ($[4Fe4S]_H$) was also demonstrated to be involved in electron transport whereas the other, low potential FeS cluster ($[4Fe4S]_L$) is involved in the stabilization of the thiyl intermediate that is formed during catalysis. For more details, see text. Blue colour indicates the membrane integral cytochrome *b* subunit.

Welte & Deppenmeier, 2014

H_2 uptake in methanogenic archaea

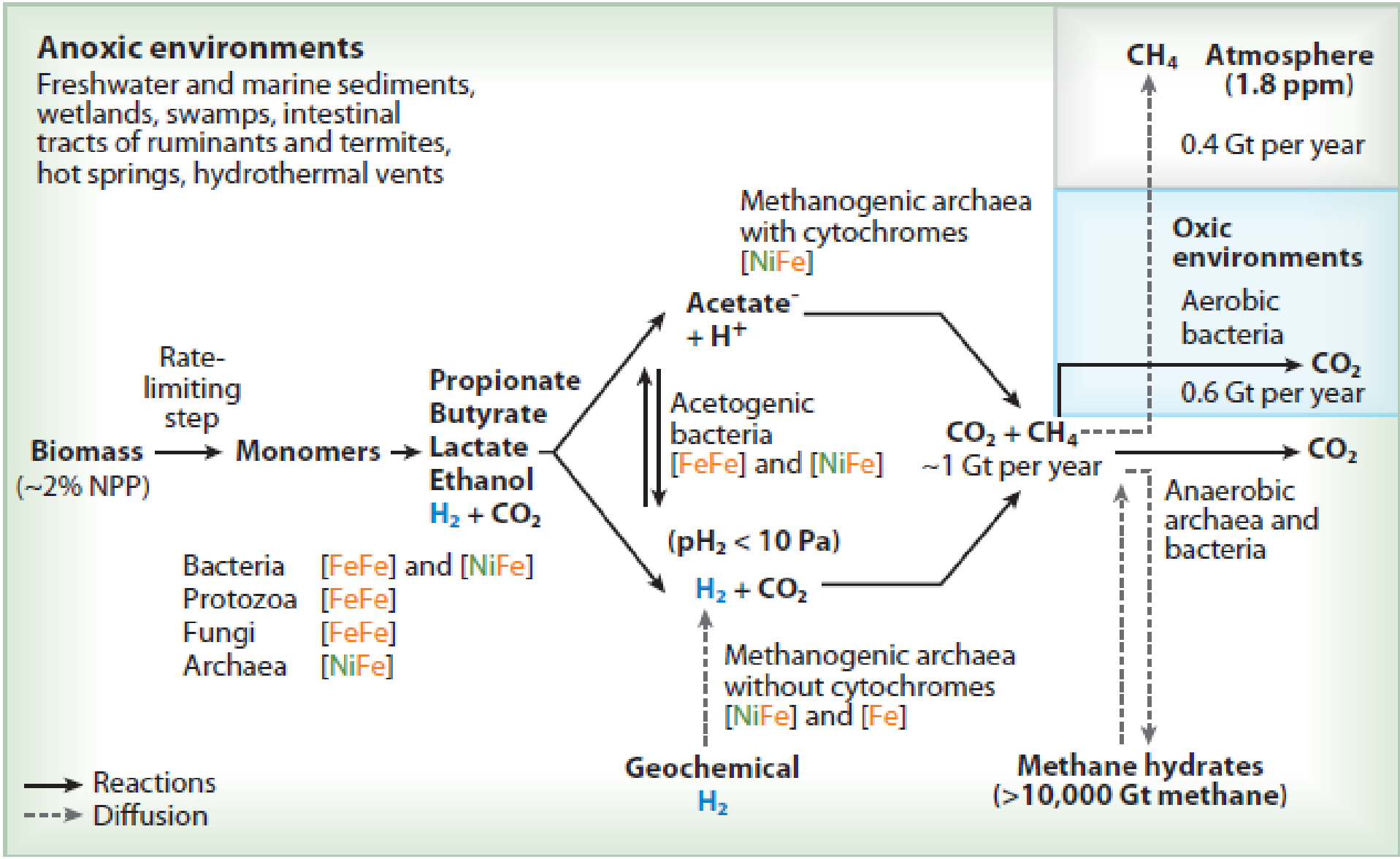

Thauer *et al.* 2010

H_2 uptake in methanogenic archaea

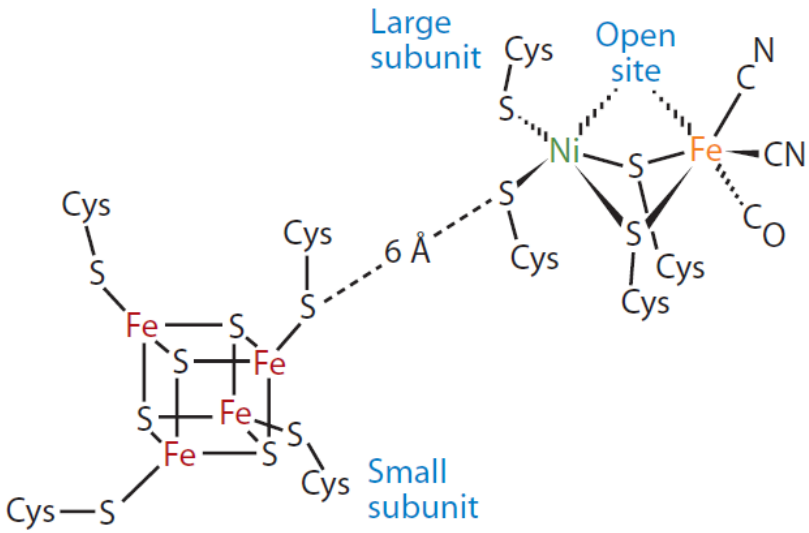

[NiFe]-hydrogenase

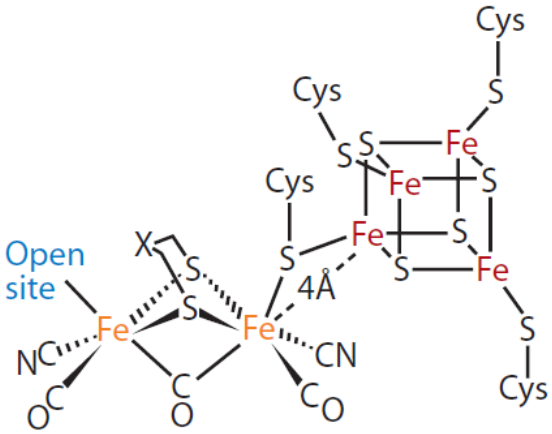

[FeFe]-hydrogenase

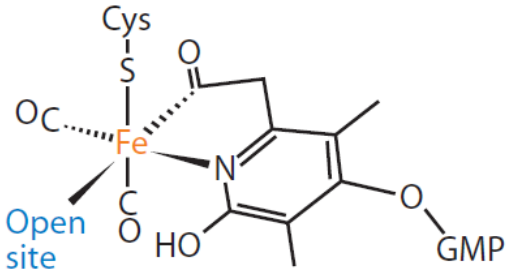

[Fe]-hydrogenase

The metal sites of the three types of hydrogenases involved in interspecies hydrogen transfer (see **Figure 2**) have unusual structural features in common, such as intrinsic CO ligands. Despite this fact, [NiFe]-hydrogenases (5–8), [FeFe]-hydrogenases (9–11), and [Fe]-hydrogenase (12–14) are not phylogenetically related at the level of their primary structure or at the level of the enzymes involved in their active-site biosynthesis (12). Abbreviation: GMP, guanylyl rest.

Thauer *et al.* 2010

H_2 uptake in methanogenic archaea

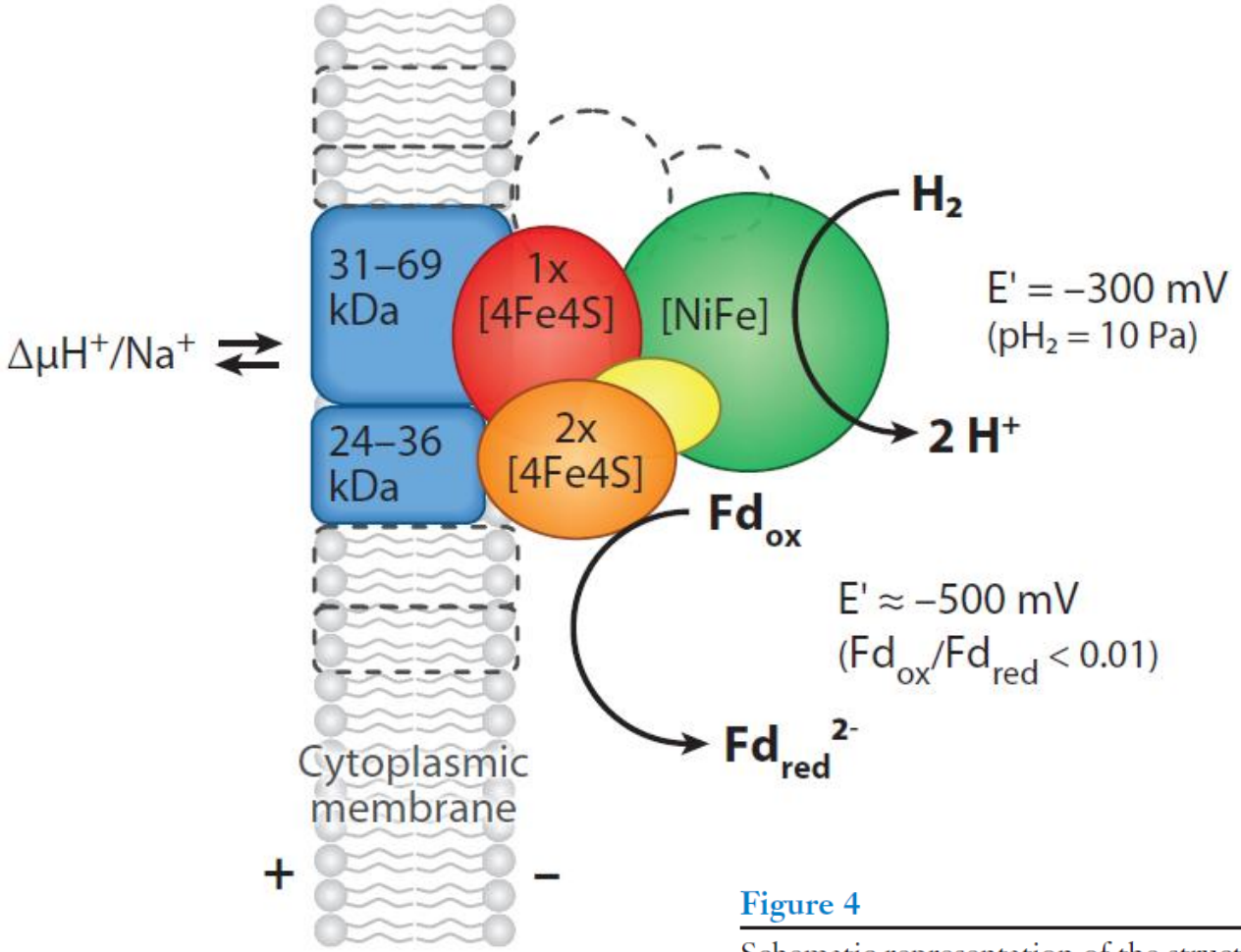

Figure 4

Schematic representation of the structure and function of the energy-converting [NiFe]-hydrogenases EchA-F, EhaA-T, EhbA-Q, and MbhA-N found in methanogenic archaea. The energy-converting hydrogenase EchA-F is composed only of the six conserved core subunits, which are highlighted in color. The energy-converting hydrogenases EhaA-T, EhbA-Q, and MbhA-N also contain several hydrophobic and hydrophilic subunits of unknown function. These subunits are symbolized by areas with dashed boundaries. Abbreviation: Fd, ferredoxin with two [4Fe4S]-clusters.

Thauer *et al.* 2010

H_2 uptake in methanogenic archaea

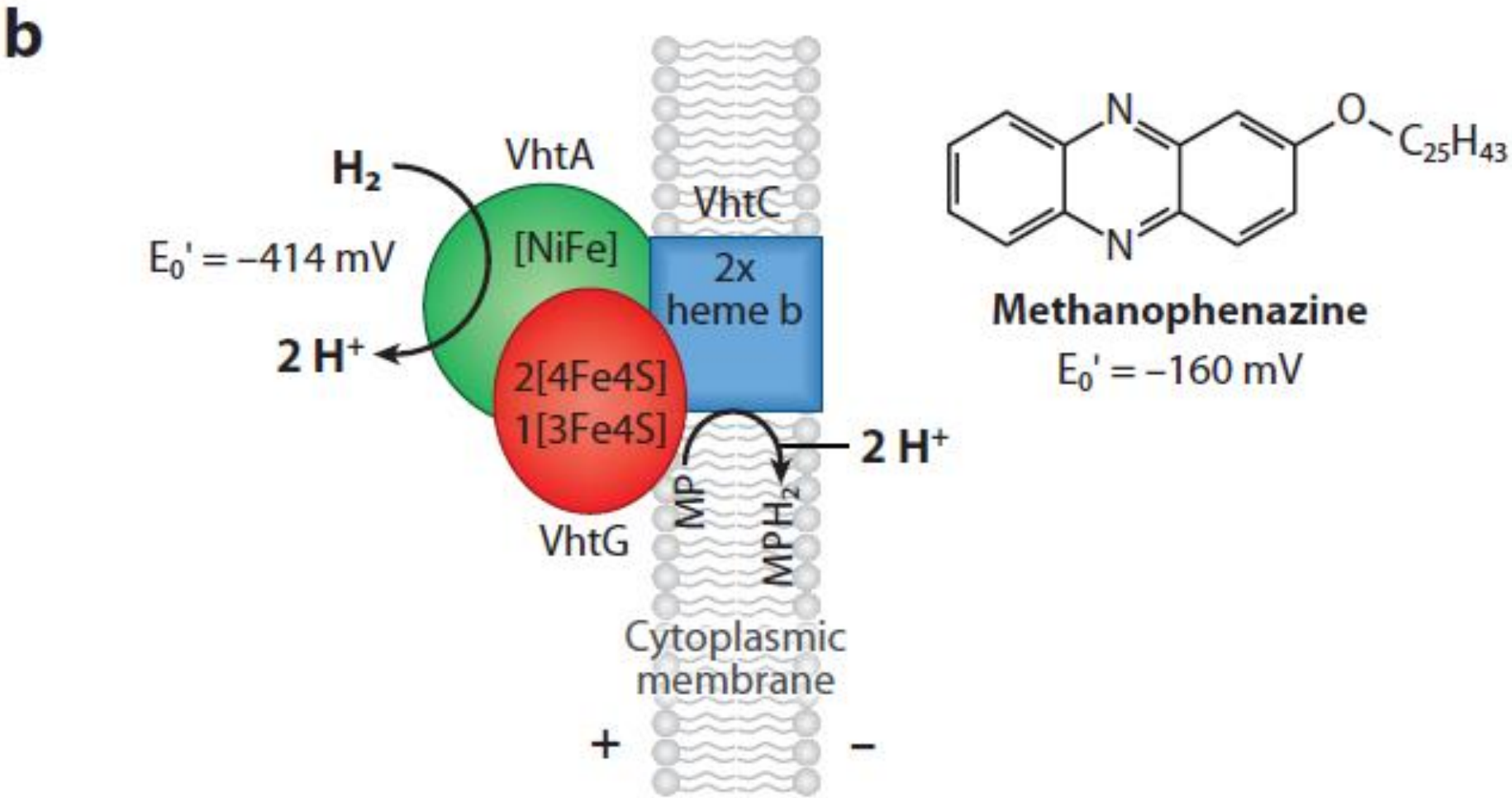

The structures and functions of (*b*) the VhtACG complex. The Vht complex is found only in methanogens with cytochromes.

Thauer *et al*. 2010

H_2 uptake in methanogenic archaea

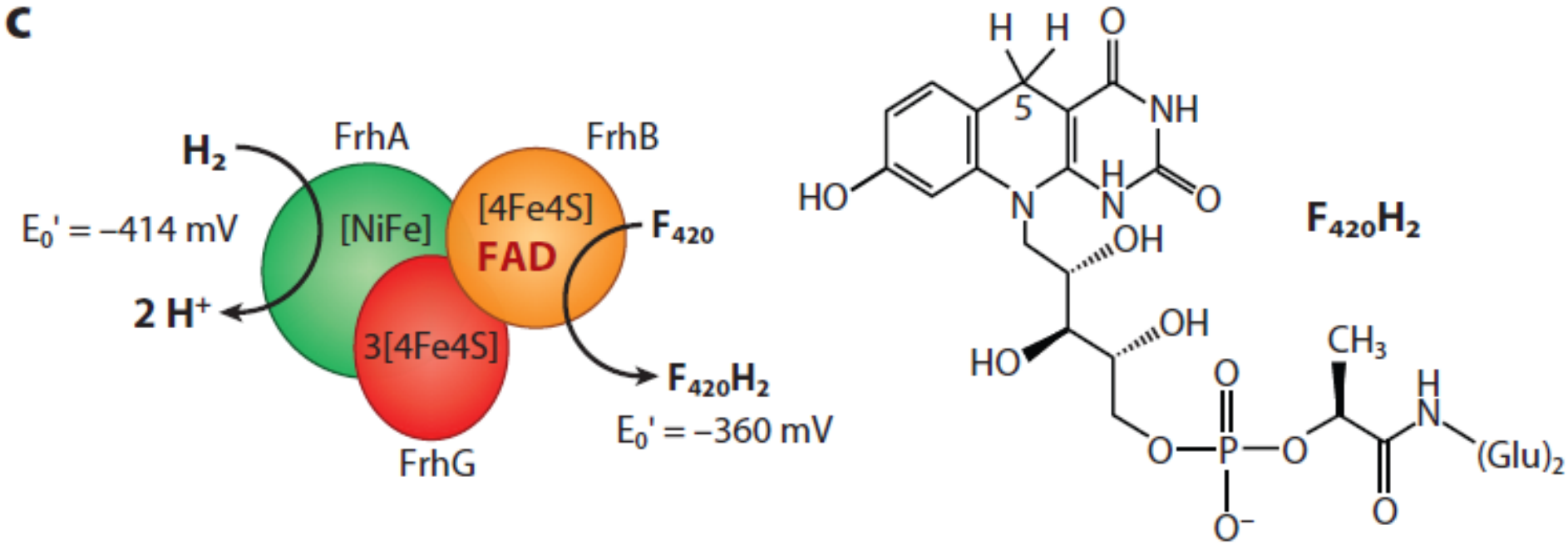

The structures and functions of (*c*) the FrhABG complex.

Thauer *et al*. 2010

H_2 uptake in methanogenic archaea

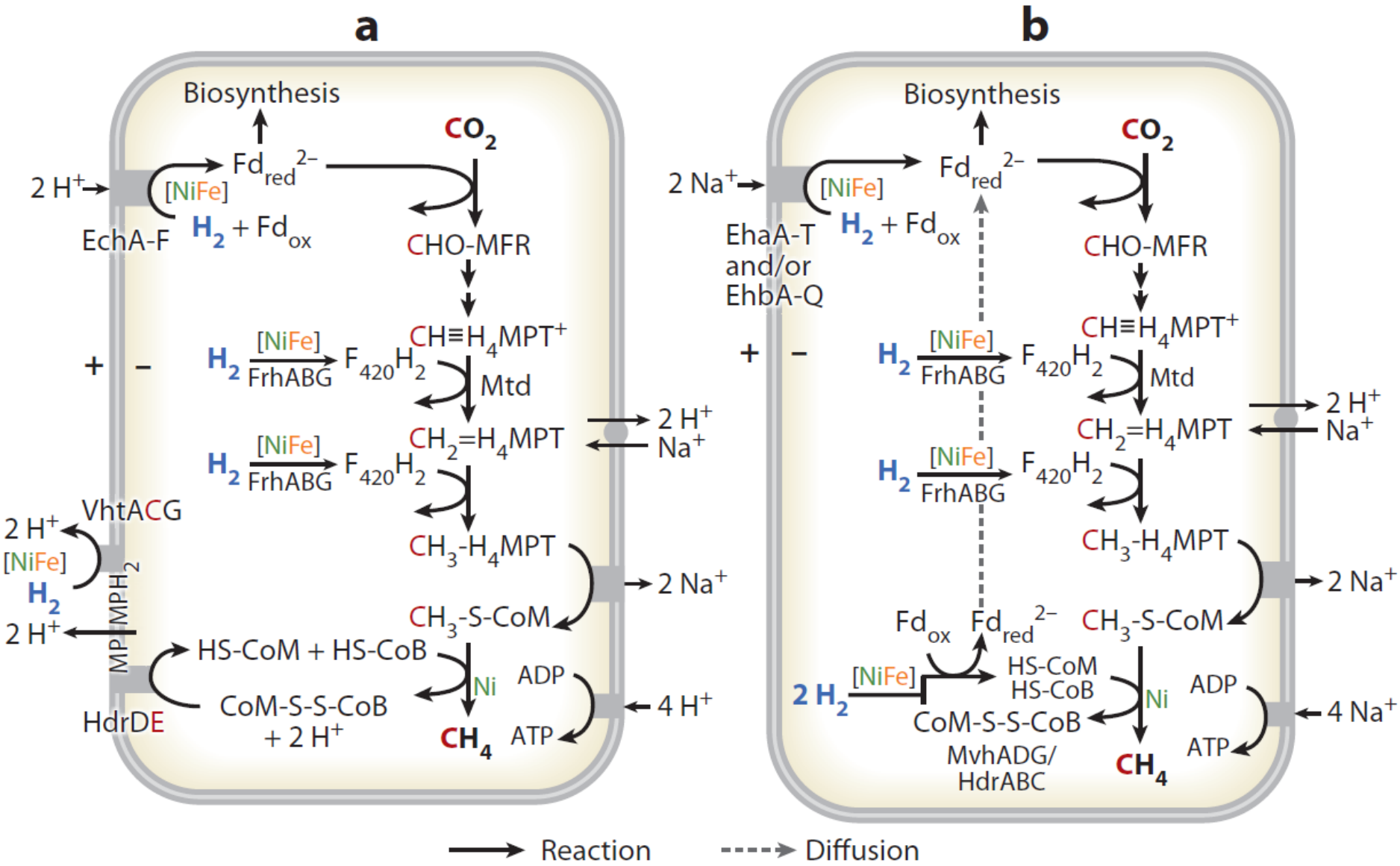

The proposed function and localization within the cell of the [NiFe]-hydrogenases involved in methanogenesis from H2 and CO2 are shown for methanogens (*a*) with cytochromes and (*b*) without cytochromes

Thauer *et al*. 2010

Methanogens without cytochromes

Methanobacteriales
Methanococcales
Methanopyrales
Methanomicrobiales
(all without cytochromes)

$4\,H_2 + CO_2 \rightarrow CH_4 + 2\,H_2O$

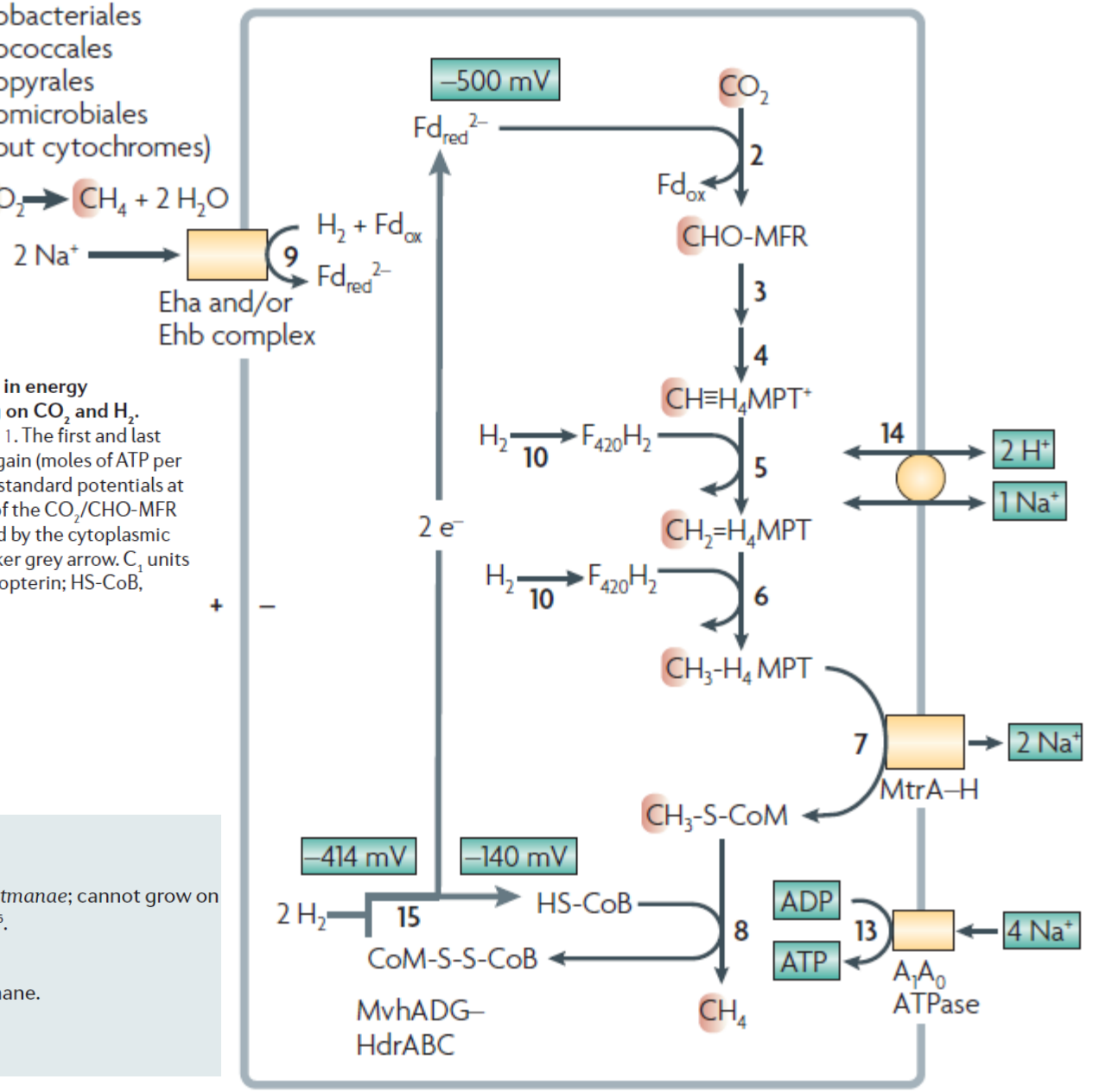

Figure 5 | **The coupling sites that are proposed to be involved in energy conservation in methanogens without cytochromes growing on CO_2 and H_2.** The numbers in bold correspond to the reaction numbers in BOX 1. The first and last steps are coupled by flavin-based electron bifurcation. The ATP gain (moles of ATP per mole of methane) is assumed to be 0.5. The redox potentials are standard potentials at pH 7.0. The $E^{0\prime}$ of ferredoxin was set at –500 mV, which is the $E^{0\prime}$ of the CO_2/CHO-MFR couple (discussed in the main text). The reaction that is catalysed by the cytoplasmic MvhADG–HdrABC complex (reaction 15) is delineated by a thicker grey arrow. C_1 units are highlighted in red. Fd, ferredoxin; H_4MPT, tetrahydromethanopterin; HS-CoB, coenzyme B; HS-CoM, coenzyme M; MFR, methanofuran.

Methanogens without cytochromes

- Do not contain methanophenazine.
- Can grow on H_2 and CO_2, except for *Methanosphaera stadtmanae*; cannot grow on acetate or methylamines and many can grow on formate[36].
- Threshold H_2 partial pressure is generally <10 Pa.
- Growth yields on H_2 and CO_2 of up to 3 g per mole of methane.
- Doubling times can be as low as 1 hour.
- Many hyperthermophilic species.

Thauer *et al.*, 2008

Methanogens without cytochromes

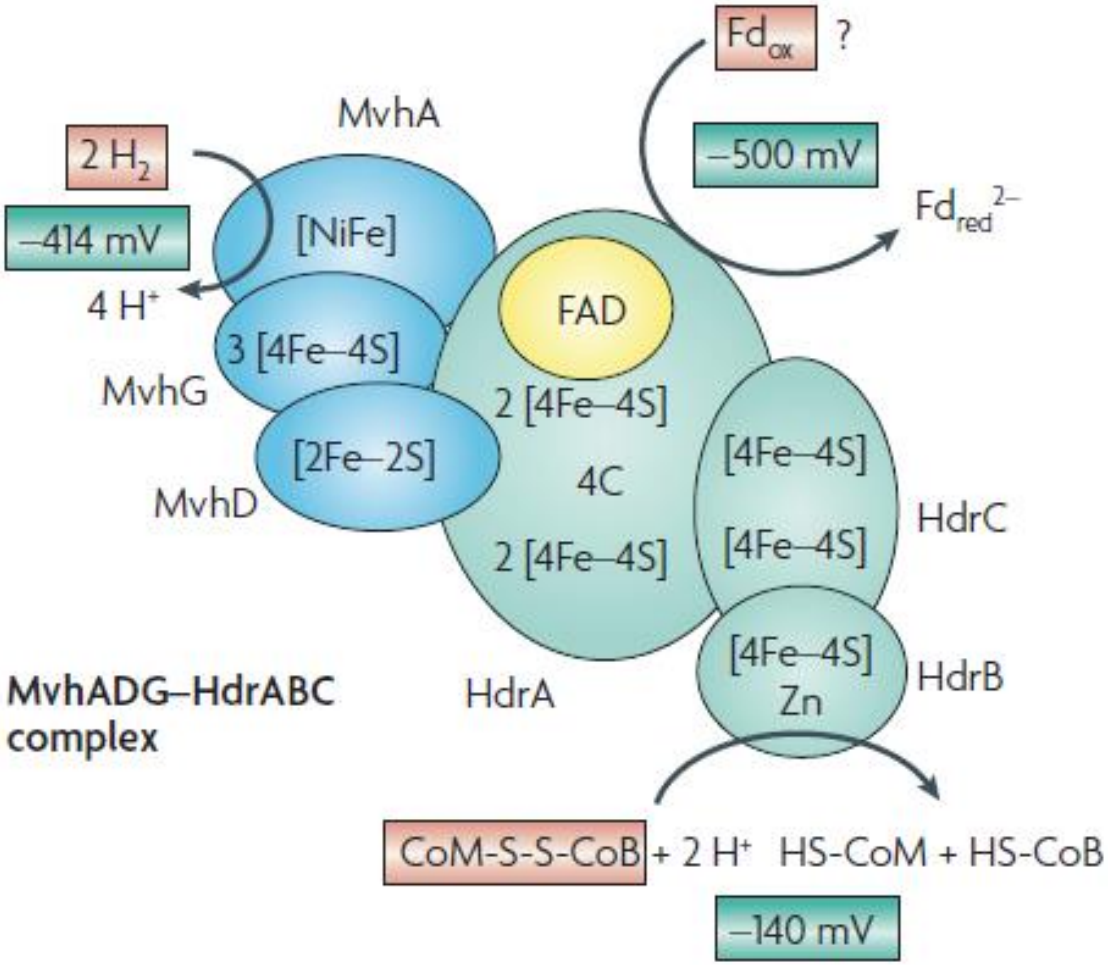

Figure 4 | **Proposed scheme for the reduction of CoM-S-S-CoB with H_2 that is catalysed by the hydrogenase (MvhADG)–heterodisulphide reductase (HdrABC) complex in methanogens without cytochromes.** The enzyme complex is proposed to couple the endergonic reduction of ferredoxin with H_2 to the exergonic reduction of CoM-S-S-CoB with H_2 by flavin-based electron dismutation that involves the FAD in HdrA. The redox potentials are standard potentials at pH 7.0 ($E^{0\prime}$). The $E^{0\prime}$ of ferredoxin was set at –500 mV, which is the $E^{0\prime}$ of the CO_2/CHO-MFR couple (discussed in the main text). The sequence of HdrB contains ten conserved cysteines that are organized into two so-called CCG domains ($CX_{31–39}CCX_{35–36}CXXC$). The carboxy-terminal CCG domain is involved in an unusual [4 Fe–4 S] cluster formation and the amino-terminal domain is involved in zinc binding. The zinc in HdrB is ligated by three sulphurs and one histidine nitrogen, as revealed by Zn-K-edge X-ray absorption spectroscopy[82]. The '4C' in HdrA represents a conserved sequence motif that contains four cysteines, and in HdrA from *Methanococcus* spp., one of the four cysteines is a selenocysteine. Fd, ferredoxin; HS-CoB, coenzyme B; HS-CoM, coenzyme M.

Thauer *et al.*, 2008

H_2 uptake in methanogenic archaea

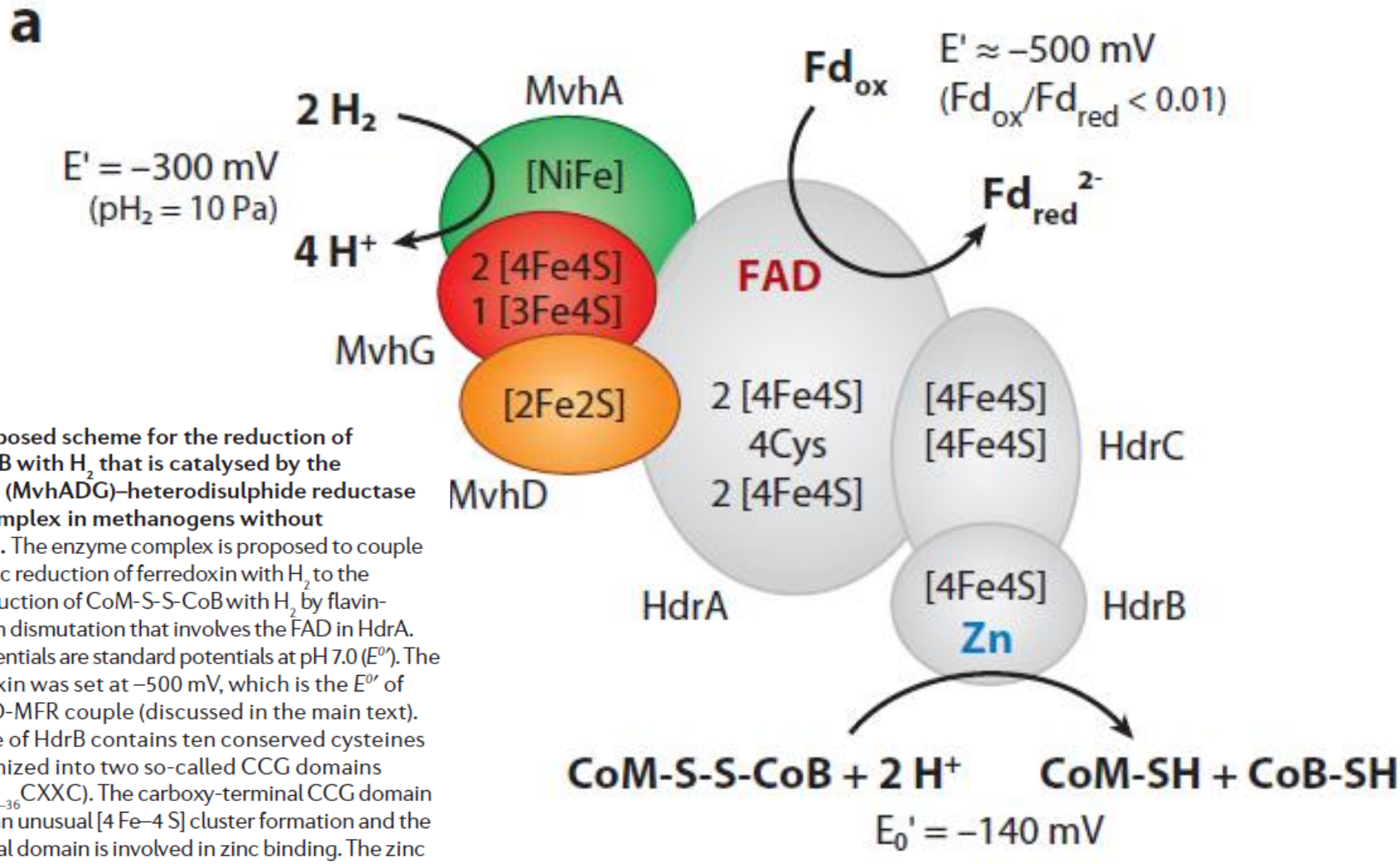

Figure 4 | **Proposed scheme for the reduction of CoM-S-S-CoB with H_2 that is catalysed by the hydrogenase (MvhADG)–heterodisulphide reductase (HdrABC) complex in methanogens without cytochromes.** The enzyme complex is proposed to couple the endergonic reduction of ferredoxin with H_2 to the exergonic reduction of CoM-S-S-CoB with H_2 by flavin-based electron dismutation that involves the FAD in HdrA. The redox potentials are standard potentials at pH 7.0 ($E^{0\prime}$). The $E^{0\prime}$ of ferredoxin was set at –500 mV, which is the $E^{0\prime}$ of the CO_2/CHO-MFR couple (discussed in the main text). The sequence of HdrB contains ten conserved cysteines that are organized into two so-called CCG domains ($CX_{31–39}CCX_{35–36}CXXC$). The carboxy-terminal CCG domain is involved in an unusual [4 Fe–4 S] cluster formation and the amino-terminal domain is involved in zinc binding. The zinc in HdrB is ligated by three sulphurs and one histidine nitrogen, as revealed by Zn-K-edge X-ray absorption spectroscopy[82]. The '4C' in HdrA represents a conserved sequence motif that contains four cysteines, and in HdrA from *Methanococcus* spp., one of the four cysteines is a selenocysteine. Fd, ferredoxin; HS-CoB, coenzyme B; HS-CoM, coenzyme M.

The structures and functions of (*a*) the MvhADG/HdrABC complex. The Mvh/Hdr complex is found mainly in methanogens without cytochromes, The stoichiometry of the MvhADG/HdrABC-catalyzed reaction has not yet been ascertained.

Thauer *et al*., 2008, 2010

Methanogens – e⁻ bifurcation

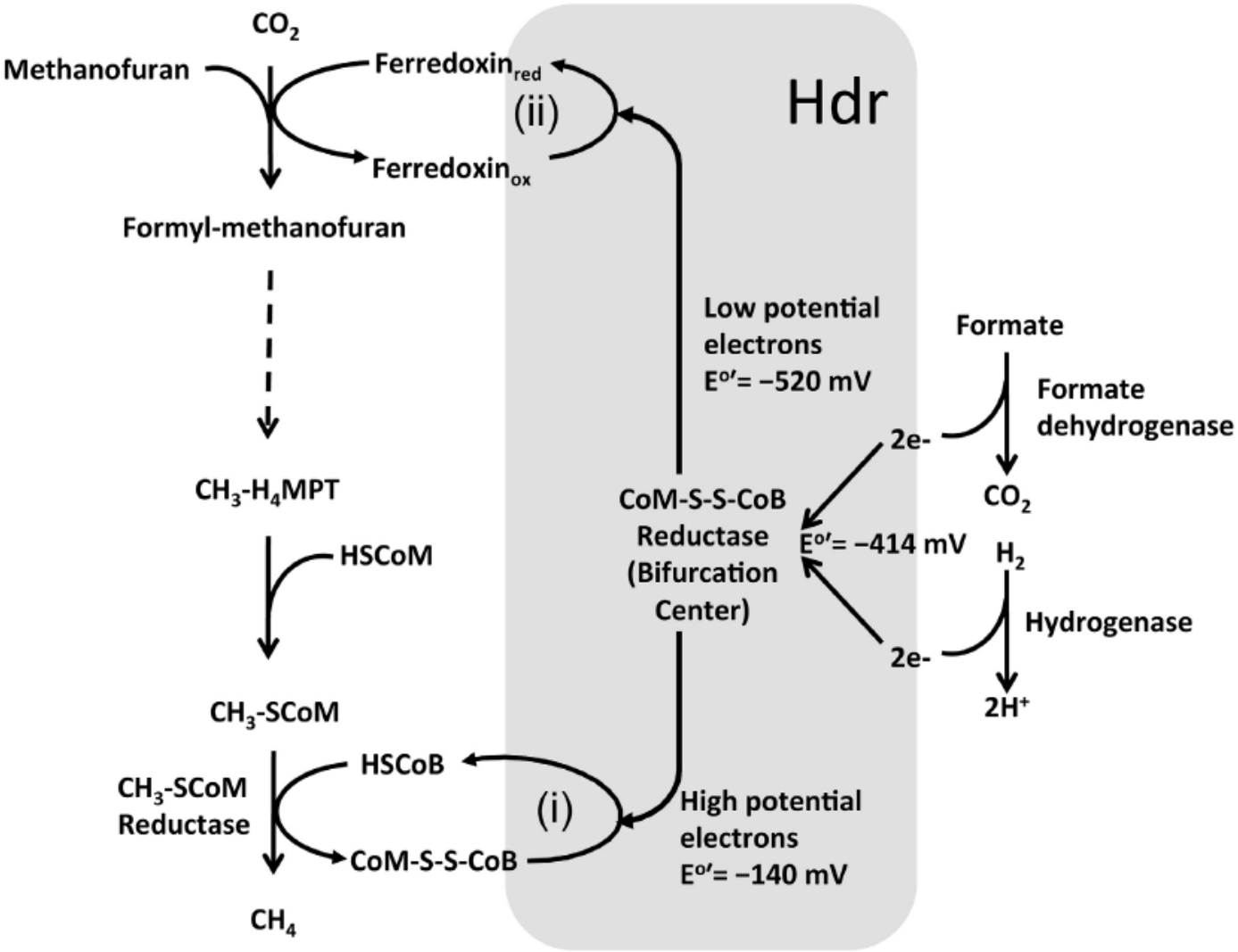

FIGURE 5 | Electron bifurcation in Methanogenesis. HS-CoB or HS-HTP, coenzyme B; HS-CoM, coenzyme M; CoM-S-S-CoB, heterodisulfide of coenzyme M and coenzyme B. Heterodisulfide reductase (Hdr) utilizes bifurcated energy electrons for two purposes: (i) converting CoM-S-S-CoB to HS-CoM and HS-CoB, using high potential electrons; and (ii) reducing a low potential ferredoxin using low potential electrons, which is energetically suitable for the highly endergonic reduction of CO_2 and generation of formyl-MF (Thauer et al., 2008; Thauer, 2012; Costa and Leigh, 2014).

Purwatini et al., 2014

Methanogens – e⁻ bifurcation

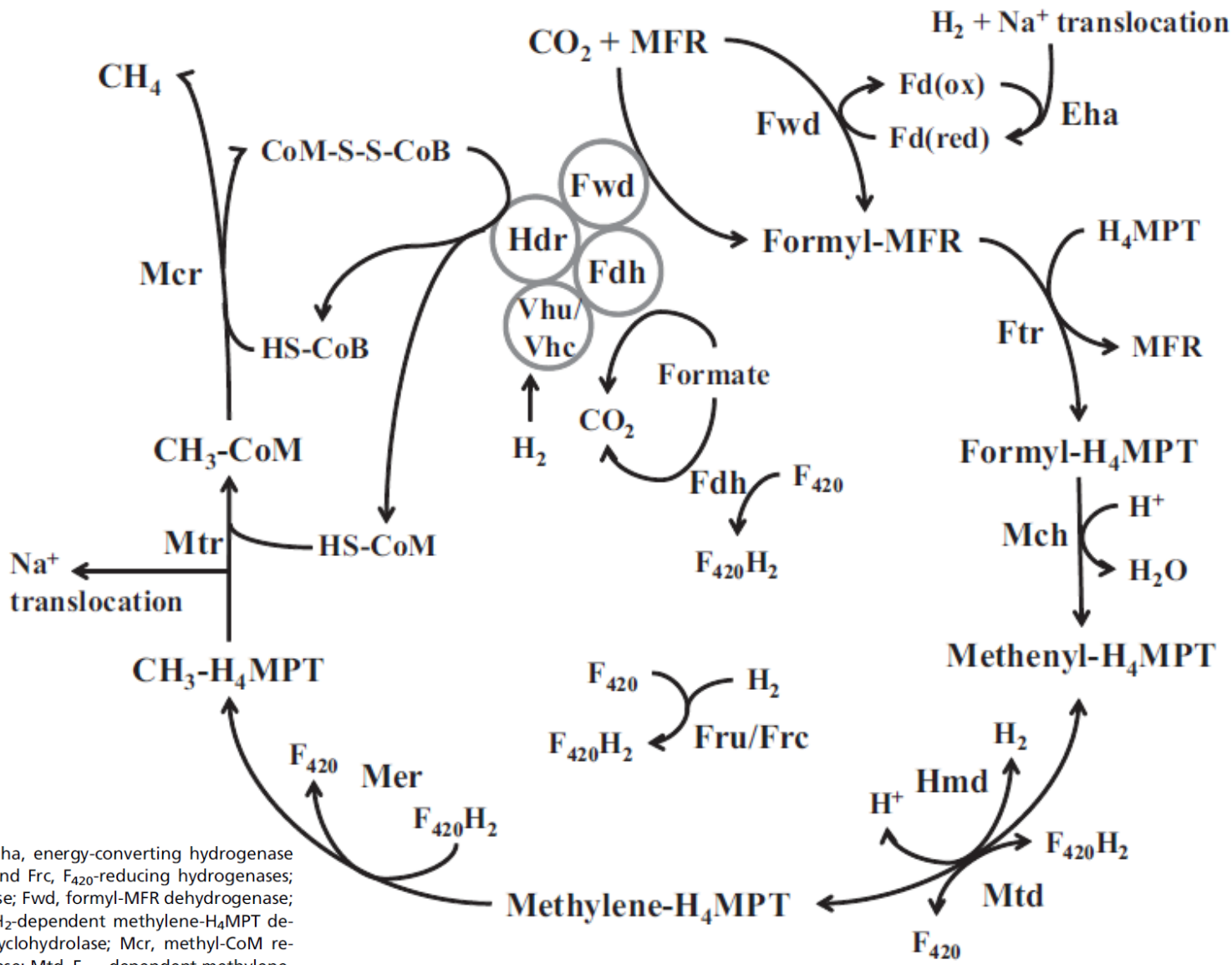

Fig. 1. The methanogenic pathway. Eha, energy-converting hydrogenase A; Fdh, formate dehydrogenase; Fru and Frc, F_{420}-reducing hydrogenases; Ftr, formyl-MFR:H_4MPT formyltransferase; Fwd, formyl-MFR dehydrogenase; Hdr, heterodisulfide reductase; Hmd, H_2-dependent methylene-H_4MPT dehydrogenase; Mch, methenyl-H_4MPT cyclohydrolase; Mcr, methyl-CoM reductase; Mer, methylene-H_4MPT reductase; Mtd, F_{420}-dependent methylene-H_4MPT dehydrogenase; Mtr, methyl-H_4MPT-CoM methyltransferase; Vhu and Vhc, F_{420}-nonreducing (Hdr-associated) hydrogenases.

Lie *et al*. 2012

Methanogens – e⁻ bifurcation

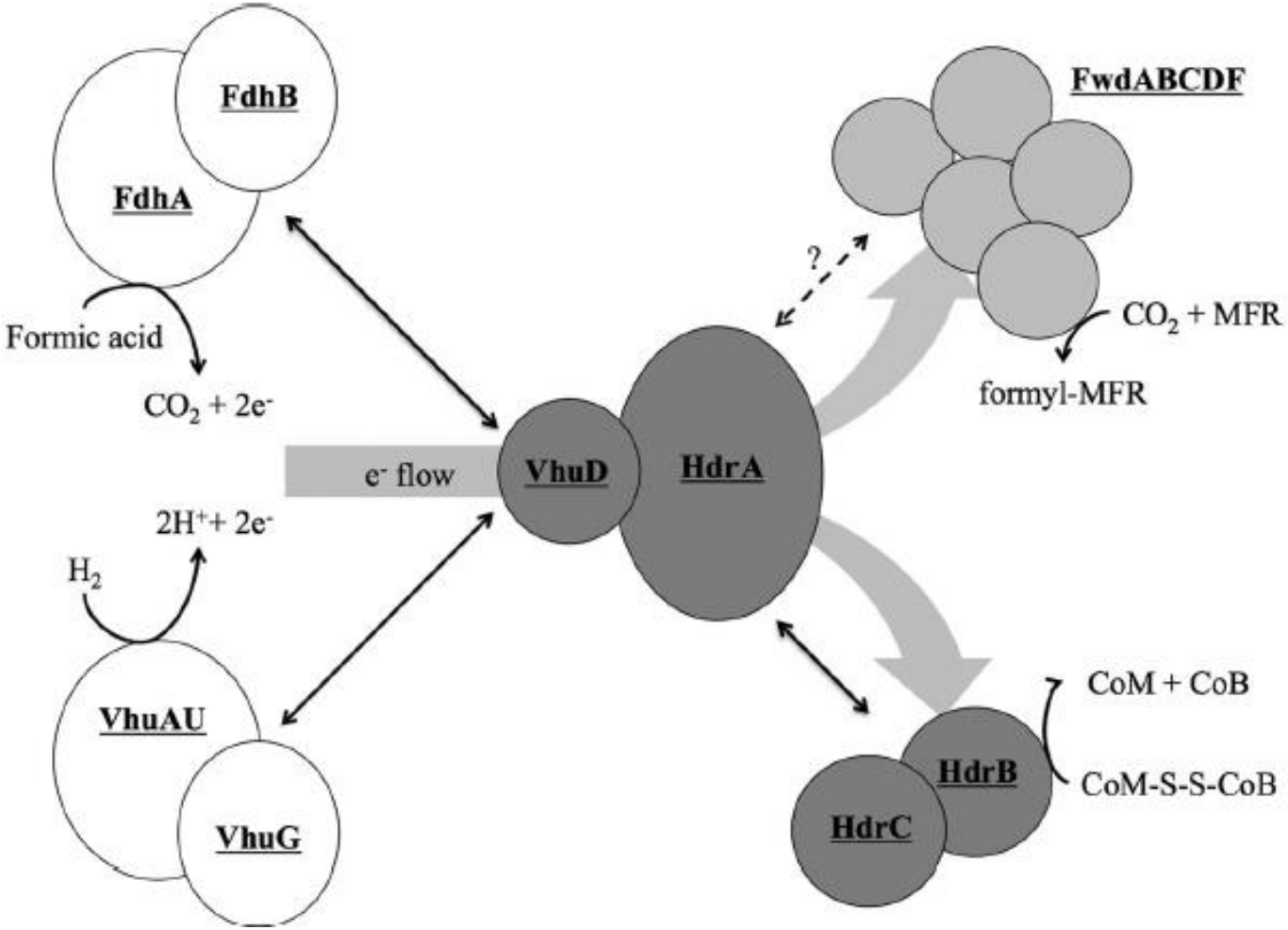

FIG 5 Protein interactions in the Hdr supercomplex. Formate dehydrogenase (FdhAB) and hydrogenase (VhuAGU) compete for binding to VhuD. VhuA and VhuU are drawn together, since they form the catalytic site of H_2 oxidation (30, 31). Electrons flow to HdrA, where their path is bifurcated to both FwdABCDF and HdrBC. Black double arrows indicate known interactions between subcomplexes. The dashed line between HdrA and Fwd signifies a hypothesized site of interaction between these subcomplexes. Reactions catalyzed by the individual enzymes are shown. The model only shows one of each enzyme, despite the fact that two of each are in the *M. maripaludis* genome (8). This reflects that, for the most part, the alternative forms are not expressed under the growth conditions used. HdrA, Vhu, and Fwd (as well as Fru) contain selenocysteine. *M. maripaludis* also encodes cysteine-containing versions, but these are repressed by selenium (19, 32). Additionally, Fwd contains tungsten, and its paralog, the molybdenum-containing formylmethanofuran dehydrogenase Fmd, requires high molybdenum for expression (33). In the case of Fdh, the genes for the alternative form of the enzyme are only expressed when cells are grown with limiting concentrations of formate in the absence of H_2 (20). Analysis of the *M. maripaludis* proteome verifies that only one form of these enzymes is highly expressed under our culture conditions (28, 34).

Costa et al., 2013(c)

Methanogens without cytochromes

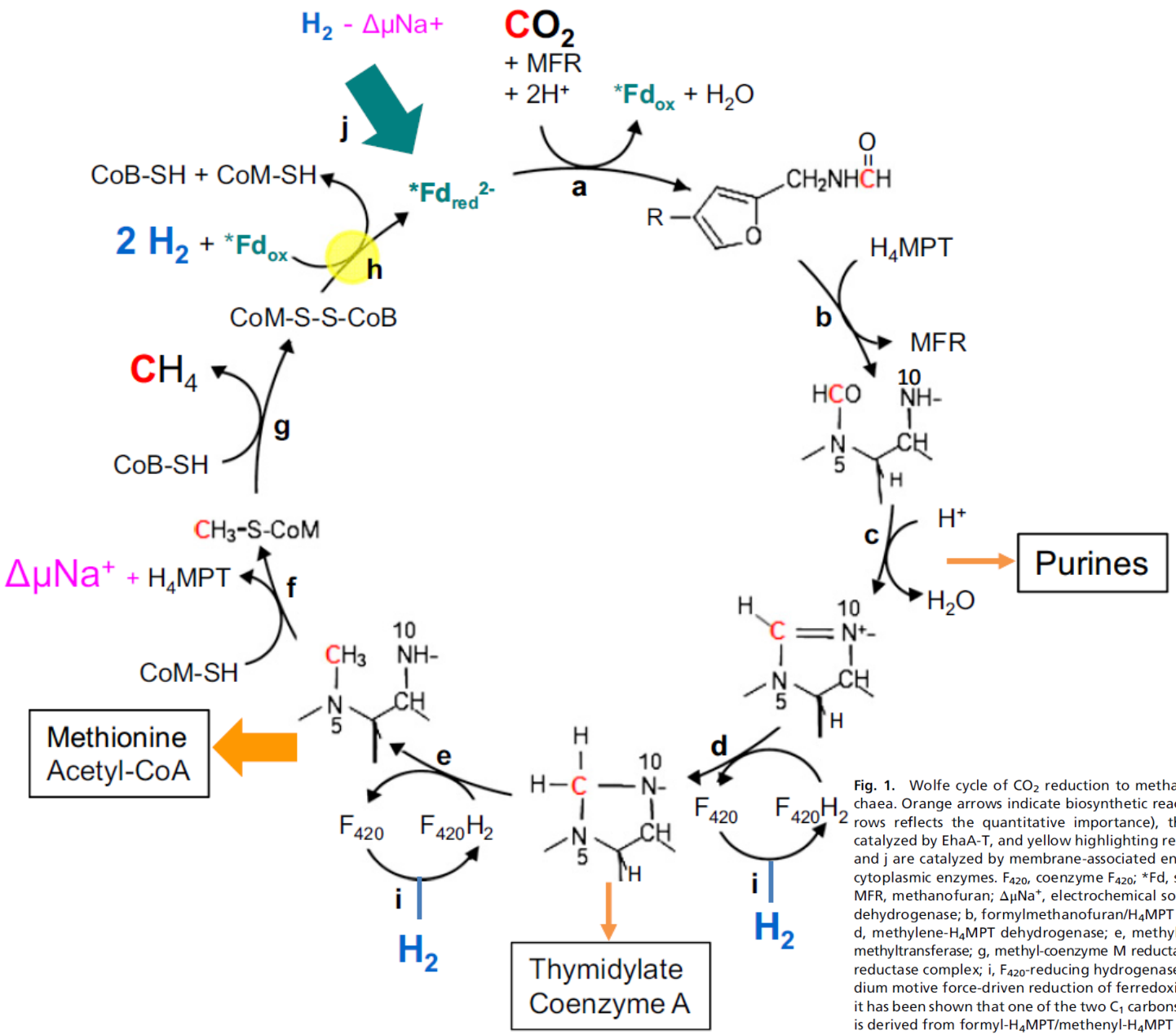

Fig. 1. Wolfe cycle of CO_2 reduction to methane with 4 H_2 in hydrogenotrophic methanogenic archaea. Orange arrows indicate biosynthetic reactions that remove intermediates (thickness of the arrows reflects the quantitative importance), the green arrow illustrates the anaplerotic reaction catalyzed by EhaA-T, and yellow highlighting represents the electron-bifurcating reaction. Reactions f and j are catalyzed by membrane-associated enzyme complexes. All other reactions are catalyzed by cytoplasmic enzymes. F_{420}, coenzyme F_{420}; *Fd, specific ferredoxin; H_4MPT, tetrahydromethanopterin; MFR, methanofuran; $\Delta\mu Na^+$, electrochemical sodium ion potential. Enzymes: a, formylmethanofuran dehydrogenase; b, formylmethanofuran/H_4MPT formyltransferase; c, methenyl-H_4MPT cyclohydrolase; d, methylene-H_4MPT dehydrogenase; e, methylene-H_4MPT reductase; f, methyl-H_4MPT/coenzyme M methyltransferase; g, methyl-coenzyme M reductase; h, electron-bifurcating hydrogenase–heterodisulfide reductase complex; i, F_{420}-reducing hydrogenase; j, energy-converting hydrogenase catalyzing the sodium motive force-driven reduction of ferredoxin with H_2. With *Methanothermobacter marburgensis*, it has been shown that one of the two C_1 carbons in purines is derived from formate (C-2) and the other is derived from formyl-H_4MPT/methenyl-H_4MPT (C-8) (25).

Thauer 2012

Methanogens without cytochromes

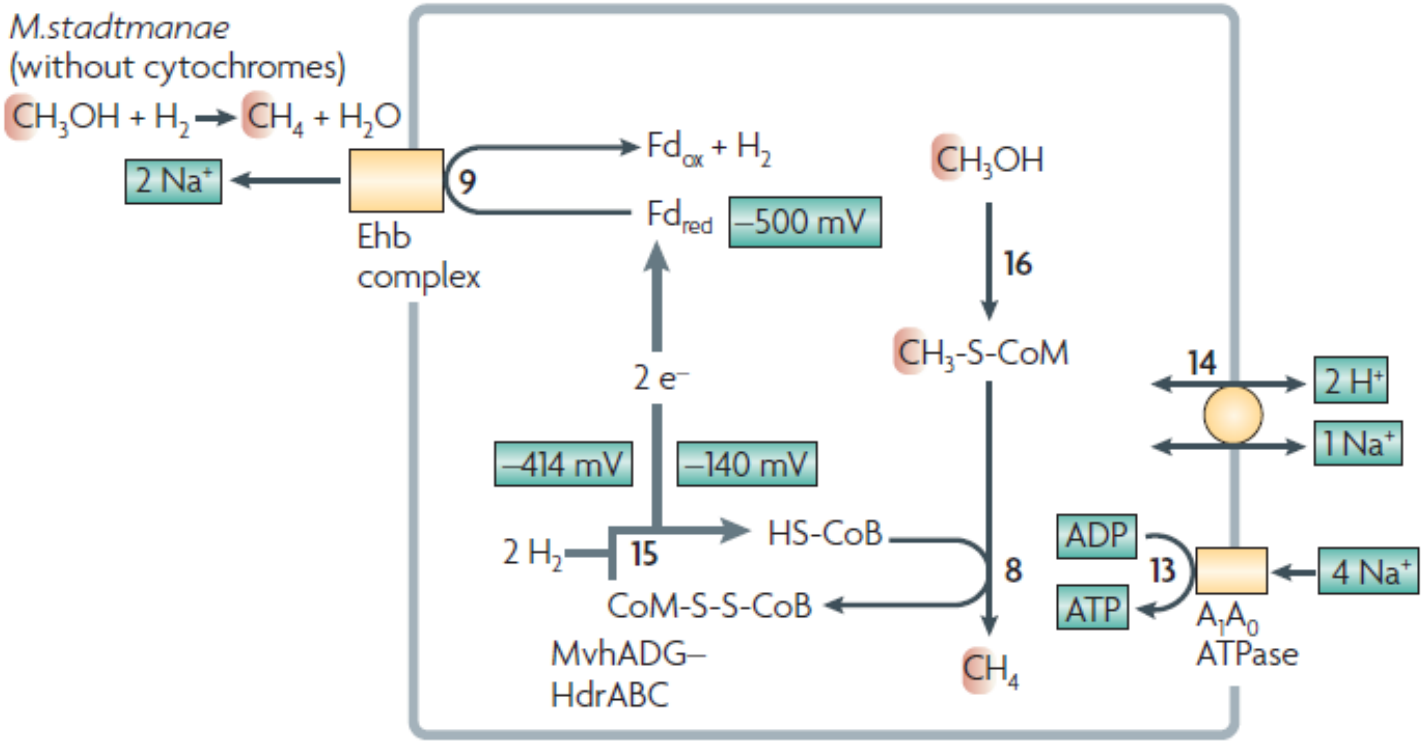

Figure 6 | **Proposed energy conservation by the Ehb complex in *Methanosphaera stadtmanae* growing on methanol and H_2.** The numbers in bold correspond to the reaction numbers in BOX 1. Reactions 9 and 15 are coupled by flavin-based electron bifurcation. The redox potentials are standard potentials at pH 7.0 ($E^{0\prime}$). The $E^{0\prime}$ of ferredoxin was set at –500 mV (discussed in the main text). The scheme can explain the described effects of dicyclohexylcarbodiimide, protonophores and sodium ionophores at high and low sodium ion concentrations[67] if the presence of an active electrogenic $Na^+/2\ H^+$ antiporter is taken into account. The reaction that is catalysed by the cytoplasmic MvhADG–HdrABC complex (reaction 15) is delineated by a thicker grey arrow. C_1 units are highlighted in red. Fd, ferredoxin; HS-CoB, coenzyme B; HS-CoM, coenzyme M.

Thauer *et al.*, 2008

Metabolism of methanogens – *Ca.* M. termitum

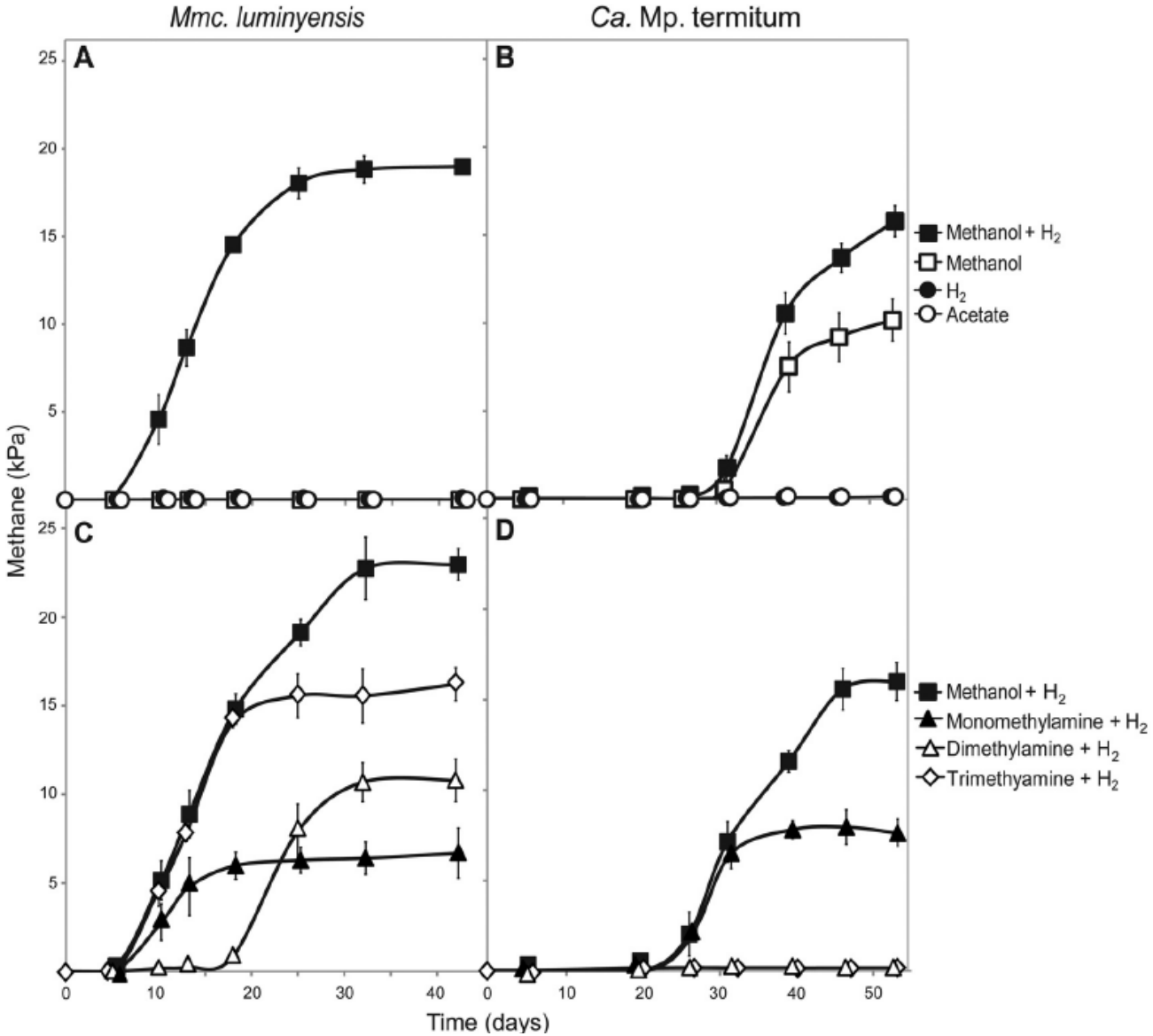

FIG 3 Time course of methane accumulation in the culture headspace of *Methanomassiliicoccus luminyensis* (A and C) and "*Ca*. Methanoplasma termitum" (B and D) incubated in bicarbonate-buffered medium supplemented with H_2 (ca. 50 kPa), methanol (50 mM), or acetate (30 mM) (A and B) or H_2 combined with different methylamines (10 mM) (C and D). To avoid a transfer of residual methanol with the inoculum, the precultures were grown under methanol limitation. The values are means of three replicate cultures; standard deviations are shown only if they are larger than the symbols.

Metabolism of methanogens – *Ca.* M. termitum

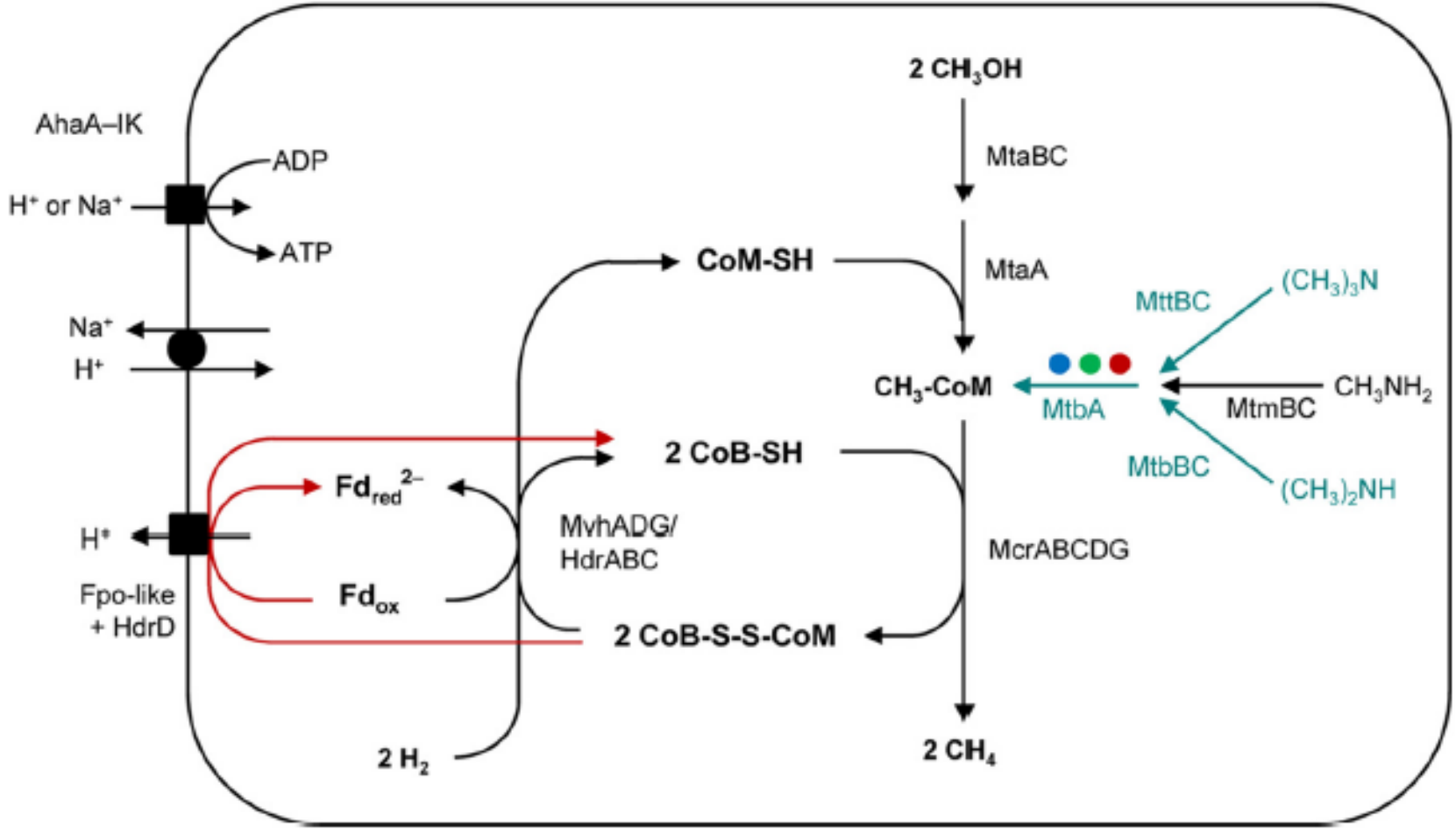

FIG 2 Energy metabolism of "*Ca.* Methanoplasma termitum" and other members of the order *Methanomassiliicoccales*. Black arrows indicate reactions whose enzymes are encoded in all genomes; red arrows indicate the proposed reaction of the heterodisulfide reductase (HdrD) coupled to the Fpo-like complex (Fig. 6). Blue-green arrows indicate that the enzymes are not present in "*Ca.* Methanoplasma termitum" but are present in the genomes indicated by colored dots (blue, *Methanomassiliicoccus luminyensis*; green, "*Ca.* Methanomassiliicoccus intestinalis," red, "*Ca.* Methanomethylophilus alvus"). Abbreviations: Mta, methanol:CoM methyltransferase; Mvh, non-F_{420}-reducing hydrogenase; Hdr, heterodisulfide reductase; Mcr, methyl-CoM reductase; Fpo-like, $F_{420}H_2$-dehydrogenase-like complex; MtbA, methylcobamide:CoM methyltransferase; Mtm, monomethylamine methyltransferase; Mtb, dimethylamine methyltransferase; Mtt, trimethylamine methyltransferase; Aha, A_oA_1-ATP synthase.

Lang *et al.*, 2015

Metabolism of methanogens – *Ca.* M. termitum

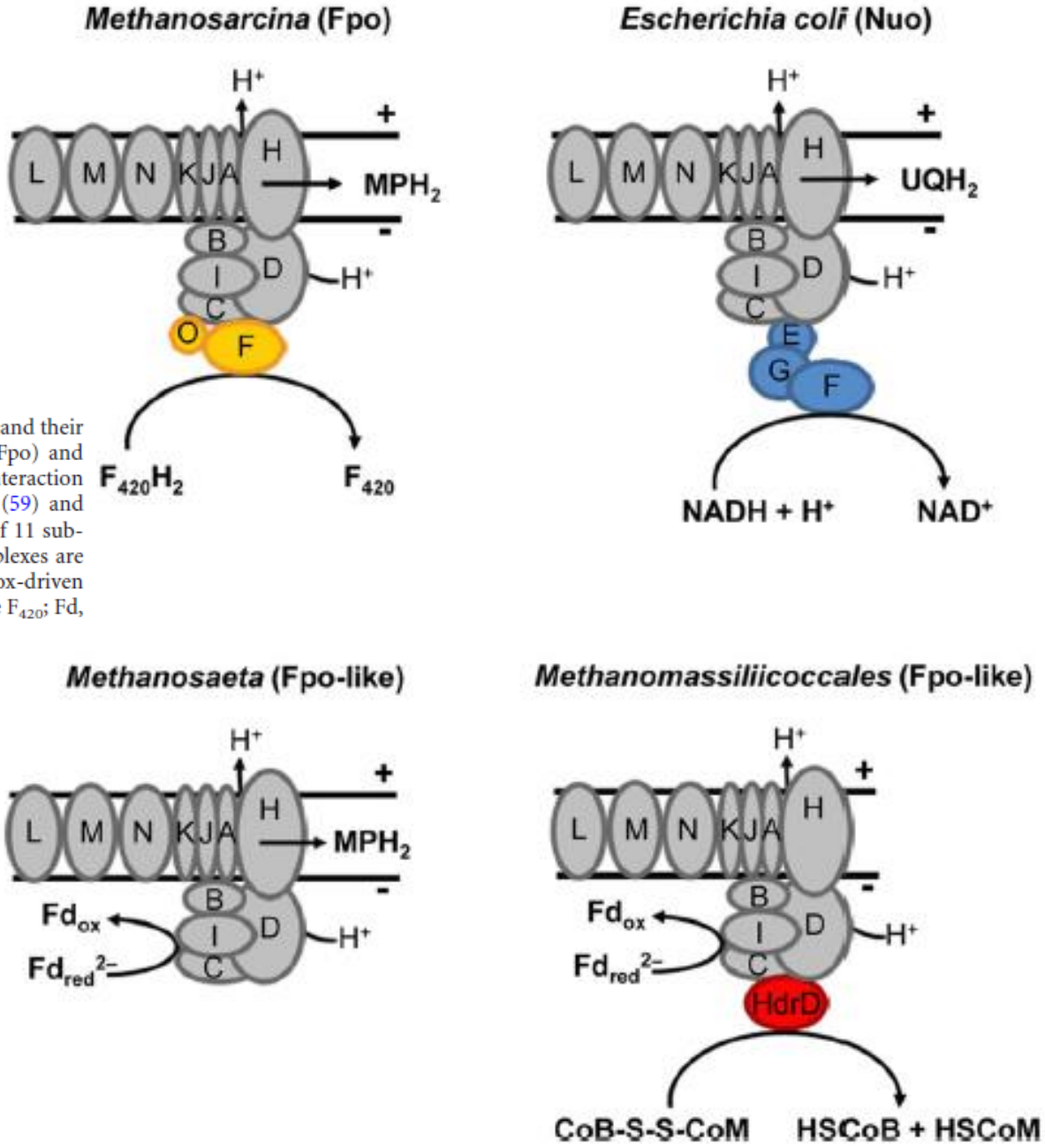

FIG 6 Redox processes catalyzed by the 11-subunit core complexes and their specific electron-transferring modules in *Methanosarcina mazei* (Fpo) and *Escherichia coli* (Nuo) and hypothetical processes and potential interaction partners of the Fpo-like complexes in *Methanosaeta thermophila* (59) and *Methanomassiliicoccales* (this study). The common core complex of 11 subunits is shown in gray, and specific subunits of the different complexes are indicated by different colors. In all cases, the complex serves as a redox-driven proton pump. For further explanations, see the text. F_{420}, coenzyme F_{420}; Fd, ferredoxin; MP, methanophenazine; UQ, ubiquinone.

Lang *et al.*, 2015

Candidatus phylum Barthyarchaeota

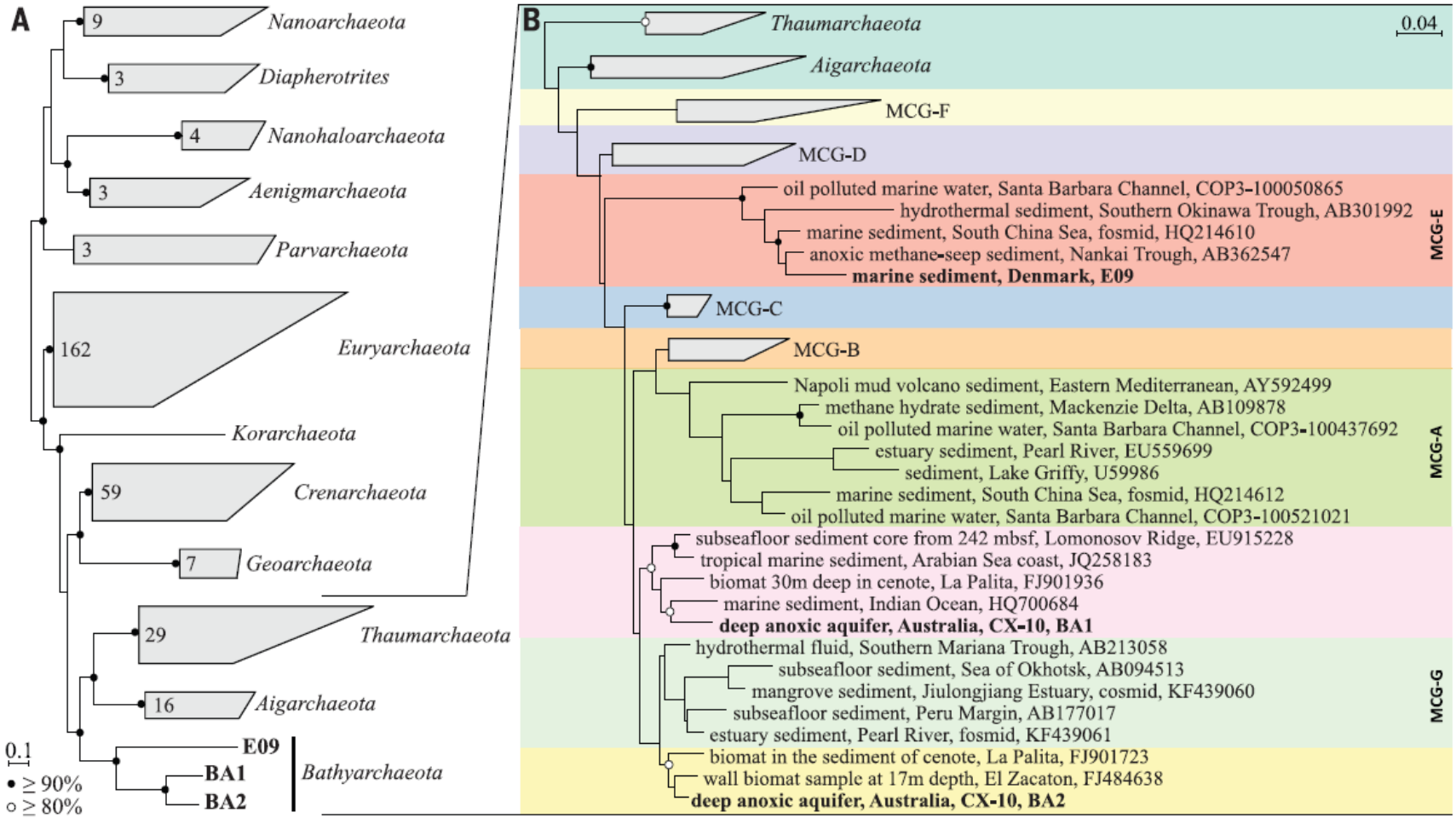

Fig. 1. Phylogenetic trees showing the placement of the BA1, BA2, and E09 genomes in the archaeal phylum Bathyarchaeota. (**A**) Maximum-likelihood tree of 295 archaea, inferred from a concatenated alignment of 144 proteins and rooted with the DPANN (Diapherotrites Parvarchaeota Aenigmarchaeota Nanoarchaeota Nanohaloarchaeota) superphyla (*27*). Support values are shown with white (≥80%) and black (≥90%) circles and indicate the minimum support under nonparametric bootstrapping, gene jackknifing, and taxon jackknifing (supplementary materials). (**B**) Maximum-likelihood 16*S* rRNA gene tree showing the placement of bathyarchaeotal representatives relative to environmental sequences, including genes recovered from Coal Oil Point. Thaumarchaeota and Aigarchaeota 16*S* rRNA sequences from reference genomes were used as an outgroup. Bathyarchaeota (formerly MCG) groups are based on the classification in (*9*). Nonparametric support values are shown with white (≥80%) and black (≥90%) circles. Environmental context and genomes or National Center for Biotechnology Information accession numbers are given. Scale bars indicate expected number of substitutions per site.

Evans *et al*. 2015

Candidatus phylum Barthyarchaeota

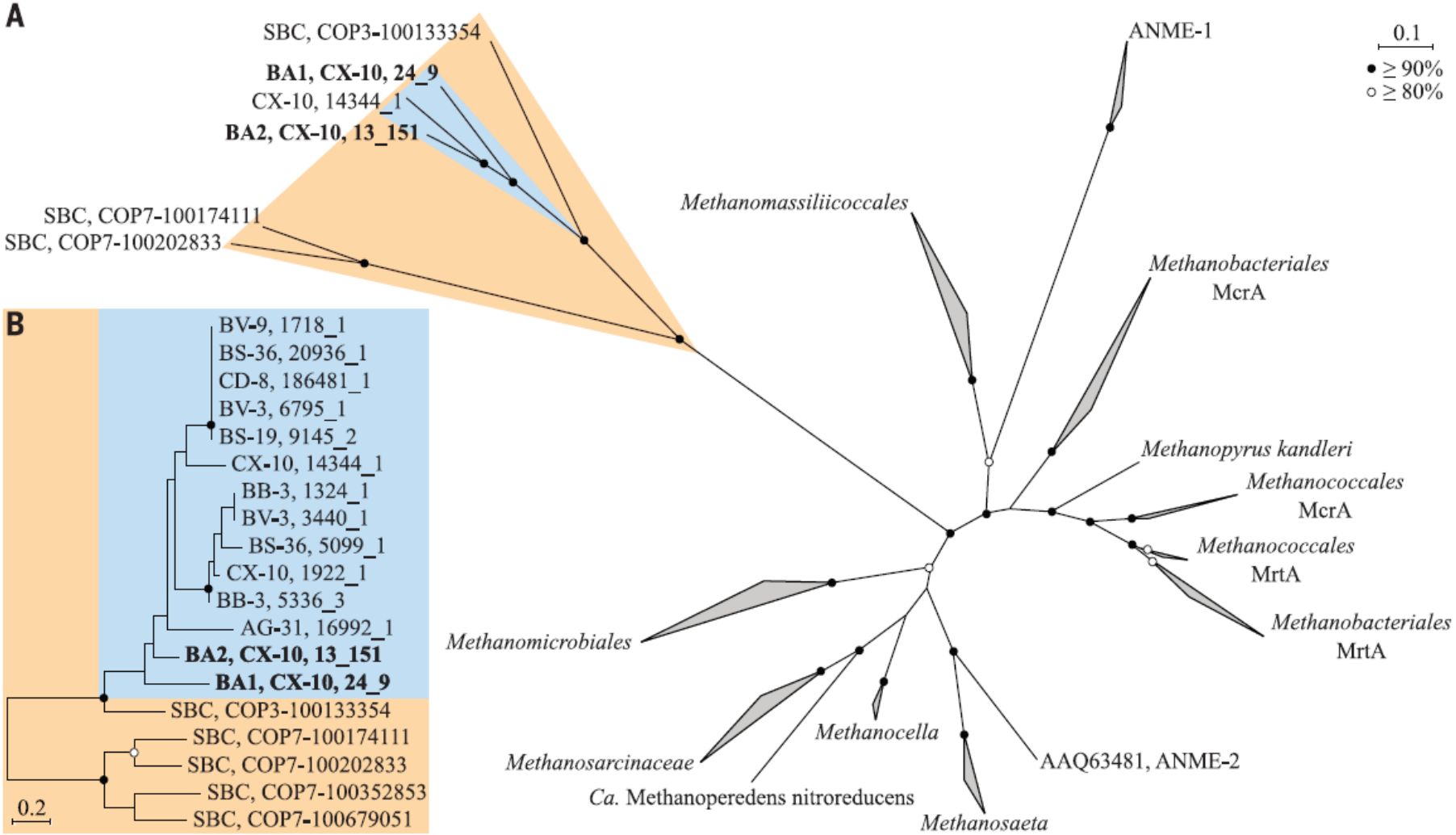

Fig. 3. Maximum-likelihood trees of McrA. (**A**) Placement of nearly full-length McrA protein sequences (≥400 amino acids) identified within the Surat Basin and Coal Oil Point metagenomes, in relation to 153 proteins obtained from GenBank. Lineages were collapsed (depicted as wedges) and labeled according to the lowest common ancestor of all taxa in the lineage. (**B**) Maximum-likelihood tree of nearly full-length and partial McrA sequences identified within the Surat Basin and Coal Oil Point metagenomes. Nonparametric support values are shown with white (≥80%) and black (≥90%) circles. Information about the Surat Basin wells is given in fig. S1. SBC, Santa Barbara Channel.

Evans *et al*. (2015) Science

Candidatus phylum Barthyarchaeota

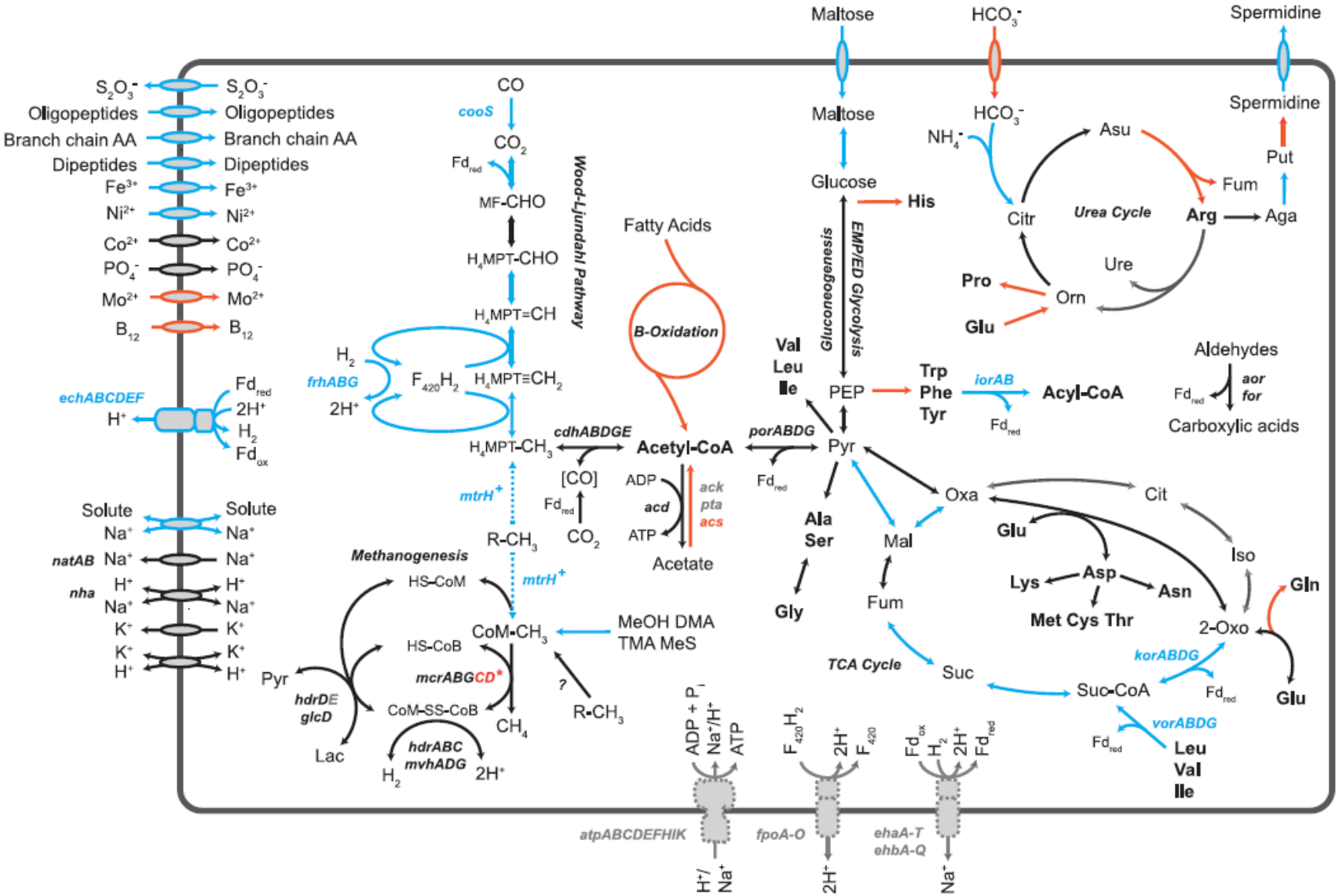

Fig. 2. Key metabolic pathways in the BA1 and BA2 genomes. Genes and pathways found in both BA1 and BA2 (black), only found in BA1 (blue), only found in BA2 (orange), or missing from both genomes (gray) are indicated. Genes associated with the pathways highlighted in this figure are presented in tables S9 (BA1) and S10 (BA2). In the BA1 genome, *+mtrH* genes are adjacent to corrinoid proteins. A bathyarchaeotal contig containing *mcrCD* genes was identified in the metagenome, which probably belongs to the BA1 genome (supplementary text). EMP/ED, Embden-Meyerhof-Parnas/Entner–Doudoroff pathway; TCA, tricarboxcylic acid.

Evans *et al*., 2015

Candidatus phylum Verstraetearchaeota

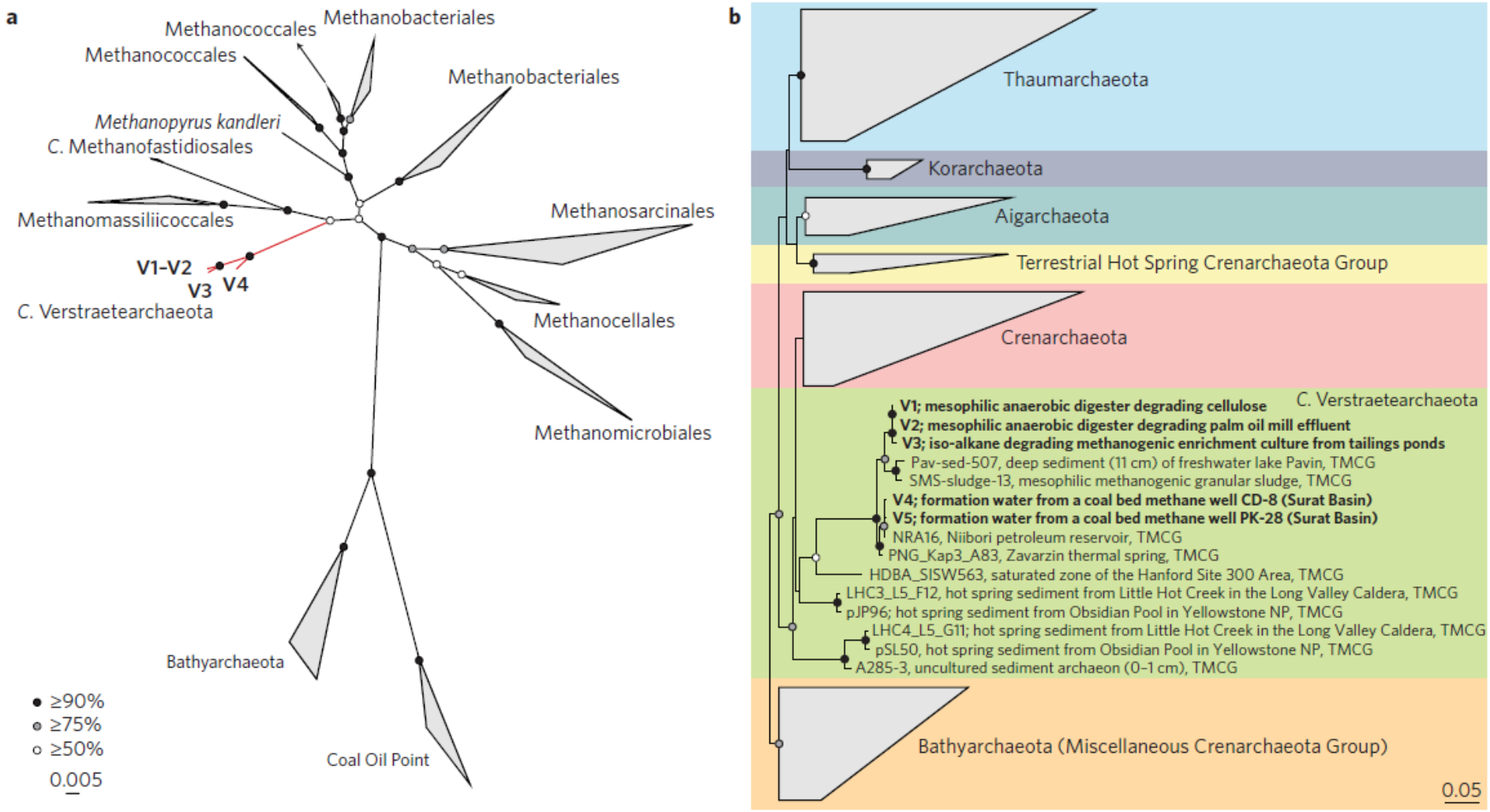

Figure 1 | Phylogenetic trees showing the placement of the Verstraetearchaeota *mcrA* and 16S rRNA genes. a, McrA protein tree showing monophyletic clustering of the divergent McrA sequences from V1–V4 (red) outside known euryarchaeotal and bathyarchaeotal methanogenic lineages. **b**, 16S rRNA gene tree showing the placement of V1–V5 (bolded) with environmental sequences classified as the Terrestrial Miscellaneous Crenarchaeota Group (TMCG), using the Bathyarchaeota 16S rRNA sequences as the outgroup. Bootstrap values were calculated via non-parametric bootstrapping with 100 replicates, and are represented by circles.

Vanvonterghem *et al.*, 2016

Candidatus phylum Verstraetearchaeota

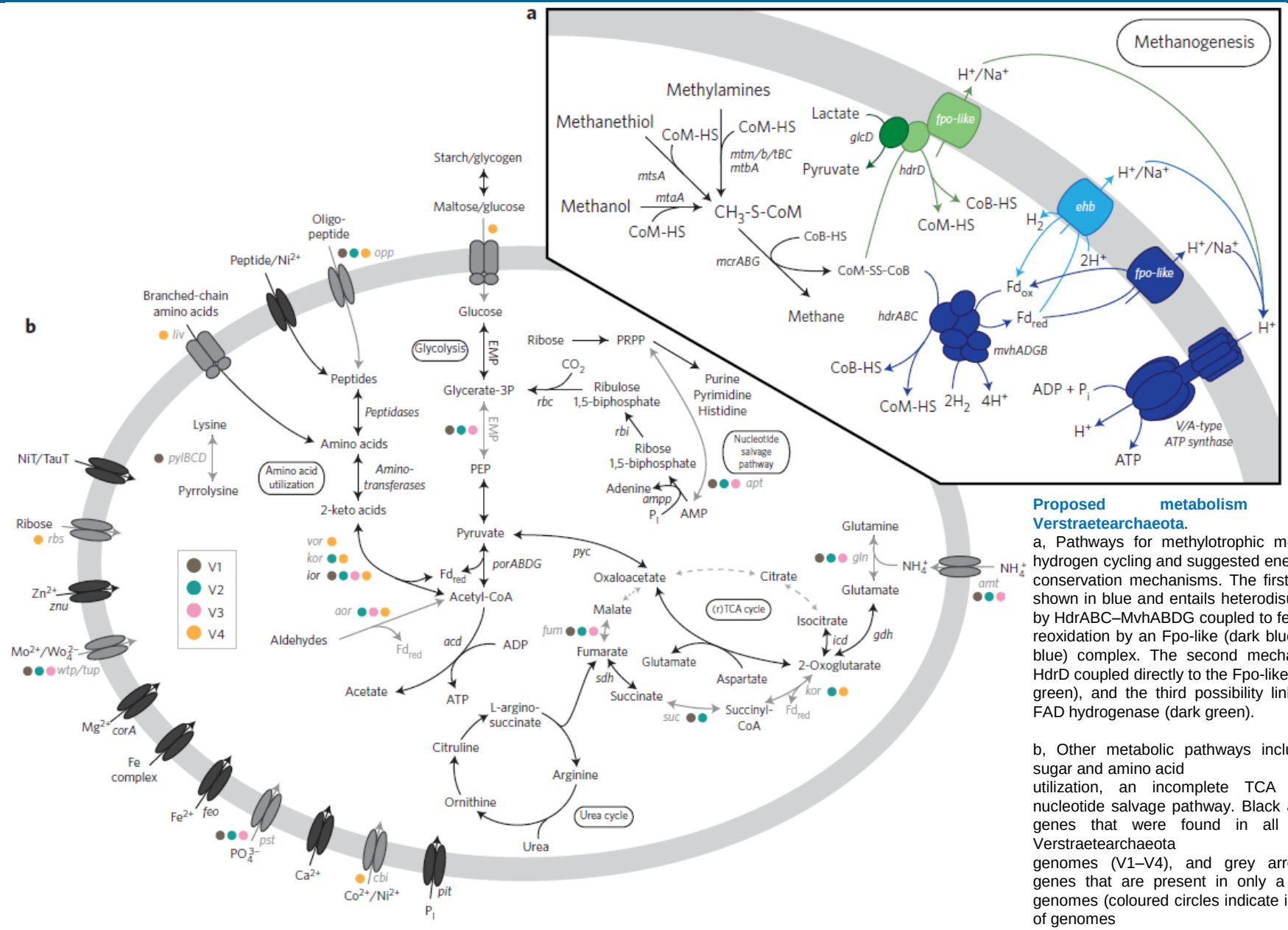

Proposed metabolism of the Verstraetearchaeota.
a, Pathways for methylotrophic methanogenesis, hydrogen cycling and suggested energy conservation mechanisms. The first mechanism is shown in blue and entails heterodisulfide reduction by HdrABC–MvhABDG coupled to ferredoxin reoxidation by an Fpo-like (dark blue) or Ehb (light blue) complex. The second mechanism involves HdrD coupled directly to the Fpo-like complex (light green), and the third possibility links HdrD to an FAD hydrogenase (dark green).

b, Other metabolic pathways including potential sugar and amino acid utilization, an incomplete TCA cycle and a nucleotide salvage pathway. Black arrows indicate genes that were found in all near-complete Verstraetearchaeota genomes (V1–V4), and grey arrows represent genes that are present in only a subset of the genomes (coloured circles indicate in which subset of genomes they are found). Dashed light grey arrows show parts of a pathway that are missing in all genomes.

Vanvonterghem *et al*., 2016

Candidatus phylum Methanofastidiosa

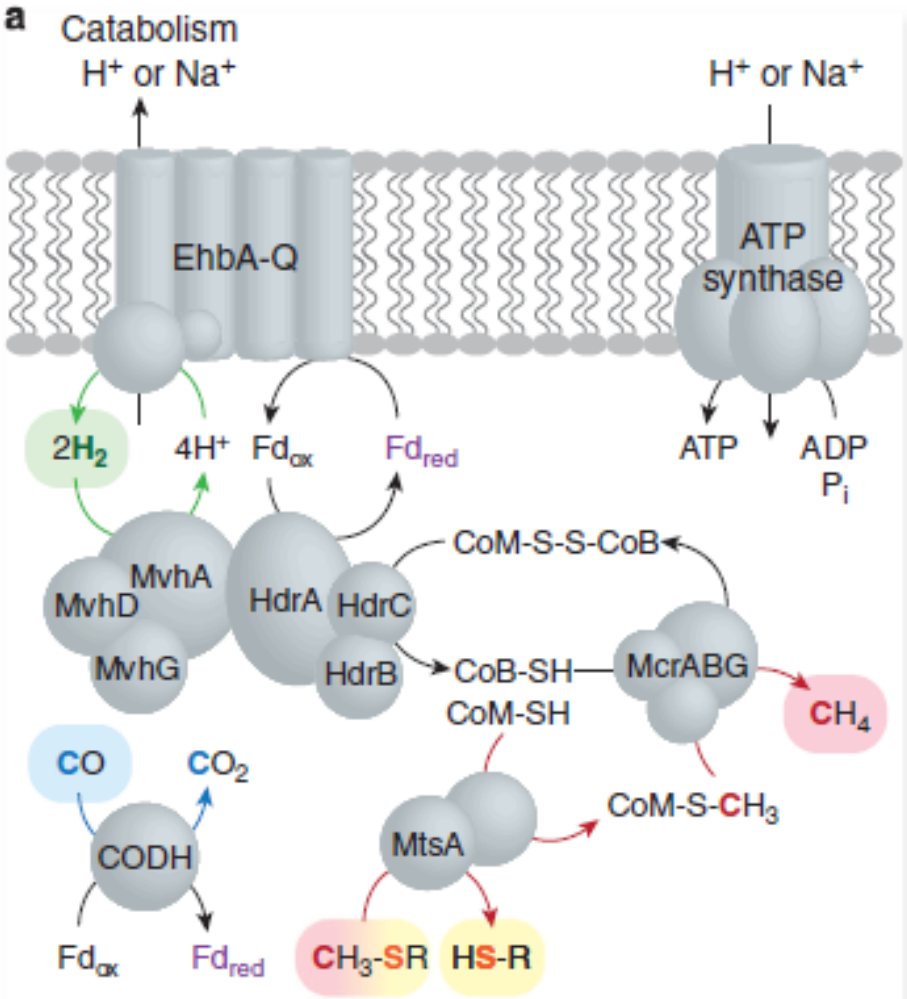

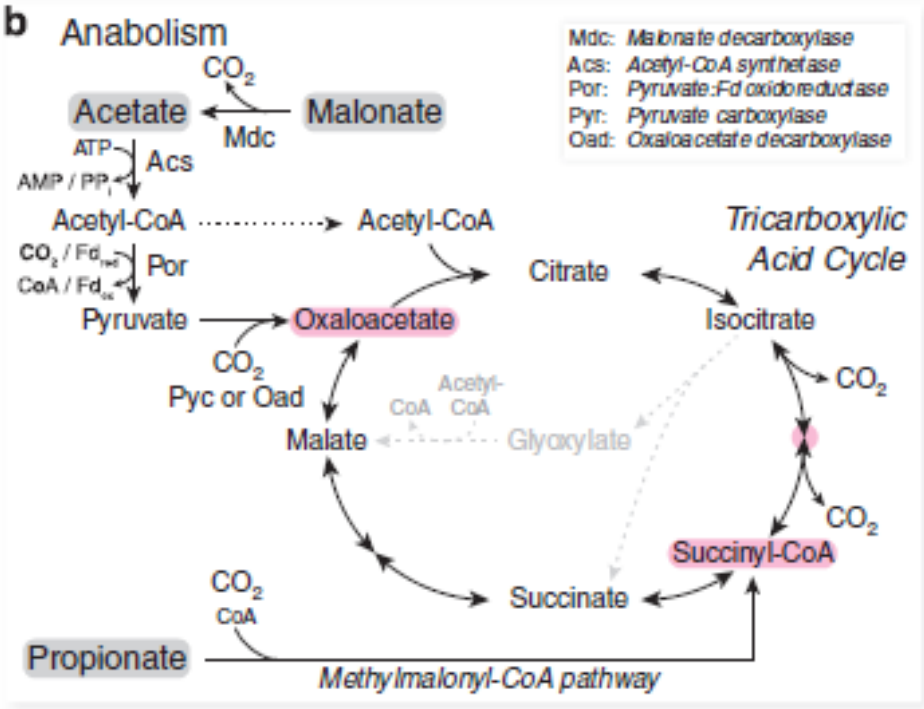

Nobu *et al.*, 2016

***Candidatus* Methanofastidiosa**
***Candidatus* Methanofastidiosum methylthiophilus**

WSA2 (a) catabolism and (b) anabolism. (a) WSA2 has genes for H2 oxidation through electron-bifurcating hydrogenase (HdrABC–MvhDGA) and H2 cycling by energy-converting hydrogenase (EhbA-Q); CO oxidation by carbon monoxide dehydrogenase (CODH); and methylated thiol reduction and methanogenesis by methylated thiol Coenzyme M methyltransferase corrinoid fusion protein (MtsA) and methyl coenzyme M reductase (McrABG). The proton motive force (or cation gradient) generated by Ehb can support ATP production by ATP synthase. (b) Malonate decarboxylase and acetyl-CoA synthetase can convert malonate and acetate into acetyl-CoA for downstream co-assimilation with CO2 (bolded) through pyruvate:ferredoxin oxidoreductase, pyruvate carboxylase and tricarboxylic acid (TCA) cycle. As identified for other heterotrophic methanogens, WSA2 does not encode the glyoxylate shunt for acetate assimilation (gray with dotted line). The methylmalonyl-CoA pathway can facilitate co-assimilation of propionate and CO2 also into the TCA cycle. WSA2 can use key TCA cycle intermediates (pink) as building blocks for biosynthesis.

Methanogenesis – cofactors

2-Mercaptoethanesulfonic acid (coenzyme M, HS-CoM)

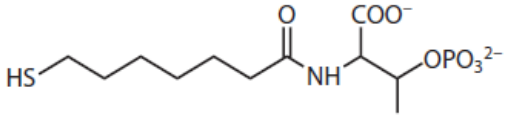

7-Mercaptoheptanoylthreonine phosphate (coenzyme B, HS-CoB)

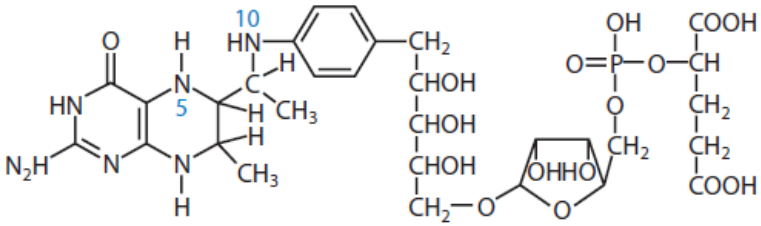

5,6,7,8-Tetrahydromethanopterin (H_4MPT)

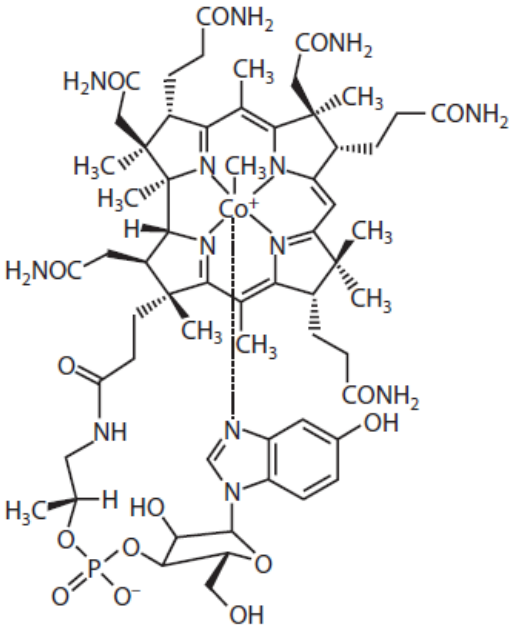

5-Hydroxybenzimidazolylcobamide (factor III)

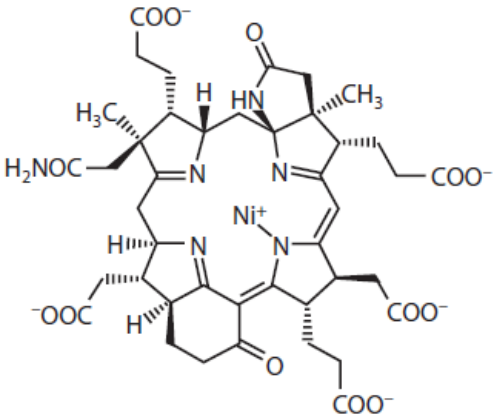

Nickel porphyrinoid factor F_{430}(F_{430})

Coenzymes and cofactors participating in reactions common to all methanogenic pathways. *Methanosarcina* species synthesize tetrahydrosarcinapterin (H4SPT), which serves the same function as tetrahydromethanopterin (H4MPT) and has a similar structure except for a terminal α-linked glutamate (113).

Ferry *et al*. 2010

Methanogenesis – cofactors

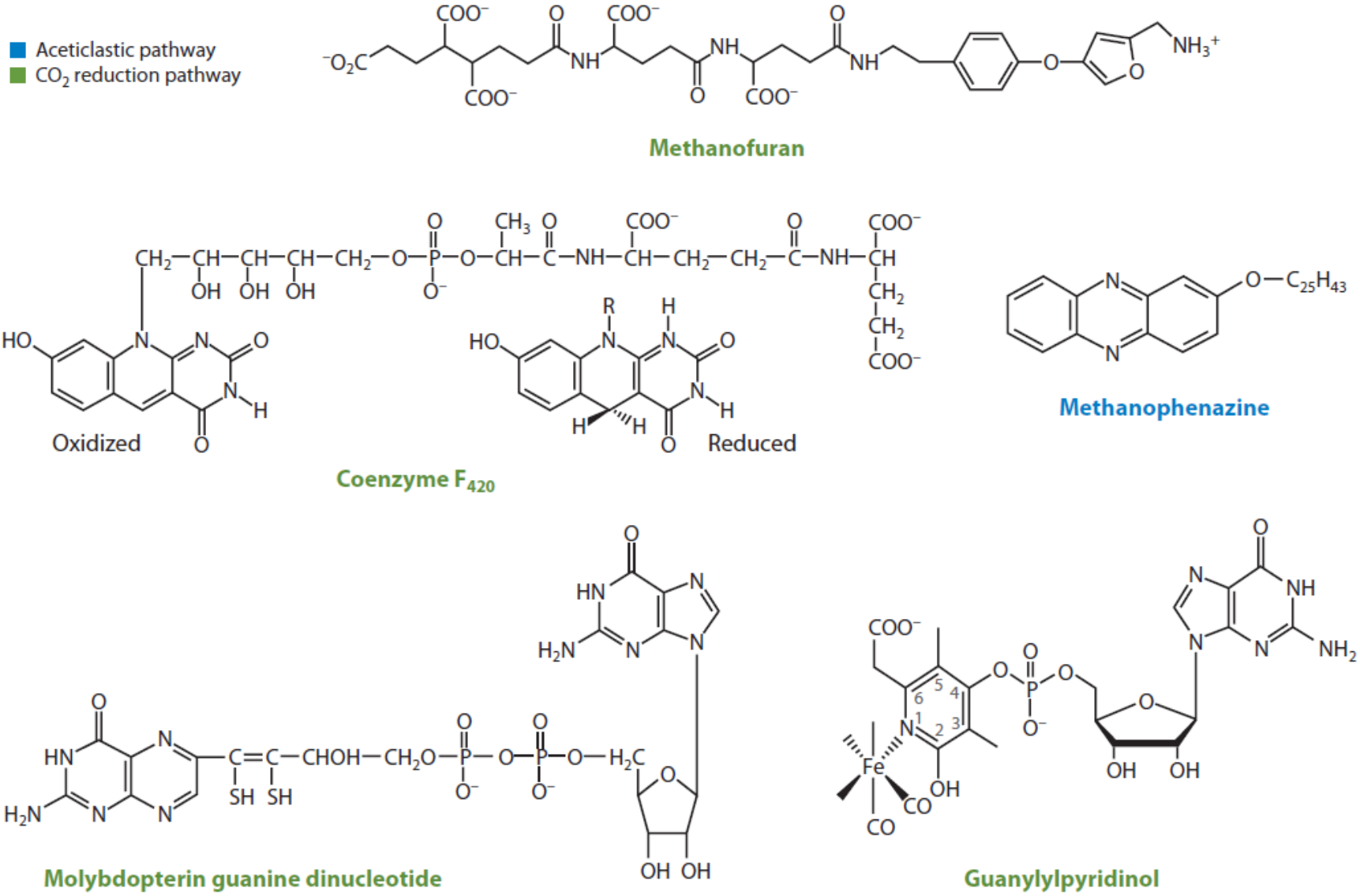

Figure 6

Coenzymes and cofactors unique to either the aceticlastic or the CO_2 reduction pathway.

Ferry *et al.* 2010

Methyl-coenzyme M reductase

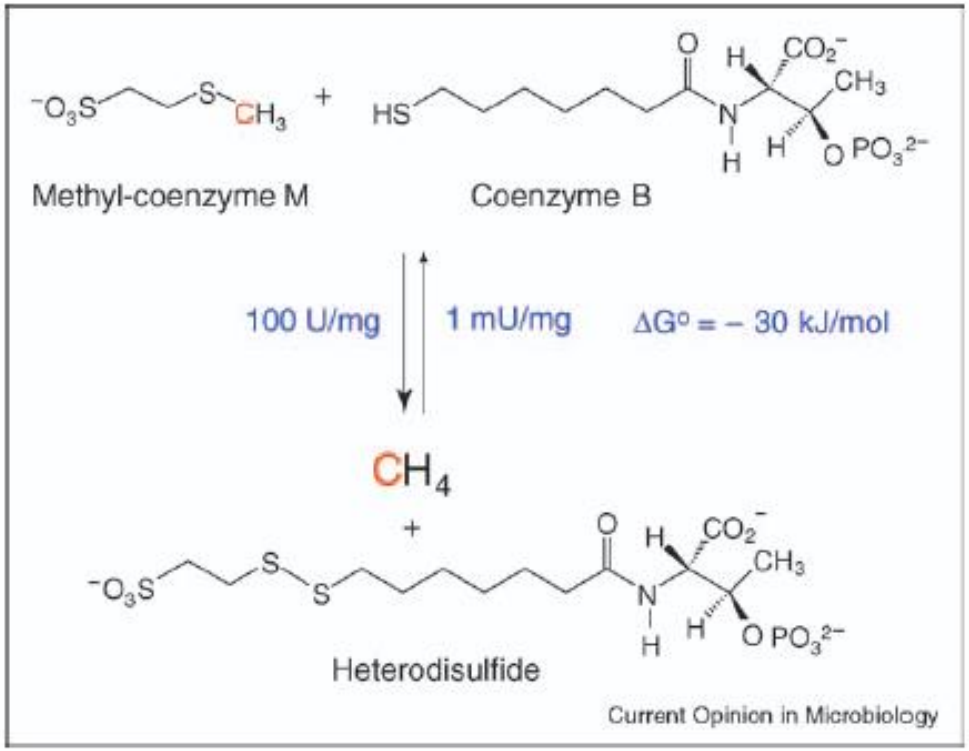

Reaction catalyzed by methyl-coenzyme M reductase (MCR) from *Methanothermobacter marburgensis*. The highest specific rate of methyl-coenzyme M reduction reported for the purified nickel enzyme is 100 U/mg protein (1 U = 1 μmol/min) [25]. The rate for the back reaction (1 mU/mg protein) was estimated using the Haldane equation (see text).

Shima & Thauer, 2005

a2b2g2

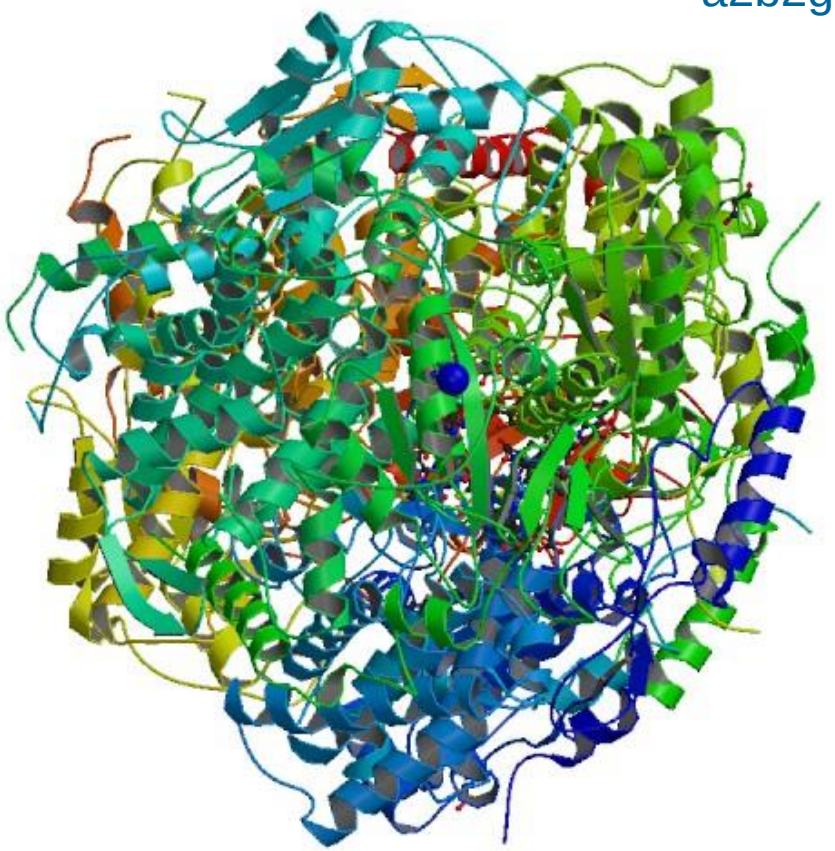

Ermler *et al.*, 1997

mcrA/mrtA isoenzymes are used as molecular marker for detection of methanogens!

Methyl-coenzyme M reductase

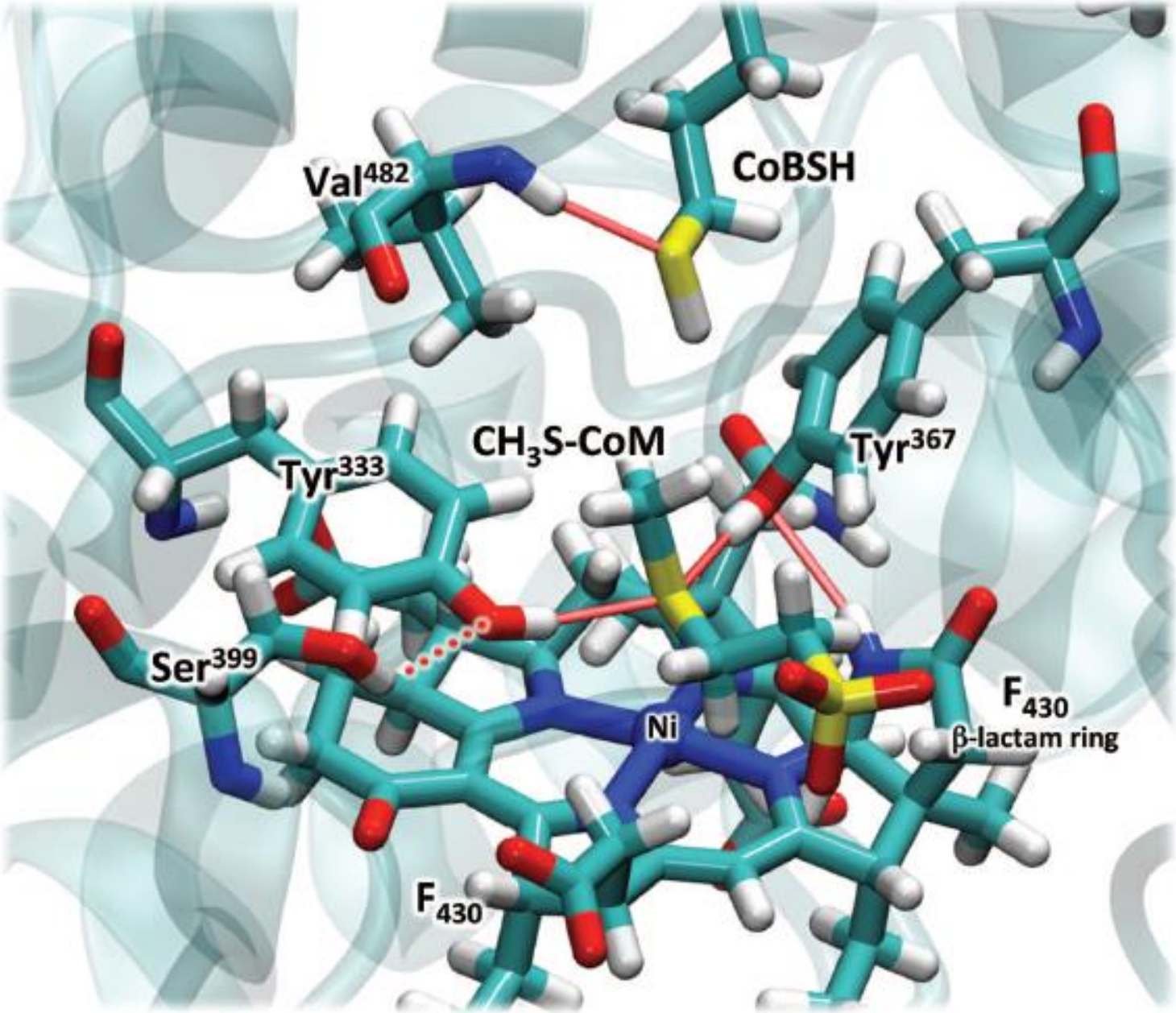

Fig. 5. Hydrogen bonding interactions among MCR active site residues. Red sticks indicate hydrogen bonds at 25°C. The dashed line indicates the weak hydrogen bond between Ser^{399} and Tyr^{333} above 30°C. Residues are numbered according to MCR from *Methanothermobacter marburgensis*. See also table S1.

Wongnate *et al.*, 2016

Methyl-coenzyme M reductase

Wongnate *et al.*, 2016

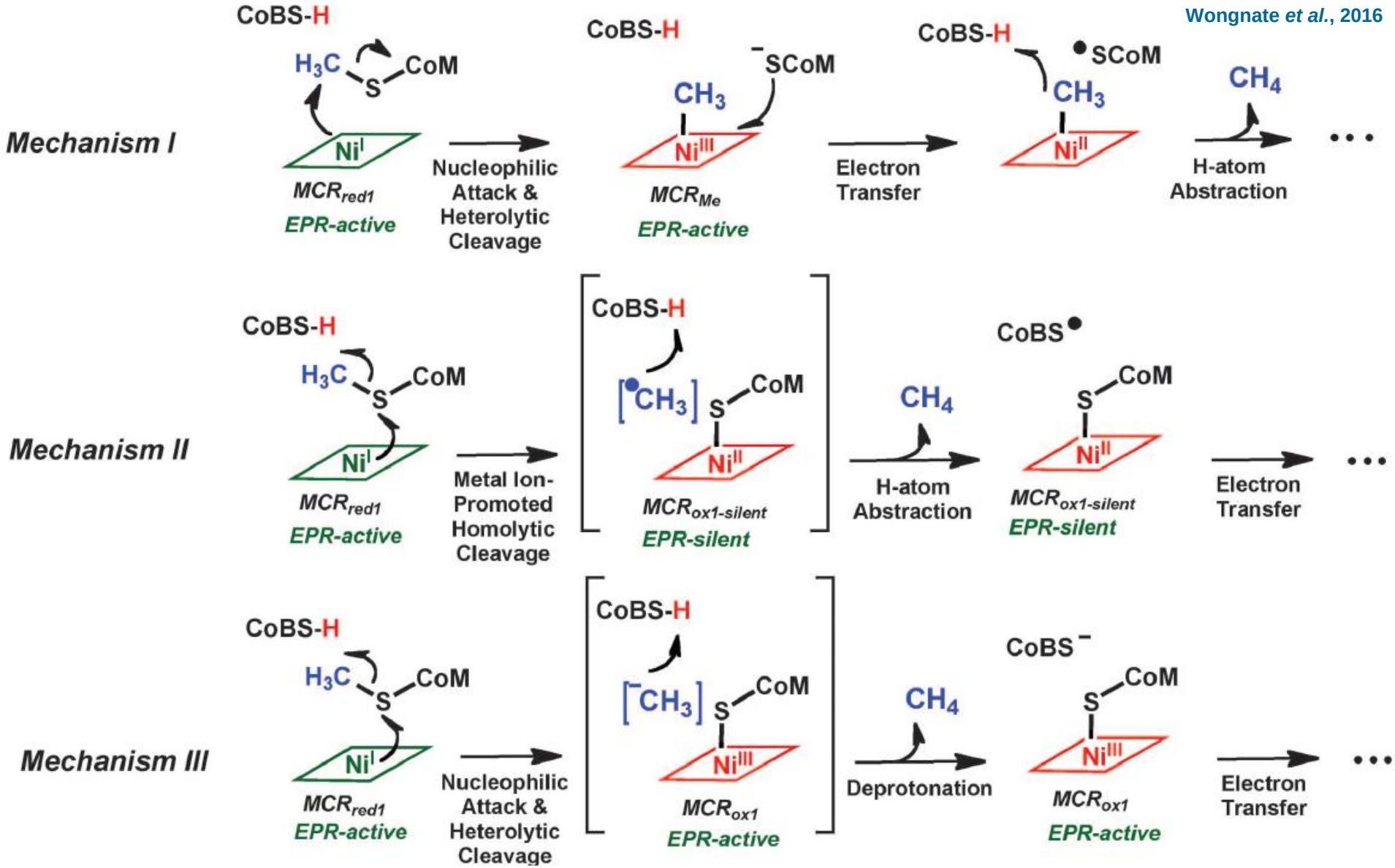

Initial steps in three mechanisms of MCR catalysis. Mechanism I involves nucleophilic attack of Ni(I)-MCRred1 on the methyl group of methyl-SCoM to generate a methyl-Ni(III) intermediate (34). This mechanism is similar to that of B12-dependent methyltransferases (48), which generate a methyl-cob(III) alamin intermediate. In mechanism II, Ni(I) attack on the sulfur atom of methyl-SCoM promotes the homolytic cleavage of the methyl-sulfur bond to produce a methyl radical (•CH3) and a Ni(II)-thiolate. Mechanism III involves nucleophilic attack of Ni(I) on the sulfur of methyl-SCoM to form a highly reactive methyl anion and Ni(III)-SCoM (MCRox1).

Methyl-coenzyme M reductase

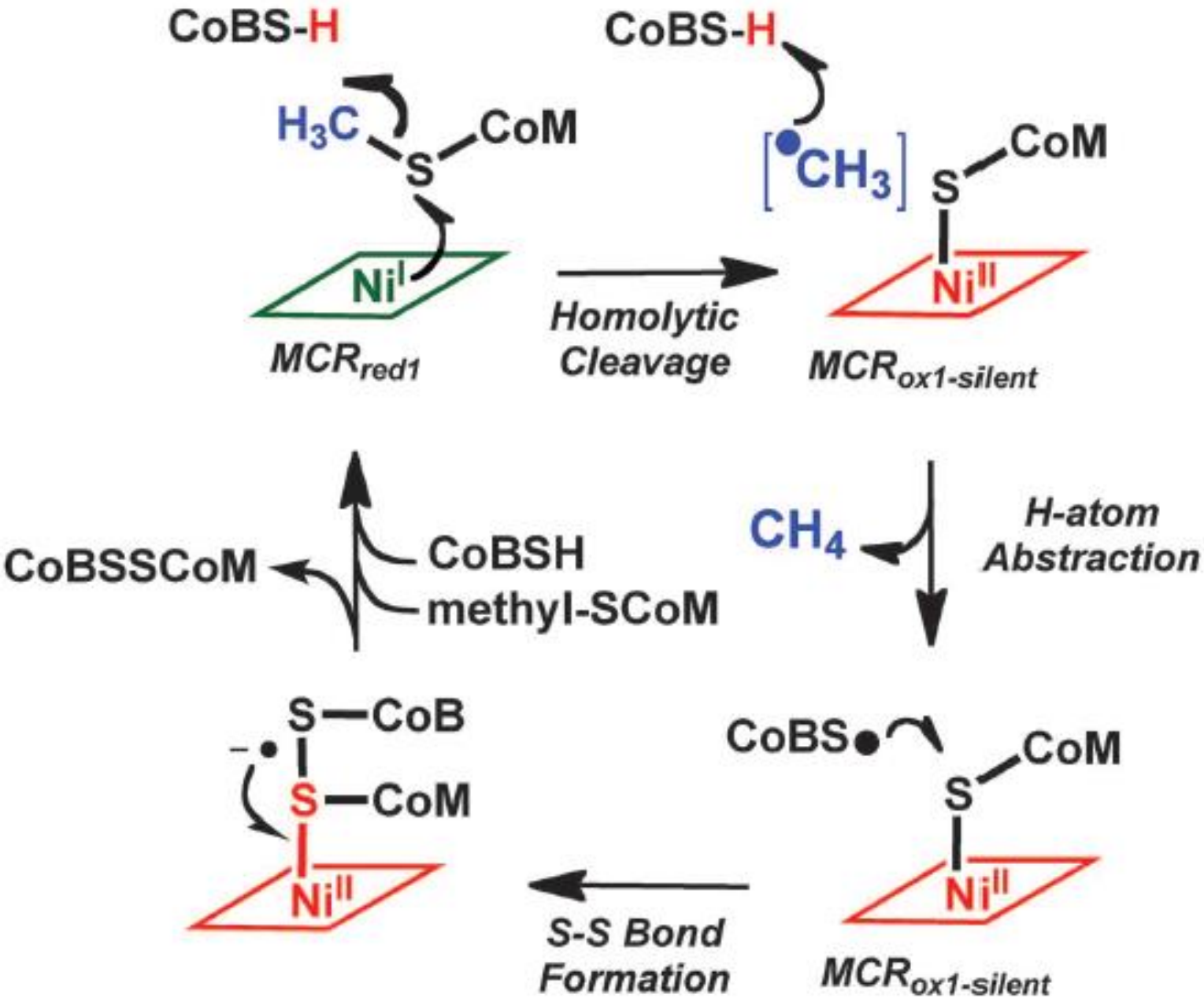

Proposed steps of mechanism II.

In the first step, Ni(I) attack on the sulfur of methyl-SCoM leads to homolytic cleavage of the C-S bond and generation of a methyl radical and a Ni(II)-thiolate (MCRox1-silent). Next, H-atom abstraction from CoBSH generates methane and the CoBS• radical, which in the third step combines with the Ni-bound thiolate of CoM to generate the Ni(II)-disulfide anion radical. Then, one-electron transfer to Ni(II) generates MCRred1 and the heterodisulfide (CoBSSCoM) product, which dissociates leading to ordered binding of methyl-SCoM and CoBSH and initiation of the next catalytic cycle.

Wongnate *et al.*, 2016